Optimization of an aero engine using both inter-cooling and inter-turbine burning

T. Blondeel

Optimization of an aero engine

using both intercooling and inter-turbine burning

by

T. Blondeel

to obtain the degree of Master of Science
at the Delft University of Technology,
to be defended publicly on Friday October 30, 2020 at 13:30 AM.

Student number:	4160681	
Project duration:	September 7, 2019 – October 30, 2020	
Thesis committee:	Prof. dr. ir. A. Gangoli Rao,	TU Delft, Chair & Supervisor
	Dr. ir. F. Yin,	TU Delft, Supervisor
	Dr I.C. Dedoussi,	TU Delft, Examiner
	–,	–

This thesis is confidential and cannot be made public until 2022.

TU Delft

Preface

The thesis titled ”Optimization of an aero engine using both intercooling and inter-turbine burning” is a research about the effects that an intercooler and an inter-turbine burner have when combined in an aero engine. 4 aero-engines are optimized with the TSFC in mind. The model focusses on the thermodynamic aspect of the aero-engine. The results are that advantages and disadvantages of the combined cycle can be concluded and which elements are important in improving the efficiency of the combined cycle and reducing the NO_X emissions. The thesis has been performed by me as partial fulfilment of requirements of a Master of Science degree at the faculty of Aerospace engineering, TU Delft, The Netherlands.

Aerospace is an innovative industry which always aims to reduce costs and emissions. For aero-engines this is mainly by improving used materials and techniques and by implementing new methods. One such method is the introduction of new engine architectures such as intercooling and inter-turbine burning. The main motivation was to contribute to engine innovations by investigating the effect that an intercooler and inter-turbine burner have on an aero-engine.

I would like to thank my supervisors Dr. Arvind G. Rao and Dr. Feijia Yin for their assistance on the thesis. Because of their assistance, I was able to deliver the results. They also helped when problems were encountered and made me think of new solutions when a problem arose during the thesis. I would also like to thank my parent whose constant support was always helpful during my studies.

T. Blondeel
Delft, September 2020

Summary

The thesis focusses on the effects that an intercooler (IC) and an inter-turbine burner (ITB) have on the cycle performance of a UBPR engine. The IC is located between the low-pressure compressor (LPC) and the high-pressure compressor (HPC). It exchanges heat between the core flow and the bypass flow reducing the temperature in the core flow. This has the advantage of a lower HPC-inlet temperature reducing the work needed to reach maximum compression. This also reduces the combustion inlet temperature which reduces the turbine inlet temperature (TIT) or increases the power density of the core. The ITB reduces the TIT by transferring some of the fuel to the ITB. This reduces the NOx emissions. The objective is to analysis the effect that several design parameters have on the on-design performance and to analyze the optimized cycles to compare the advantages and disadvantages of each. Both the IC and ITB improve the thrust specific fuel consumption (TSFC) of the cycle. They also both reduces the NOx emissions. The ITB reduces the NOx emissions more because of the extra degree of freedom during take-off. Varying the ITB energy fraction dependent on the ambient conditions has a positive effect on the NOx emissions during take-off at a slight TSFC increase. Combining an IC and an ITB in the cycle does not add the benefit of each for the TSFC but does add the benefit for NOx emissions as it reduces this even more. The IC-ITB engine is thus found to be optimal over the other engines because the NOx emissions are substantially lower than for the other investigated cycles.

Contents

List of Figures

List of Tables

Nomenclature

Abbreviations

c_1	Main combustion chamber
c_2	ITB combustion chamber
CO_2	Carbon Dioxide
$cold_e$	cold exhaust
hot_e	hot exhaust
IC_e	intercooler exhaust
NO_X	Nitrogen oxides
TIT	Turbine inlet temperature
BPR	Bypass ratio
cd	cold duct
EIS	Entry into service
FAR	Fuel to Air ratio
FPR	Fan Pressure ratio
GSP	Gas turbine simulation program
HPC	High pressure compressor
HPT	High pressure turbine
IC	Intercooler
icd	intercooler duct
ICxx	Engine with an effectiveness of 0.xx
ISA+x	International standard atmosphere + T[K]
ITB	Inter-turbine burner
ITBxx	Engine with ITB fuel fraction of of 0.xx
LEAP	Leading Edge Aviation Propulsion (aero-engine)
LHV	Lower heating value
LPC	Low pressure compressor
LPT	Low pressure turbine
MTOW	maximum take-off weight
OEW	Operational empty weight
OPR	Overall pressure ratio

PR Pressure ratio

SLS Sea level static

ST Specific thrust [kN/kg]

TOC Top of Climb

TSFC Thrust Specific fuel consumption [g/kN/s]

Parameter

ΔH Change in enthalpy during the process [W]

ΔS Change in entropy during the process [W]

$\dot{m}$ mass flow [kg/s]

ϵ Specific exergy [J/kg]

η_{th} Thermal efficiency

γ Heat capacity ratio

μ viscosity $[Ns/m^2]$

ρ density $[kg/m^3]$

A Area $[K/W]$

c_p Heat capacity at constant pressure [J/(K kg)]

$EINO_x$ Emission index for NO_X [g/kg]

$EISNO_x$ Standardized Emission index for NO_X [g/kg]

H/C hydrogen over carbon ratio

k Thermal conductivity $[W/(mK)]$

L^* specific lost exergy [-]

m_f Fuel mass [kg/s]

Nu Nusselt number

P_S Shaft Power [W]

P_T Thrust Power [W]

Pr Prandtl number

PT_x Total pressure at stage x [Pa]

R Thermal resistance $[K/W]$

Re Reynolds number

T_b blade temperature

T_c coolant temperature [K]

T_g gas temperature [K]

TT_x Total temperature at stage x [K]

U_i Internal energy [W]

W_x	Mass flow at stage x [kg/s]
W_{rev}	Reversible work [W]
b	Steady flow availability [W]
b	constant to define conductive cooling
b	constant to define film cooling
C	Relative speed to the earth [m/s]
E	Exergy [W]
e	effectiveness
H	Enthalpy [W]
h	specific enthalpy [J/kg]
KE	Kinetic energy [W]
L	Lost exergy [L]
P	pressure
PE	Potential energy [W]
q	Heat [W]
QE	Chemical energy [W]
S	Entropy [J/K]
T	Temperature [K]
U	Flight speed [m/s]
V	speed [m/s]

1

Introduction

This chapter introduces the thesis. First the general backline is given followed by a small introduction to the used methodology. Secondly, the lay-out of the thesis is explained.

1.1. Previous work and motivation

Aviation is an important contributor to greenhouse gasses and other emissions. It is one of the sectors that has the fastest growth. There is an incentive to reduce these emissions on a global scale. Since aviation accounts for more than 2% of the total emissions globally and is a fast growing sector, it is an important sector to keep an eye on to reduce emissions. A person flying a transatlantic flight will have the same impact on the climate as the average European has by heating their home a whole year-round as it produces 986 kg CO_2 [1]. The original estimates for 2020 were that the emissions in aviation would be 70% higher than in 2005. The International Civil Aviation Organization (ICAO) estimated that these could rise to 300-700% by 2050. [2]

Through the International Airline Transport Association (IATA), the aviation industry has given itself targets: a decrease in fuel used by 1-1.5% per year, stabilize the CO_2 levels at a 2020 target and halve the emissions by 2050 compared to 2005. In general, these changes should come from technological enhancements such as improving the engine or developing alternative fuels, improving infrastructure, and operational measures such as improved flight procedures. When no action is undertaken, the red line in figure 1.1 is the prospected CO_2 growth. Some measures have to be taken to meet the 2550 goal. Such as technology increase, biofuels and possible radical technologies as seen in the figure. [3]

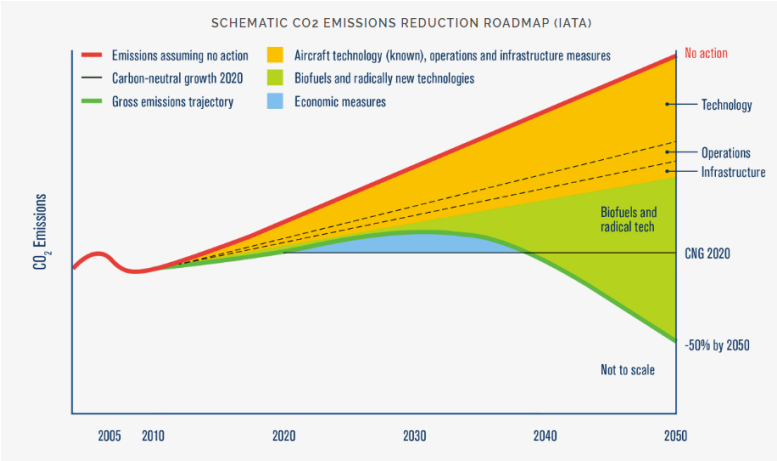

Figure 1.1: Schematic of CO_2 prediction in 2050. [3]

One option of reducing the emissions of aviation is looking at innovative engine architectures. Most aero-engines used in modern aircraft are Brayton cycles. Adapting this cycle allows for changes that

may improve the performance of these engines. The first improvement in history was to increase the turbine inlet temperature and the pressure ratio. Then a fan was included to increase the propulsive efficiency by bypassing some air around the core cycle. The effect was a reduction in thrust specific fuel consumption (TSFC), which also reduces the CO_2 output. This fan had the effect that a more energetic core was needed and this increased the production of NO_X. This contributes to ozone (O_3) formation and methane depletion in the upper layer of the atmosphere. The overall effect of NO_X emissions is that the atmosphere heats up [4].

Lowering the pressure and the temperature in combustion will result in less NO_X emission. However, a more fuel-efficient engine generally prefers a higher pressure, which will also increase the temperatures, resulting in more NO_X. Other emission gasses are also investigated, such as carbon oxide, but the engine's architecture has little impact on this. Unburned hydrocarbons generally follow the same trend as CO. There is also soot, which is predominantly carbon particles with a diameter larger than 6nm. SOOT is a known carcinogen. No immediate influence of pressure and temperature in the engine is found to the production of SOOT.

The two architectures that are investigated are inter-stage turbine buring and intercooling. Intercooling is the process where air is cooled during the compression. For aero-engines, this mostly happens between the low pressure compressor (LPC) and the high pressure compressor (HPC). The air is bypassed after the LPC and exchanges heat with the bypass flow via the intercooler (IC). This cooler air has some pressure losses because of the physical implementations of the heat exchanger. This cooled air is then fed to the HPC where it will continue the regular cycle. Inter-turbine burning happens between the high pressure turbine (HPT) and low pressure turbine (LPT). Extra combustion chambers are added in between the turbines. Generally, this happens between the HPT and the LPT. In this location, an extra combustion chamber is attached, where fuel can be added to the flow independent of the main combustion chamber. By using an inter-stage turbine burner, the engine specific power output increases. An inter-turbine burner (ITB) also allows for a higher degree of freedom during off-design operations and a lower maximum temperature in the main combustion chamber.[5] It could also be used to implement a new alternative fuel into this second combustion chamber.

Most of the research done on intercooling is performed at Chalmers University by Thomas Grondstedt and Konstantinos Kyprianidis[6–11] and at MTU by Michael Flouros[12–17]. At Chalmers, an average fuel reduction of 3-5% was found over all the papers and all the intercooling configurations. This is mainly due to the reduced work needed for the HPC because the cooling flow is at a lower temperature and the combustion inlet temperature no longer limits the overall pressure ratio (OPR). Different architectures were investigated, a single pass IC, a double pass IC, and a reverse flow IC. The architectures all had the same advantages and disadvantages. A lower engine weight was found. The IC added weight but the reduction in weight from the HPC was greater. The nacelle was larger since the addition of the IC made the bypass larger in size. Intercooling resulted overall in a fuel reduction of 3-5%. Another possible advantage was a reduction in NO_X since a lower temperature in the HPC could mean a lower temperature in the combustion chamber, which would result in less thermal NO_X formation. The disadvantages are an increased complexity of the design and that the cycle prefers higher OPR. The OPR was limited by the HPC blade height and the fan sizing, which could be improved using a geared fan. The geared fan architecture was not investigated previously. At MTU, the IC-engines were also all equipped with a recuperator. The recuperation system uses the hot exhaust gas to preheat the combustion inlet air. A TSFC reduction between 9.1 and 13.1% was found for the intercooled recuperated systems. It was not clear how much was from the IC, how much was from the recuperator and how much was from combining the systems.

Inter-turbine burning in modern aero-engines is previously investigated by Feijia Yin and Arvind Gangoli Rao at Delft University of Technology[5, 18]. In inter-turbine burning, the results showed that it had worse fuel performance when only on-design performance was analysed. It did however already show a reduction in NO_X of up to 40% while the TSFC increased by 5%. Including off-design performance showed that an engine architecture with an ITB was better in achieving the hot-day-take-off constraint than a conventional engine. This meant that the inter-turbine burned engine could be smaller, or the conventional engine needs to be sized up to accommodate the off-design performance. When this was included, a TSFC reduction of 4% in cruise and up to 7% in take-off was the result.

The methodology used is to create four engine architectures. A conventional (baseline) engine, an intercooled engine (IC-engine), an inter-stage turbine burning engine (ITB-engine) and an engine which combines an IC and an ITB (IC-ITB engine). These 4 engines will be optimized using Gas

turbine simulation program (GSP) and a MATLAB optimization sequence based on sequential quadratic programming. All 4 engines are optimized to the same operating conditions with the same inlet mass flow at cruise condition. The optimized variable is the minimization of the TSFC. Then, the engine architectures are compared to each other. This is done for the TSFC, the NO_X emissions and maximum temperatures in the cycles.

1.2. Research question, aims and objectives

This section explains what the goals and the questions are for the thesis. The research questions are given as well as the research objective.

Intercooling has positive effects on the fuel economy of a jet engine and possibly on the produced NOx in the combustion chamber since the combustion chamber inlet temperature can be lower. It does make the architecture more difficult since there is an extra component and the installation penalty is most likely higher than for a conventional aero-engine. inter-turbine burning has positive effects on the produced NOx emissions, on the off-design performance of an aero-engine and on the lifetime of an aero-engine since the maximum temperature can be lower. It makes the architecture more difficult since it needs an extra combustion chamber between the HPT and LPT and might need cooling of this LPT. The planned research will combine the two approaches together to find the advantages and disadvantages of the new setup. The addition of the 2 architectures can be seen in figure 1.2. The IC is defined as the added green block and the ITB is the added purple block.

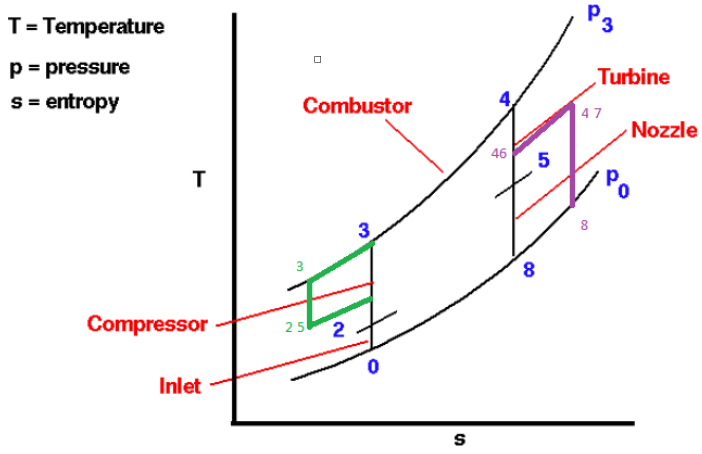

Figure 1.2: T-S diagram of Brayton cycle with IC and inter-turbine burning.[19]

The main research question is: Is an engine architecture using intercooling and inter-turbine burning advantageous in comparison with the currently used architecture that does not use these two components or one of the two components? Since this is a broad scope towards the research, this can be split into multiple research sub-questions.

1. Is the proposed architecture better from an emission viewpoint?
   - Can the CO_2 emission be reduced with the new architectures?
   - Can the NO_X emission be reduced with the new architectures?
2. Is the proposed architecture better from a fuel economy viewpoint?
3. Is the idea better from an operation viewpoint, considering maintenance?
   - What is the maximum temperature in the engine?
   - What is the maximum temperature during cruise flight?
4. What are the design and operational challenges?

The research objective is then as follows. Find advantages and disadvantages of an engine architecture using intercooling and inter-turbine burning and make recommendations based on the findings by simulating and optimizing the jet engine with the use of the Gas Turbine Simulation program (GSP).

1.3. Lay-out

The first following chapter is the literature review. The literature review focuses on the basics of an aircraft engine and what the effect is adding an IC and an ITB separate. It explains the used methodologies by the other researchers and summarized their results. A part is also used to note the effects of turbine blade cooling. The most common emissions are laid out and followed by a description of the used software, GSP and MATLAB. Following this, the own methodology is explained. The models are laid out. The cooling model is validated. The emission model is derived and the exergy calculations are explained. After this, a chapter is dedicated to a parameter analysis. In this chapter, all the relevant parameters that influence the cycle are varied in cruise flight to measure the effect of changing a single parameter on the models. The variables changed are: bypass ratio (BPR), fan pressure ratio (FPR), LPC pressure ratio, HPC pressure ratio, turbine inlet temperature (TIT), IC effectiveness (explained in the methodology), IC pressure loss, bypass split ratio (how much of the bypass goes through the IC and the ITB energy fraction (how much of the energy is added in the ITB). The chapter after this is the on-design optimization. In this chapter, the 4 engine architectures are optimized. This results in tables that quantify the optimized results. This is done for the baseline engine, for multiple IC-engines with varying IC effectiveness, for multiple ITB-engines with varying ITB energy fraction and for multiple IC-ITB engines that with varying IC effectiveness and ITB energy fraction. Then, the off-design analysis is laid out in the following chapter. In this chapter, a top of climb condition is added and a spool speed limiter is added in the take-off operation. The effect is that the engines change to satisfy these conditions. These new 4 engines are now compared to see the effect on these off-design conditions. This done for both the TSFC and the NO_X emissions. The exergy analysis is presented after this in the next chapter. In this chapter, the results of the exergy analysis on the 4 engines created in the off-design optimization are presented. All components can now be compared to see how much each component contributes to the losses. After this, the conclusion is presented with recommendations.

2

State of the art / Literature review

All the research presented in this section has to do with improving the fuel economy of an aero-engine or improving the emissions. It is divided into 6 sections: a section on intercooling, inter-turbine burning, turbine blade cooling, emissions, exergy, and a 0D simulation program called GSP.

2.1. Aircraft Engine

A current turbofan engine is a machine that has been designed based on a Brayton cycle. It takes in inlet air, which then goes through a fan. The air splits between a bypass and a core cycle. In this core cycle, the air gets compressed through a compressor. Then it enters a combustion chamber where fuel is injected into the core flow, adding energy to the flow at a nearly constant pressure, which raises the temperature of the flow and the specific heat capacity. The hot gas expands further through a turbine to produce turbine power, which is then used to drive compressor mounted on the same shaft as the turbine. The extra power is left after the turbine exits this core section to the ambient air at an increased velocity and increased temperature. The bypass flow gets a total pressure increase from the fan and accelerates and exits the engine to the ambient air. Both these flows exert a thrust force to the aircraft and accelerate it or keep it at a constant velocity counteracting the drag of the aircraft.

The ideal Brayton cycle is shown in figure 2.1.The compressing stage is shown between point 0 and point 3 while the compressor is from 2 to 3. The combustion happens in the combustor shown between 3 and 4 (at constant pressure) and the turbine driving the compressor is shown between 4 and 5. The net work from the ideal Brayton cycle is then from point 5 to point 8. In a real cycle the compressor and turbine lines are not vertical anymore since efficiencies are not 100%. The temperature at point 3 will be slightly higher for the same pressure, and the extracted net work will be slightly lower.

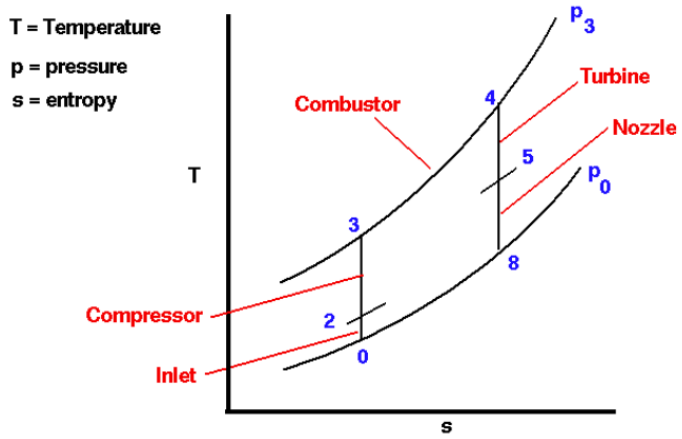

Figure 2.1: T-S diagram of ideal Brayton cycle. [19]

The amount of net work that can be taken out of the engine is related to the maximum temperature of the engine and the pressure ratio. A higher pressure ratio will result in higher thermal efficiency(η_{th}), as seen in equation 2.1. The heat capacity ratio (γ) is dependent on the gas composition.

$$\eta_{th} = 1 - \frac{1}{OPR^{\gamma-1/\gamma}} \tag{2.1}$$

The optimal pressure ratio is however not the one giving the highest thermal efficiency. It is the one giving the maximum net work output. This means maximizing the area inside the T-S diagram in figure 2.1. This Brayton cycle can then be adapted by adding extra components such as an IC or an ITB or a recuperation system that heats the flow before the combustion chamber with hot air from the exhaust.

2.2. Intercooling

Research about intercooling has already been done widely. This will be summarized here. The effects this might have on the cooling flow will be described and studied in section 2.4.

The basic thermodynamic process of intercooling is visible in figure 2.2. The green cycle is the added process compared to the conventional Brayton cycle. The fan and the LPC compress the core flow. Cooling happens trough the IC with the bypass flow. After the IC, the air gets compressed further to the desired pressure ratio. For the same pressure ratio as a conventional cycle, a lower combustion inlet temperature is achieved. This changes the optimal cycle and thus also the optimal pressure ratio. Other benefits are that the air is at a lower temperature and less work is needed to compress the colder flow. Some disadvantages are pressure losses, weight addition, installation penalty from the wider engine body and the optimal pressure ratio being too high for the current level of technology.

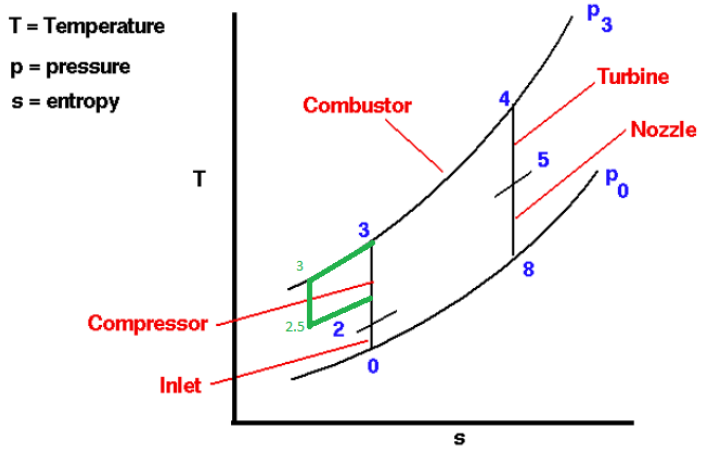

Figure 2.2: T-S diagram of aero-engine with IC

2.2.1. Intercooling in Gas Turbines

A first paper by Caniere et al. [20] investigates how intercooling can raise the cycle efficiency in an air-cooled gas turbine. They found that an increased cycle efficiency is not necessarily the result of a higher turbine inlet temperature (TIT). A found result was the importance of the pressure ratio split between the LPC and the HPC at which the IC was installed. The intercooling should happen early in the compression to maximize the HPC's benefit and minimize the pressure losses. This corresponded with the IC position in a turbine built by GE, the LMS100 [21]. The LMS100 is however a gas turbine for ground operations. The design range was an OPR between 20 and 50, and the TIT was between 1100 and 1600. In this region they found that using an IC gave a better cycle efficiency than a conventional engine. This was mostly from the reduced work needed to further compress the flow and the cooling flow extracted from the HPC had a lower temperature. Maximum efficiency was not found in this research. It was expected that this was mainly due to the design range of the OPR, since the optimum was expected to be found at a higher OPR than 50. The results of the cycle efficiency shown as the contour lines can be seen in figures 2.3 and 2.4. It is noticeable that indeed the IC finds better

efficiencies but that the optimum efficiency for this intercooled engine is above the graph (higher OPR).

The method in which they modeled the compression and the expansion is not useful since in total there were only 4 stators and 4 rotors. This is less than for modern aero-engines. It is however useful that they found the best results were for high OPR and that the intercooling itself should happen at a relatively low pressure ratio. An external supply of water performed the cooling of the IC itself. This will not be the case in aero-engines since the only cooling flow for the IC will be the bypass flow or the ambient air.

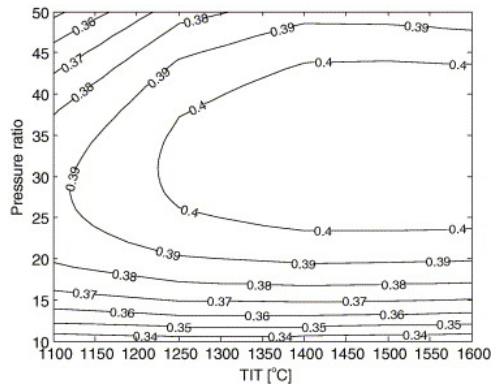

Figure 2.3: Cycle efficiencies for conventional [20]

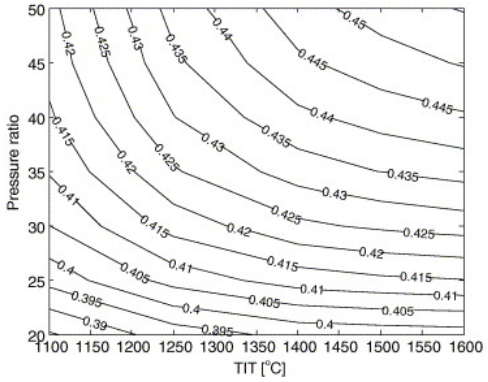

Figure 2.4: Cycle efficiencies with intercooling [20]

2.2.2. Intercooling in early aero-engines

Saravanamuttoo et al. [22] investigated the IC and concluded a positive effect on the thermal efficiency compared to a conventional engine. Walsh et al. [23] expanded upon this investigation by including an optimization for an intercooled engine which found that an intercooled engine works better at a higher OPR. They found a correlation between the thermal efficiency and a multitude of variables and it can be lower or higher than the thermal efficiency of a conventional engine. The typical variation can be seen in figure 2.5 where the thermal efficiency becomes significantly better at high OPR.

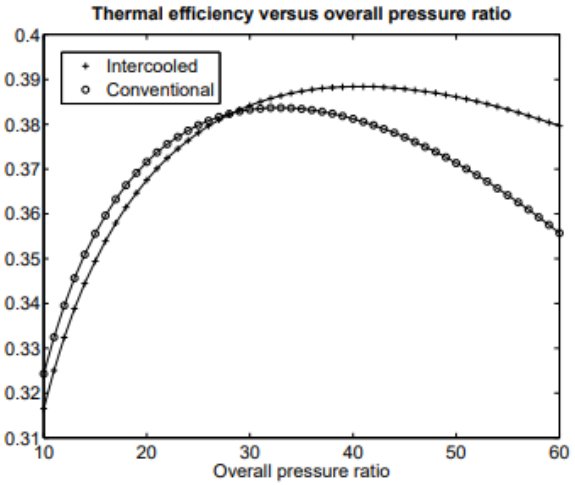

Figure 2.5: Typical thermal efficiency variations for an intercooled and a convention turbofan[23]

2.2.3. Intercooling in modern aero-engines

Gröndstedt et al. [9] investigated the performance of an intercooled turbofan engine in 2010. A fuel burn reduction of 4.3% was found, which was optimized to 5.5% using a multidisciplinary design optimization. This was mostly achieved by the IC allowing for higher OPR, which was previously limited by the combustor inlet temperature. The intercooled engine also had a higher specific thrust, which allowed the engine to be 163kg lighter.

Kyprianidis et al. [6] further elaborated on this design by adding a recuperated core. A recuperated core is where the airflow after the HPC is going through a heat exchanger that exchanges the heat between the air out of the HPC and the exhaust gasses after the LPT, as can be seen in figure 2.6. In this figure, the IC is the outward part of the engine where the bypass flow crosses the core flow. The recuperator is rearward, where the core exhaust gasses pass the core combustion inlet to exchange the heat. The benefits of having variable geometry and different combustion technologies were investigated.

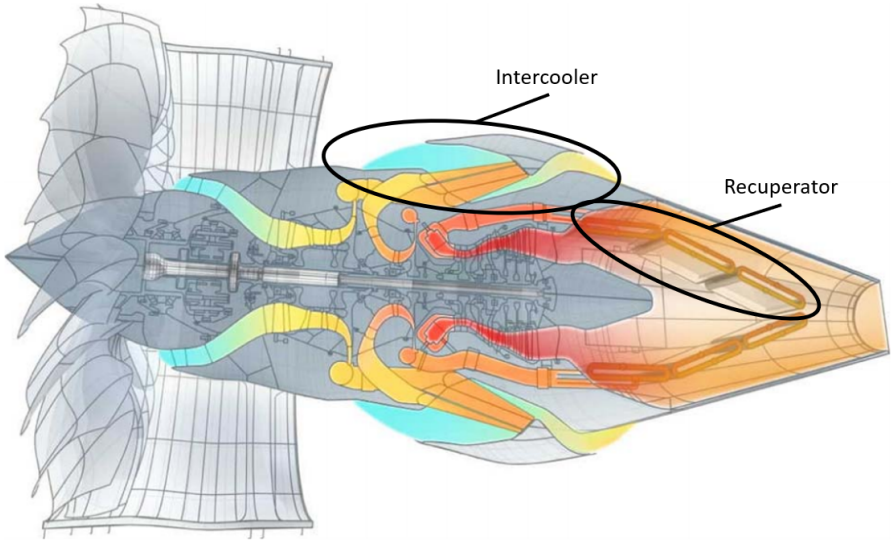

Figure 2.6: Intercooled Recuperated core turbofan engine. [6]

The design of the OPR for such an engine is no longer constrained by the HPC exit temperature as would typically be the case for a conventional engine but by the HPC blade height. The mission fuel reduction for this design was 3.2%, mainly due to the increase in thermal efficiency and the lower engine weight. The intercooled and recuperated engine is compared to conventional engine in table 2.1. This found design gave the T-S diagram seen in figure 2.7.

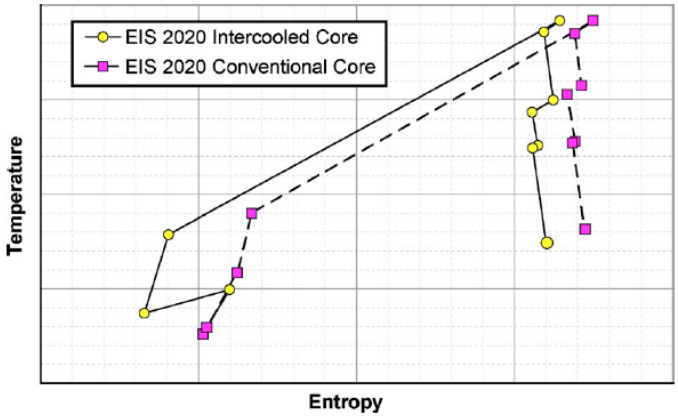

Figure 2.7: T-S diagram for intercooled core and conventional core at TOC. [6]

Table 2.1: Comparison of the parameters of an intercooled aero-engine with a conventional turbofan engine [6]

	Conventional core	IC
	EIS 2020	EIS 2020
MTOW (1000 kg)	206.5	202.6
OEW (1000 kg)	113.0	111.2
Engine dry weight	Ref.	−5.9%
LPT weight	Ref.	−27.1%
Core weight	Ref.	−32.5%
Added components weight (as % of engine dry weight)	-	7.7%
Block fuel weight	Ref.	−3.2%
Midcruise SFC	Ref.	−1.5%
Thermal efficiency	Ref.	+0.007
Propulsive efficiency	Ref.	+0.000

Having a variable IC nozzle could regulate the amount of cooling flow going into the IC influenced the pressure losses and effectiveness. Figure 2.8 shows that the net thrust can be increased by allowing more cooling mass flow through the external part of the IC. This increases the heat transfer that takes place but also increases the pressure losses. An optimum could be found, which increased the net thrust by 2%.

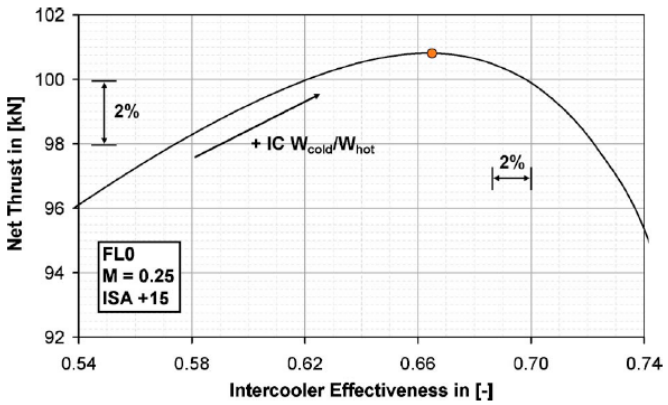

Figure 2.8: Optimized performance of a variable IC nozzle during take-off. [6]

A recuperated core with variable geometry in the LPT is then also investigated. The results of this variable LPT geometry can be seen in figure 2.9. This also gave a reduction in mission fuel.

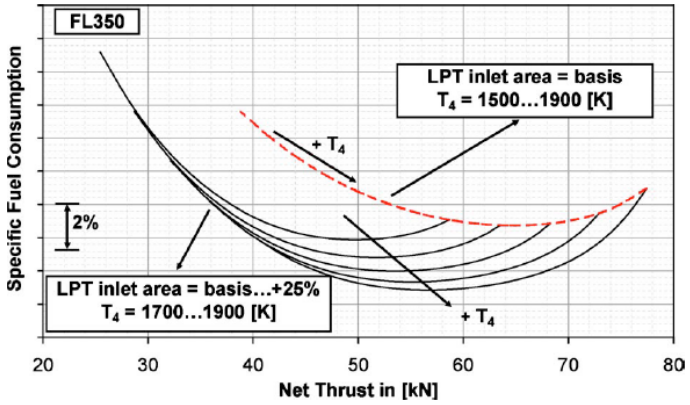

Figure 2.9: Effects of variable LPT geometry on recuperated aero-engine. [6]

The high OPR cycle gives new problems since there is a higher NO_X emission in this region. This follows the trend that higher OPR gives higher NO_X emissions, as seen in figure 2.10.

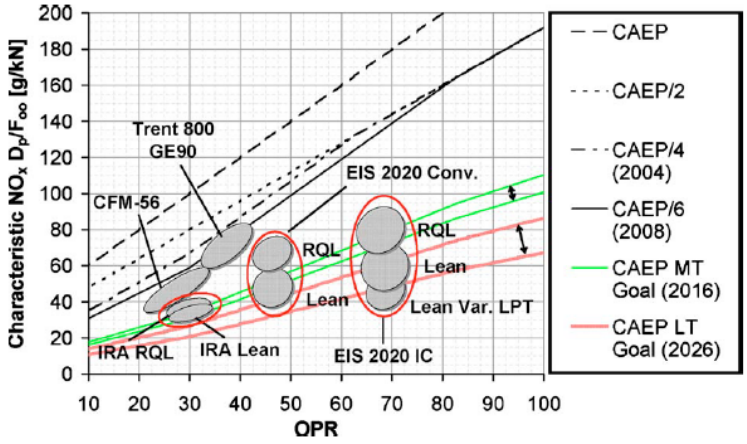

Figure 2.10: NO_X emissions for different existing and future aero-engines. [6]

Zhao et al. [10] investigated the effect of a two-pass cross-flow IC. A two-pass cross-flow IC had the advantage of low internal pressure losses, but it had relatively high external pressure losses. The author mentioned that the overall heat transfer was on the lower side, but it was enough to increase the OPR in cruise from 55 to 75. The cooler flow after the HPC resulted in less cooling flow mass needed. A variable nozzle was chosen that opened during take-off and had a smaller area in cruise. The achieved fuel burn reduction was 3.2% in comparison with a baseline conventional engine. A corresponding snowball factor gave a total net fuel burn reduction of 4.8%.

Kyprianidis et al. [7] decoupled the specific thrust optimization setting of the intercooled and conventional aero-engine since they might perform optimally at a different specific thrust. The installation of the IC was inboard of the engine between the LPC and the HPC; it featured a flow splitter and an auxiliary variable geometry nozzle. This was the same configuration as in [6]. However, now it allowed for a different specific thrust for both engines and thus a different propulsive efficiency. The found fuel reduction was lower. This was because there now was a minimum blade height requirement that set a limit on the intercooled core size and OPR. This smaller core was also a problem since this limited the size of the fan. A larger fan lowers the fan speed and increases the LPC shaft diameter. This would increase the HPC hub to tip ratio, which does not agree with a smaller core found from intercooling. The specific thrust for an intercooled core was higher. The intercooled engine had a higher thermal efficiency than the conventional engine. The propulsive efficiency of the intercooled engine was higher due to the higher ST. This counteracts the benefits of improving the core efficiency. A possible solution

to this problem might be to install a geared fan such that the minimum shaft constraints on the LPC are removed. The benefits however, were found highly dependent on pressure losses in the IC.

The optimization by Grondstedt et al. [9] was done on three aspects: mechanical design, an aircraft model, and an engine performance model. The data was verified using a CFD study on the IC. Since an IC allows for a temperature reduction in the HPC exit, a higher OPR can be achieved. The current trend of increasing the bypass ratio (BPR) and thus relatively smaller cores also helps to integrate ICs. The cooling flow was modelled according to Wilcock et al. [24] The IC was verified using a parametric CFD study and a comparison to empirical data. In the conventional engine, the OPR, BPR, and fan pressure ratio (FPR) were the fundamental optimization values. Including an IC added the pressure ratio split between the HPC and the LPC. The optimization found a temperature reduction of 67K delivered by the IC, the internal pressure loss was 3.2% and the external pressure loss was 5.4%. Inside the bypass flow, an IC mass flow ratio was found most optimal at 15.9 which means 15.9 parts of the bypass flow go around the IC and 1 part enters the cold side of the IC. Since no open literature was available regarding modeling the external part of the IC, a CFD study was included to validate the heat transfer and the pressure losses. For the internal part of the IC, this data was available. The design used an auxiliary exhaust nozzle since this gave better results than a mixed nozzle which was investigated by Xu et al. [25] To optimize for the full mission, the auxiliary nozzle area was chosen as the varying parameter. A variable HPT was also investigated but was discarded because of the high temperatures in said component.

The modelling by Kyprianidis et al. [6] was done for a variable geometry. In figure 2.11 the effects of the variable geometry are plotted in cruise condition. It is shown that a smaller effectiveness is better for the TSFC in cruise since it was reduced by 2%. This was achieved with a reduced nozzle area up to 40%. Designing such a nozzle will be challenging.

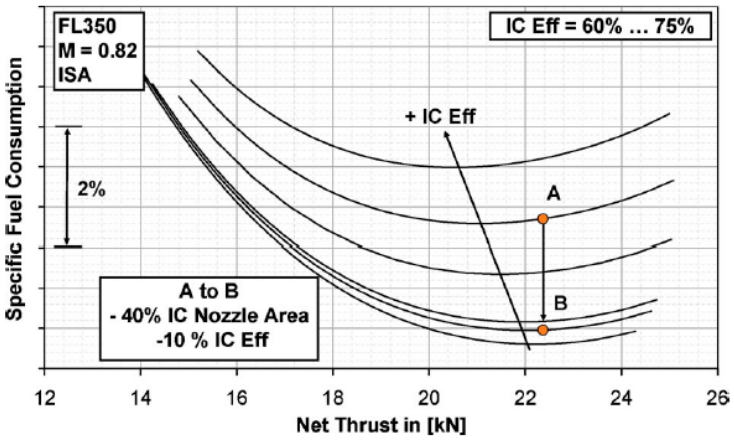

Figure 2.11: Optimized performance of a variable IC nozzle during cruise. [6]

Kyprianidis et al.[8] expanded upon this by incorporating a geared fan. It was found that reducing specific thrust increased propulsive efficiency but decreased thermal efficiency since there was less heat transfer in the IC. Increasing the BPR lowered the specific thrust but increased engine weight.

In figure 2.12, the specific thrust at TOC is always on the x-axis, and the efficiencies are given on the y-axis. The points of minimum TSFC and minimum fuel are not the same since an IC always had the disadvantage of an installation penalty. The bigger nacelle means more drag. The lowest TSFC was found for the lowest specific thrust, this aligned with the highest BPR.

The IC mass flow ratio was also varied, assuming a constant effectiveness. Low IC mass flow rates were found to be optimal. With a high IC mass flow ratio, large amount of air would go trough the cold side of the IC. This would increase the sizing of the IC and the sizing of the nacelle. This increases nacelle drag and pressure losses in the IC. The results can be seen in figure 2.13. Higher mass flow rates did lower the weight of the engine. The lowest TSFC again did not match the lowest mission fuel. An optimum was found between a lower TSFC, the weight reduction of the IC and the installation penalty.

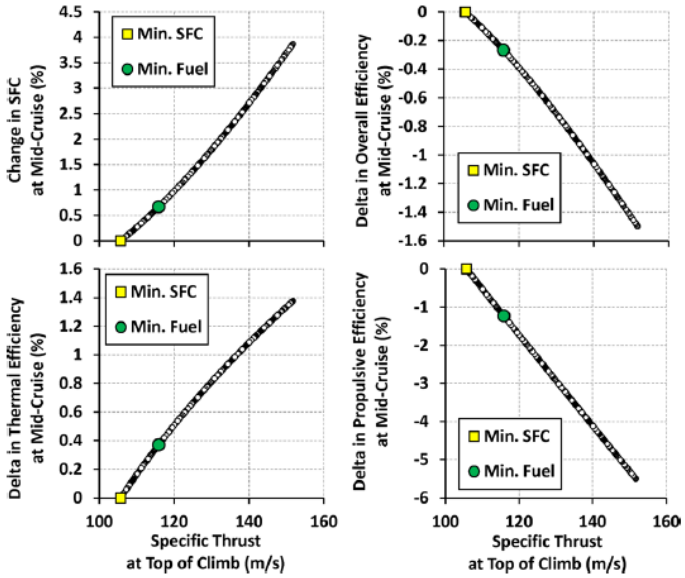

Figure 2.12: Specific thrust versus efficiency [8]

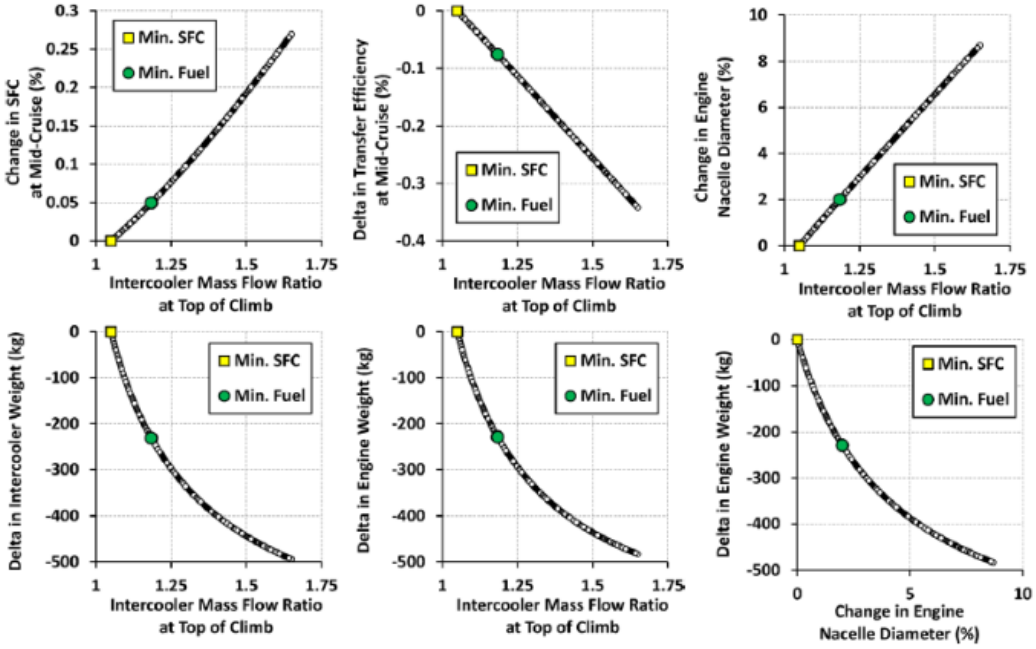

Figure 2.13: IC mass flow ratio versus efficiency [8]

The pressure ratio at which the IC was placed was found to be on the lower end. This would improve the core efficiency and lower the TSFC. The optimal IC pressure ratio for total mission fuel was higher since this meant a lower engine weight and a shorter engine. Results can be seen in figure 2.14. For a split on the higher end, the overall efficiency of the engine went down. This was because the propulsive and thermal efficiency also went down. However, the overall mission fuel was found at a slight non-optimal efficiency since again this had a positive result on the engine weight.

A higher OPR was optimal. This would increase the temperature in the inlet of the IC such that more heat could be extracted. It also increases the thermal efficiency of the core. Results can be seen in figure 2.15.

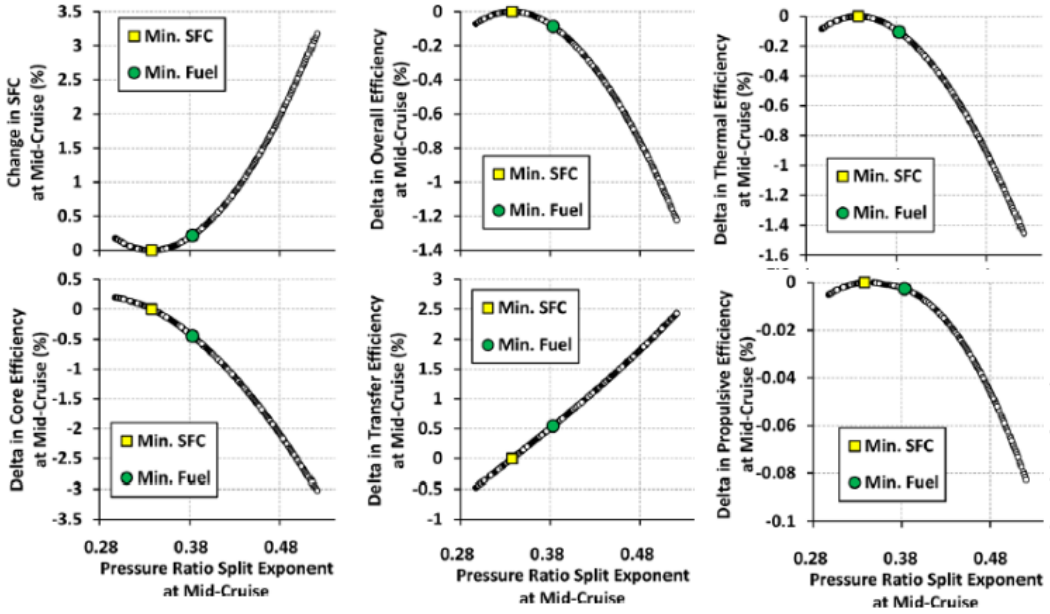

Figure 2.14: Pressure ratio split versus efficiency [8]

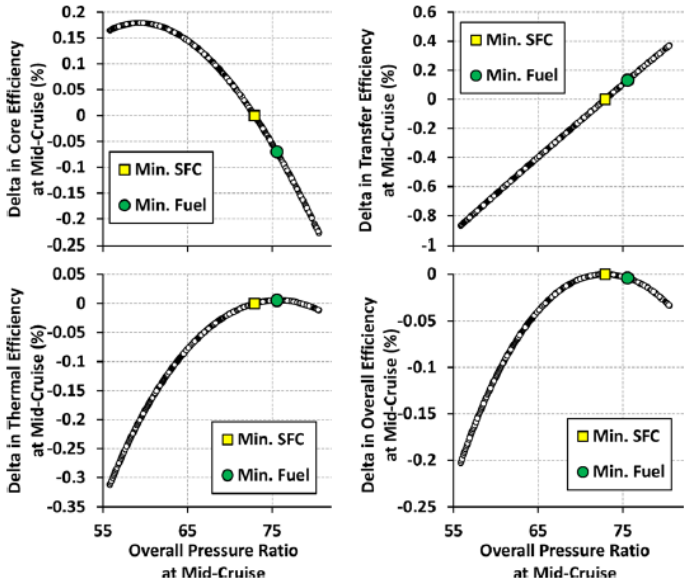

Figure 2.15: OPR vs efficiency [8]

The IC effectiveness was also varied. A higher effectiveness resulted in more pressure losses on both sides. Results can be seen in figure 2.16. It was found that optimizing the TSFC of an engine was not necessarily the same as optimizing mission fuel.

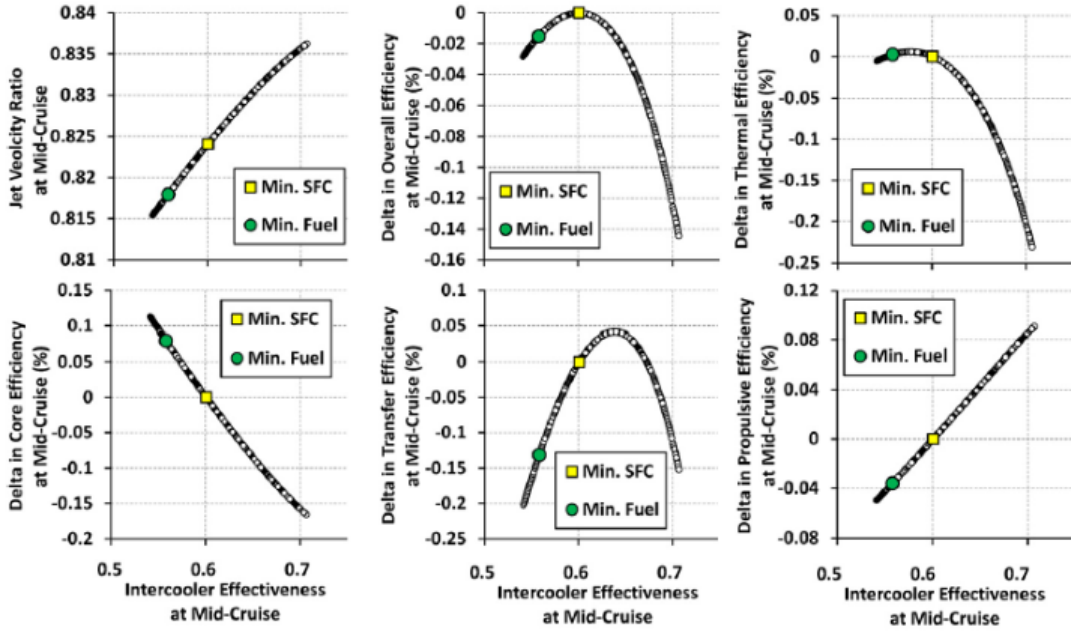

Figure 2.16: IC effectiveness versus efficiency [8]

2.2.4. IC conclusion

While it was shown that an IC has a significant effect on the TSFC, the effect on the overall used mission fuel was lower. The important aspects to account for were always the sizing of the core. Since it became smaller, limiting factors became the HPC blade height and the sizing of the fan. The sizing of the fan itself could be resolved with a geared fan. The rise in thermal efficiency counters the pressure losses going with the IC. Another significant part of the reduction in TSFC was the engine weight since the HP section could be designed for less work. The lower temperatures in the combustion chamber could help to reduce the NO_X emissions, and the fuel reduction helps the reduction in CO_2. Adding an IC to an aero-engine has the disadvantage of an increased installation penalty and a more complex design since a variable geometry was needed to ensure that the advantages during take-off and top of the climb were not lost in cruise.

2.3. inter-turbine burning

inter-turbine burning is the idea that fuel is not only added in the combustion chamber before the turbine stages, but also afterwards. This can be in a secondary combustion chamber between the generally defined HPT and LPT. It can also be at multiple locations or even a continuous burning across the whole turbine is possible.

2.3.1. inter-turbine burning in aero-engines

The effects of burning fuel in the turbine has been investigated by Liu et al. [26] for a turbojet and a turbofan engine in 2001. They investigated the base engine versus multiple configurations of inter-turbine burning, namely 1 extra combustion stage, 2 extra combustion stages and continuous burning. The focus was the effect that inter-turbine burning had on the specific thrust and on the TSFC. The result of the turbofan engines versus the compressor ratio is seen in figure 2.17. The TSFC for the ITB was slightly higher than the conventional engine but the ST was a lot higher. It was also noted that inter-turbine burning become more efficient at higher BPRs as seen in figure 2.18.

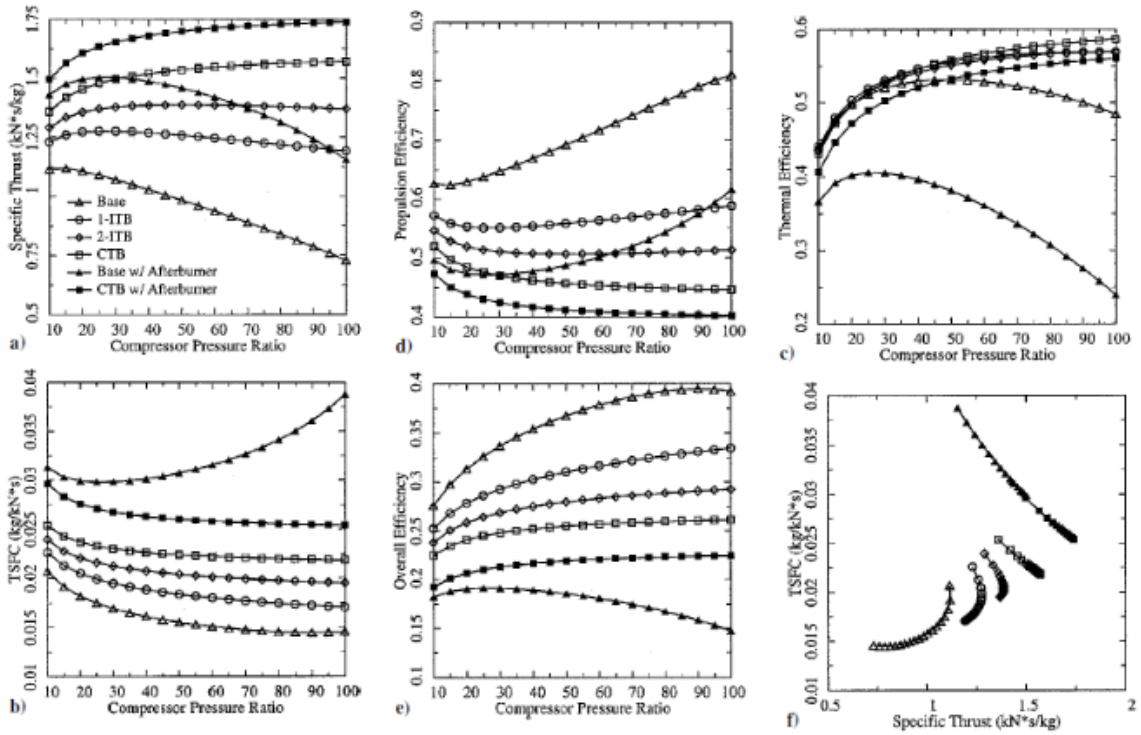

Figure 2.17: Performances of turbofan engines vs compressor pressure ratio at a Mach number of 0.87, TIT of 1500K reheat temperature of 1900K, BPR of 5 and a FPR of 1.65. [26]

It also becomes more efficient at higher FPRs as seen in figure 2.19. It is still visible that the base engine has a better TSFC. This stops however at larger BPRs since the base engine does not have the power to drive such a big fan in this case.

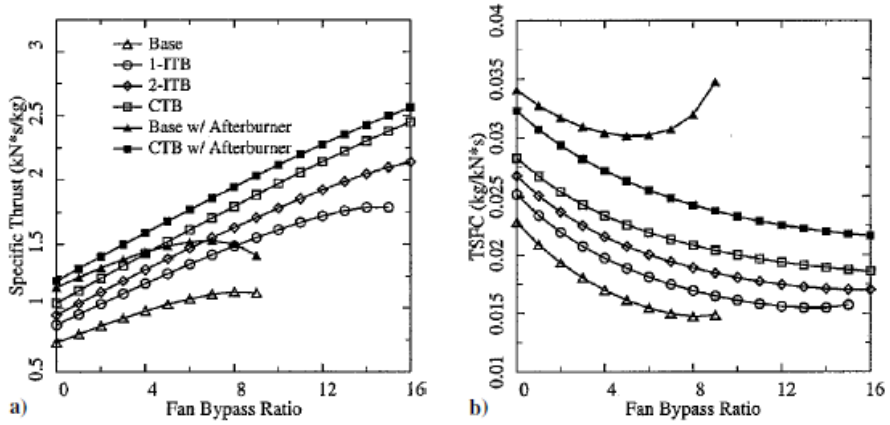

Figure 2.18: Effects of BPR on performance[26]

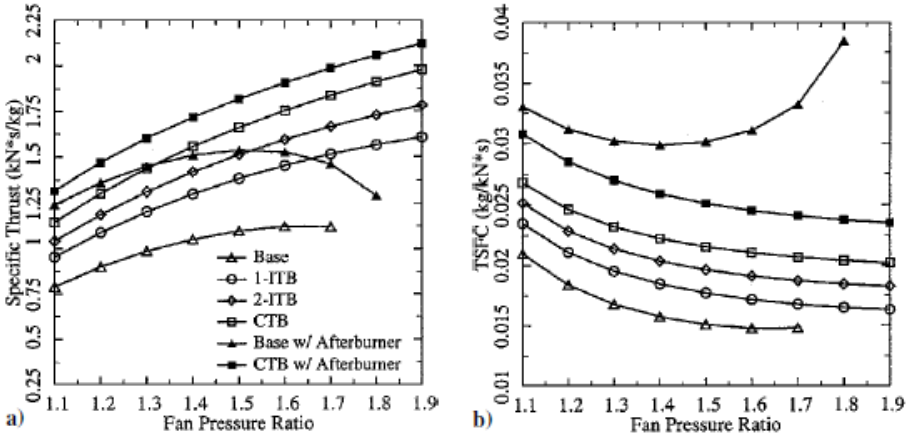

Figure 2.19: Effects of FPR on performance.[26]

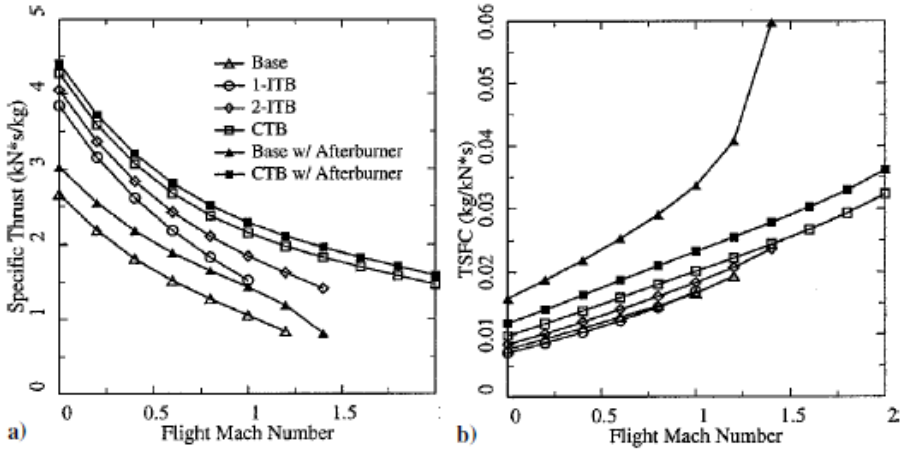

Figure 2.20: Performance comparison of ITB versus baseline engine. [26]

All the comparisons were made with the same design conditions. This already showed some advantage for the inter-turbine burning. This can be improved since the inter-turbine engine operates optimal at different conditions than the base engine. It favours a higher pressure ratio, a higher BPR

and higher fan pressure. No optimization was done to compare these 2 engines, the only change was an increase in OPR from 30 to 60, a BPR from 8 to 12 and a FPR from 1.65 to 1.72. The results are shown in 2.20.

It shows that the inter-turbine engine is better at higher compression ratios and higher BPRs. It also shows higher specific thrust which might mean the engine is better suited for off design performances.

This research was expanded by Chen et al. [27] They concluded that inter-turbine burning was most beneficial for land based applications since the cooling requirements for air based operations were too high. The research then focused on the land-based application.

A study on inter-turbine burning was also performed by Liew et al. [28], to focus on the off-design performance on a jet engine. This was a study based on a supersonic jet engine and the results found that inter-turbine burning had a positive impact on the fuel economy of the mission, both in the subsonic as in the supersonic region. Better results were found in the supersonic region.

2.3.2. inter-turbine burning in modern aero-engines

The aero-engine for commercial purposes was investigated by Yin et al. [18] It was investigated on the premise of reducing bleed air and reducing NO_X emissions in aero-engines. It followed from the trend that aero-engines are having an increased OPR and an increased TIT. This however increases the NO_X emissions. Two T-S diagrams showing 2 different approaches to inter-turbine burning are seen in figure 2.21.

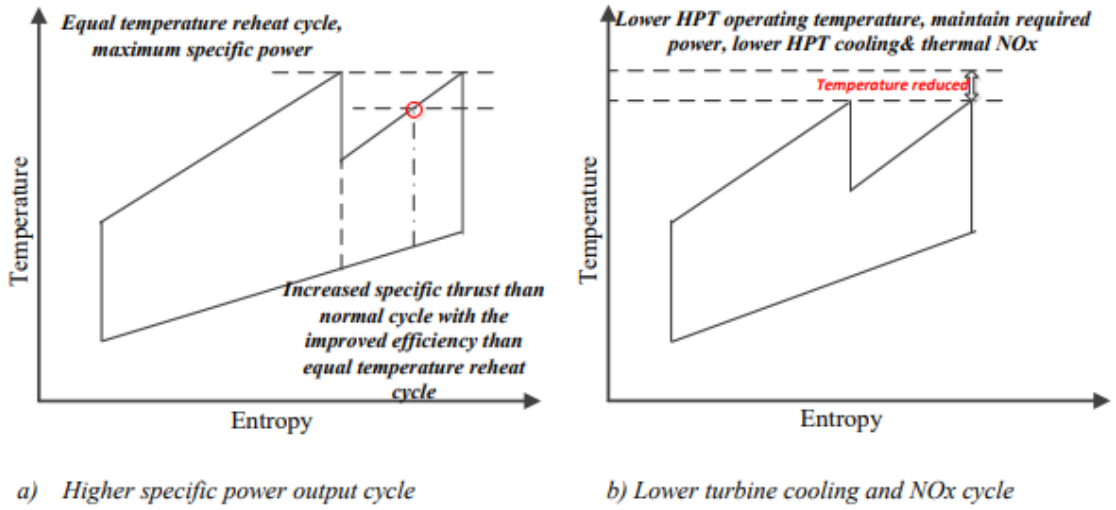

Figure 2.21: T-S diagram of inter-turbine burning aero-engine for 2 different applications. [18]

The effect of the ITB was investigated to see the effects on the NO_X emissions and on the cooling requirements in both the HPT and the LPT. An in-house cooling model was used for the latter. The engine performance was modelled in GSP. The NO_X emissions were estimated using an in-house prediction tool based on Cantera's reactor networks. [29] The geometry of the combustor is based on the same methodology as Shakariyants et al. [30]. Since kerosene is a complex fuel, the Aachen surrogate was used which has been developed at TU Aachen by Honnet et al. [31]. The results showed that an ITB reduces HPT cooling requirements since the TIT temperature is lower. The thermal efficiency of the turbine is lower since part of the heat is added at a less efficient pressure in the cycle. The turbine efficiency improvement counteracts this since there is less cooling air required. The NO_X emissions are up to 40% lower compared to a conventional engine setup as can be seen in figure 2.22.

It is expected that the ITB can increase the engine OPR while keeping the NO_X emissions low. This inter-turbine architecture is then analysed using an off-design analysis by Yin et al. [5] The difference with the on-design analysis is that now different settings were analysed to provide a better understanding in the performance during a complete flight mission. A visualization of the engine configuration can be seen in figure 2.23

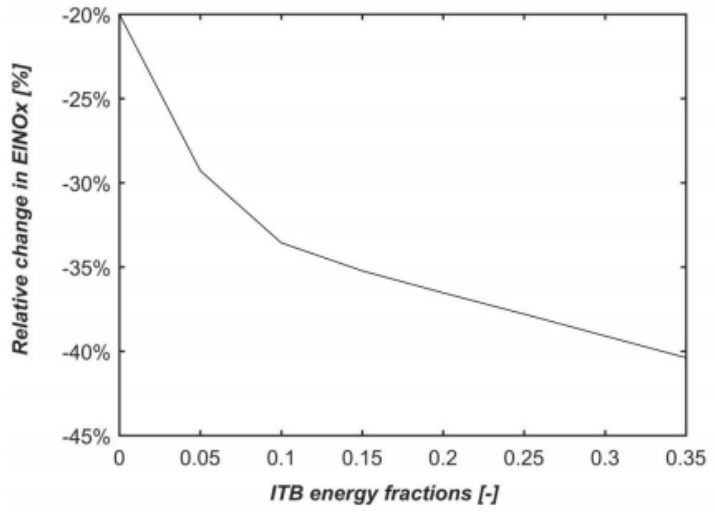

Figure 2.22: Reduction in NO_X emissions for varying ITB energy fractions [18]

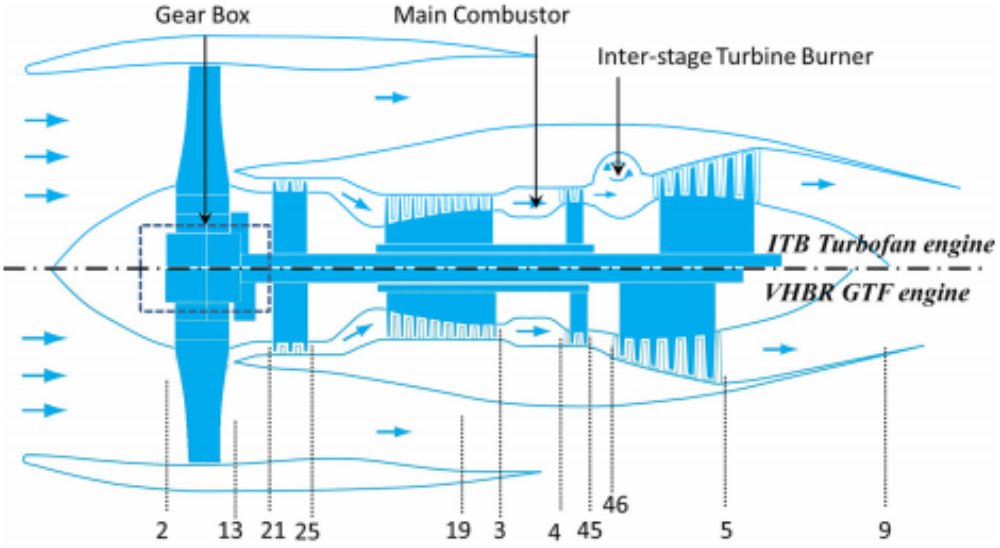

Figure 2.23: ITB turbofan comparison with Very High BPR Geared Turbofan engine. [5]

The model was again made in GSP where the same setup was used. The first optimization resulted in maximizing the BPR, the FPR, and the OPR for both the conventional and inter-turbine burning aero-engine. The TIT of the inter-burner engine was however 300K lower while the TSFC was 1.5% higher. When the off-design criteria are considered however, it followed that the baseline engine was not feasible for the hot-day take-off condition since the flat rating temperature was not high enough. The baseline engine had to be iterated to allow for a flat rating temperature of 25°C. This resulted in a bigger engine core and thus a smaller BPR and a smaller OPR which followed in an increase of the TSFC of 4.9% over the baseline engine. This made the inter-turbine burning engine more fuel efficient. The ITB gives a second combustion chamber which gave an extra degree of freedom which allowed the engine for a higher maximum thrust and thus has better off-design performance characteristics. The reduction in TSFC found is visualized in figure 2.24.

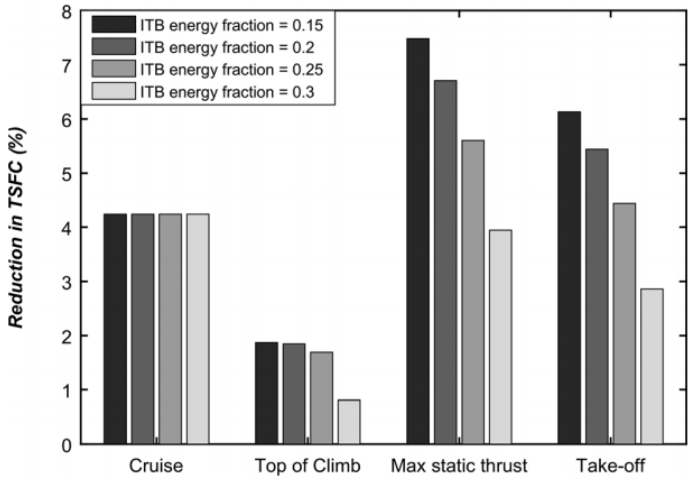

Figure 2.24: TSFC reduction of ITB compared to revised. [5]

The ITB also came out with a better maintenance and lifetime since the maximum temperature in the cycle is lower. The only disadvantage found was the need for a variable bleed valve and a variable stator vane since the surge margin for the LPC was reduced.

2.3.3. ITB conclusion

At first glance, it seemed like an ITB was only usable to give more thrust in the engine or to reduce the NO_X of the engine. When being further investigated it was found that the extra degree of freedom allowed the core to be designed smaller which resulted in a higher BPR, higher OPR and thus also a decrease in TSFC and CO_2. Besides this, also the maximum temperature in the engine became smaller which means a longer lifetime.

2.4. Turbine blade cooling

The effects of turbine blade cooling are known to be advantageous for cycle efficiency of a gas turbine. Improving the TIT has been the most important factor to increase the gas turbine efficiency. It has been so successful that not a lot of people challenge the principle. This is the best way to continue going forward to increase the efficiency of a gas turbine. It has however been shown that the efficiency gains at very high temperature may be countered by the extra losses that accompanied the larger cooling flow rates. It has already been shown that for fixed pressure ratios, changing the TIT gave maximum cycle efficiencies found temperatures close to those found in currently used jet engines.[32] One cooling model will be further explained. This is a model by Jonsson et al.[33]. It is a model that offers flexibility in usage with concise number of parameters. For turbine efficiency loss due to cooling, a linear reduction in polytropic efficiency dependent on the cooling ratio is further explained.

2.4.1. Cooling model for mass flow

There are multiple ways to model the cooling flow. Since only the mass flow is needed for the engine performance model, only correlations will be reviewed.

One publication by Jonsson et al. [33], models the cooling flow based on correlations. The cooling fluid mass flow rate was calculated following equation 2.2. The equation consists of the cooling mass flow ($\dot{m}_c$), the gas mass flow before cooling ($\dot{m}_g$), the corresponding heat capacities at constant pressure $c_{p,c}$ and $c_{p,g}$, the gas temperature at the inlet ($T_{g,cmb\ \text{exit}}$) and the coolant temperature at the inlet ($T_{c,\text{cmpr exit}}$), the blade temperature (T_b), and 2 parameters defining the efficiency of the convective cooling (b) and the film cooling (s).

$$\frac{\dot{m}_c c_{p,c}}{\dot{m}_g c_{p,g}} = b\left(\frac{T_{g,cmb\ \text{exit}} - T_b}{T_b - T_{c,\text{cmpr exit}}}\right)^s \tag{2.2}$$

The specific heat capacities $c_{p,g}$ and $c_{p,c}$ are calculated following equation 2.3. The variables used are the enthalpy of the gas/coolant at the inlet temperature($h_{g,\text{cmb exit}}$,$h_{c,\text{cmpr exit}}$) and at the blade temperature($h_{b,g}$,$h_{b,c}$). The corresponding temperatures use the same subscripts.

$$c_{p,c} = \frac{h_{b,c} - h_{c,\text{cmpr exit}}}{T_b - T_{c,\text{cmpr exit}}}; c_{p,g} = \frac{h_{g,\text{cmb exit}} - h_{b,g}}{T_{g,\text{cmb exit}} - T_b} \tag{2.3}$$

Since the mixing of the cooling flow influences the work in the turbine, a momentum balance is introduced which gives a loss in pressure which is converted to a reduction in turbine polytropic efficiency by using equations 2.4 and 2.5

$$\frac{\Delta p}{p_{tbn,\text{inlet}}} = -\frac{\dot{m}_c}{\dot{m}_g}\kappa_g M_g^2 \zeta = -\frac{\dot{m}_c}{\dot{m}_g} K; \Delta p < 0 \tag{2.4}$$

$$\eta_{p,\text{c tbn}} = \eta_{p,\text{uc tbn}} - \Delta\eta; \Delta\eta > 0 \tag{2.5}$$

In which the mixing loss factor ζ, heat capacity ratio κ_g, and the Mach number are set values based on the layout of the cooling flow and parameter K. The average values are found in [33]. These correlations might be incorrect however since they are validated based on F-class land based turbines which deliver a 10 times higher quantity of power then current aero-engines.

2.4.2. Cooling losses

Research on the cooling losses has been done by Horlock et al. [32]. It is known that implementing cooling in an aero-engine has pressure losses because the cooling air and the hot gas need to mix. In the nozzle guide vanes, the first mixing of cooling flow occurs. It is assumed that this section completely mixes before the mixture goes through the first rotor. A semi-empirical relation linking the hot gas mass flow and the cooling flow is found to define the polytropic efficiency loss($\Delta\eta_{\text{stage}}$) divided by the original polytropic efficiency (η_{stage}) is given in equation 2.6 where the cooling fraction (ξ) is defined as inlet cooling mass divided by inlet gas mass. This relation had a good comparison to experimental data. The temperature of the cooling air is however not included in the constants in this relation thus this will not be further expanded upon.

$$\Delta\eta_{\text{stage}} / \eta_{\text{stage}} = -0.125\xi \tag{2.6}$$

2.5. Emissions

The emissions in an aero-engine are one of the driving factors for developing new technologies. The main contributors are carbon dioxide (CO_2), Nitrogen oxides (NO_X), carbon monoxide (CO), and unburned hydrocarbon UHC. The production of these gasses should be limited going forward to improve the environmental impact of aviation.

The reactants producing the emissions in an engine are air existing mainly of nitrogen and oxygen ,and fuel exisiting mainly of hydrocarbons and some sulfur. [34]

$$Air = N_2 + O_2 \tag{2.7}$$

$$Fuel = C_n H_m + S \tag{2.8}$$

The products in the combustion chamber are mainly the following: The previously mentioned 4, accompanied by water (H_2O), dioxygen (O_2), Soot,and sulfur oxides (SO_X)[34]

$$\mathrm{CO_2} + \mathrm{H_2O} + \mathrm{N_2} + \mathrm{O_2} + NO_X + UHC + CO + C_{\mathrm{soot}} + SO_x \tag{2.9}$$

The 2 emissions that will be looked further upon here are the NO_X emissions and the CO_2 emissions.

2.5.1. Carbon dioxide

Carbon dioxide is a green house gas which naturally occurs from a complete combustion. It is influential to global warming. It has a linear relation to the fuel burned and is thus linearly related to the TSFC. Meaning a lower TSFC will give less CO_2.[35]

2.5.2. Nitrogen Oxides

Most of the nitrogen oxides that are emitted from an engine are in the form of NO_2. A general approach however is to combine all oxides of nitrogen under the term NO_X. There are multiple mechanisms that produces these gasses, namely thermal NO_X, nitrous oxide mechanism, prompt NO_X and fuel NO_X

The production is dependent on the flame temperature, the combustor inlet temperature is also influential to the production of NO_X since this influences the flame temperature. The pressure of the combustion chamber is very important to the formation of NO_X. Higher pressure ratios generally lead to a better TSFC but worse performance considering NO_X. Maughan et al. found that $NO_x \propto P^n$ where P is the pressure inside the combustion chamber and n ranges from 0.5 to 0.8. This n is dependent on the temperature of the combustion. For lower temperatures, n is lower. At low temperatures, prompt NO_X is the main contributor to NO_X production and at high temperature, thermal NO_X is the primary contributor to emissions. [36]

Most of the NO_X is formed by thermal NO_X at higher temperatures. It is an endothermic reaction that has an exponential growth above a flame temperature of 1800K. It is also found that, since the production is dependent on the flame temperature, the combustor inlet temperature is also influential to the production of NO_X. [35]

Generally, correlations are used to estimate the amount of NO_X produced. The variables influencing the correlations are often the mean residence time, the chemical reaction rates and mixing rates. One such correlation is given by Lefebvre et al. [37]. This correlation gives excellent results based on existing engines from 1955 and 1970 with pressure ratios of 13.5 and 26. It is only correct for spray combustors, for LPP combustors and can be used if the maximum temperature T_pz (primary zone) is changed by T_st (stoichiometric flame temperature). It is also dependent on the combustion volume and the combustor airflow rate. Not on the pressure.

$$\mathrm{NO_x} = 9 \times 10^{-8} P^{1.25} \mathrm{V_c} \exp\left(0.01 T_{\mathrm{st}}\right) / \dot{m}_{\mathrm{A}} T_{\mathrm{pz}} [\mathrm{g/kg}] \text{ fuel} \tag{2.10}$$

Another correlation is found by Odgers and Kretschmer [38]. This correlation also uses a flame temperature and the pressure but also accounts for the residence time and gives this to be between 0.8 and 1 ms. dependent if airblast atomizers or pressure atomizers are used.

$$\mathrm{NO}_x = 29 \exp - (21,670/T_{\mathrm{c}})\, P^{0.66} \times [1 - \exp -(250\tau)][\mathrm{g/kg\ fuel}] \tag{2.11}$$

One more correlation presented by Lewis [39], states that the formation of NO_X is only dependent on the pressure and the temperature after the combustion. This is because the residence time is not

used as the important time but the relaxation time of the nitrogen molecules. This is the same in all air based combustion systems. Since this correlation is based on aero-engines and in general the residence times of aero-engines are roughly all the same, this equation gave good results. This is not the case when it is used for different gas turbines since then the residence time is different.

$$\mathrm{NO_x} = 3.32 \times 10^{-6} \exp\left(0.008 T_c\right) P^{0.5} [\mathrm{ppmv}] \tag{2.12}$$

2.5.3. CO

Carbon monoxide is a gas that forms mostly in fuel-rich environments since there is then a lack of oxygen to complete the burning towards CO_2. In a lean environment, there is however also CO present. This comes due to the dissociation of CO_2. Highest CO emission values are found for low power setting with low combustion temperatures.

2.5.4. UHC

UHC emissions are the unburned hydrocarbons which is a toxic pollutant. They generally form with incomplete burning of the fuel or when the fuel gets burned and other carbon bonds of lower molecular weight form. It is difficult to model the total formation of UHC but in general it follows the same trend as for CO.

2.5.5. Soot

Soot is described as particles formed during the quenching of gases at the outer edge of flames of organic vapours, consisting predominantly of carbon, with lesser amounts of oxygen and hydrogen present as carboxyl and phenolic groups and exhibiting an imperfect graphitic structure. They are particles with a diameter larger than 6nm and are a known carcinogen. [40] Good mixing of the fuel and the air is important to minimize the formation of Soot. But since no immediate influence of pressure or temperature is present, it is assumed that adding an IC will not influence Soot and for an ITB, the mixing needs to be adequate but that is also not in 0D gas path.

2.6. Exergy

The exergy of a system is the maximum amount of work that can be obtained by bringing it to equilibrium with the environment through a reversible transformation. The capacity to generate work is a combined property of the thermodynamic state of the system and the environment. Since a system can always produce more work if it is brought towards a vacuum. This is called the useful work potential which is described by Gibbs as: the maximum amount of mechanical energy that one can obtain from a system, the difference being inevitably lost to the environment due to the implications of the second law of thermodynamics. This second law states that the total entropy of a system can never decrease and can only remain constant when all processes are reversible. The exergy of a system is always the same, the only things that can change the exergy is the state of the system and the conditions of the environment.[41]

2.6.1. Closed System

In a closed system, the thermodynamic exergy (E) is defined by the internal energy of the system (U), the entropy (S), and the pressure (P). It is defined according to equation 2.13.

$$E = W_{net} = (U_i - U_{i_0}) + P_0(V - V_0) - T_0(S - S_0) \tag{2.13}$$

The potential energy (PE), the kinetic energy (KE) and the chemical energy (QE) of the system must be added to this to give the total value of the exergy in the system as seen in equation 2.14.

$$E = (U_i - U_{i_0}) + P_0(V - V_0) - T_0(S - S_0) + PE + KE + QE \tag{2.14}$$

The chemical energy here is the maximum amount of work when its elements are chemically transformed to match the elements of the environment.

2.6.2. Open System

In an open system, a control volume (V) is added to the equation as can be seen in equation 2.15.

$$E = (U_i - U_{i_0}) + P_0(V - V_0) - T_0(S - S_0) + (P - P_0)V \tag{2.15}$$

In equation 2.15, some components cancel each other out, and other components are the definition of enthalpy (H) which is the internal energy and the product of the pressure and the volume. Thus, the exergy is now defined by equation 2.16.

$$E = (H - H_0) - T_0(S - S_0) + PE + KE + QE \tag{2.16}$$

2.6.3. Efficiency

Exergetic efficiency is then the ratio of the first law efficiency of the thermal cycle to the efficiency of the reversible cycle in the same system. It is a way of defining a system that is rather new but can be used to find where a lot of hidden losses happen in a system.

2.7. Software

This section will describe the software used to to support the research. To simulate gas turbines, a simulation application is Gas Turbine Simulation Program (GSP). This is a component based modelling system where a variation of gas turbine components can be included in the simulation. The optimization of the engine will be done by using MATLAB build in optimization toolbox.

2.7.1. Gas Turbine Simulation Program

GSP is a program that calculated gas turbine performance characteristics from a design point. It is suitable for off-design analysis. Both steady-state (off-design) and transient simulation can be performed. This is done numerically by defining the engine system states and then solving this for conservation of mass, energy and momentum. The individual components comprising the engine are selected in a menu and then accordingly connected. All these components have some driving design parameters. These variables vary from design parameters to component maps which define the characteristics of the component in steady-state or transient simulation. This allows for adapting models such that extra components can be added and a new engine model is easily created. This model is solved using a generic solver. The solver creates a set of non-linear equation which are sent to a solver. The components in GSP are modelled using the component maps which represent their multi-dimensional non-linear characteristics. The standard model in GSP is 0-dimensional, which means only averaged gas properties at the inlet and exit of each component are used to model the component. This 0-dimensional assumption creates only small inaccuracies. The model also solves processes which span multiple components. such as shaft power, secondary air flows (cooling), sensor and fuel pumps.[42]

Different components add different sets of states and equations. The object oriented solving offer a lot of freedom to simulate different architectures. The different types of components are visible in figure 2.25.

The system is modelled according to the model architecture seen in figure2.26. First the system is initialized. Following the design point is calculated. from this point, the steady states are calculated. This is all done using Newton-Raphson method to find the roots of the state equations. The transient simulation will not be used in this research.

2.7.2. Optimization

The optimization will be done in MATLAB using the optimization toolbox and an API connection to GSP. The used optimizing algorithm is sequential quadratic programming (sqp). This is an iterative method for a constraint non-linear problem. It solves a series of subproblems which each linearise the non-linear problem. This is extensively described by Nocedal et all. [43]

The constraints tolerance used is 1e-6. The tolerance for the first-order optimality is also 1e-6.

2.7.3. Example usage

The models that will be used in this research will all have the design condition as cruise. This requires cruise conditions such as altitude and cruise speed. The design point will have the design parameters changed such that the design thrust is as required and the TSFC is minimized. The steady-state model is then solved at an off-design condition with a specified thrust. This gives corresponding parameters. These parameters are now used to do a boundary check. For example the TIT might not agree with the cooling air temperature and mass flow. This means that the cooling flow fraction in the design point has to be changed. This is done until the equality and inequality constraints are satisfied with respect to minimizing the TSFC during cruise flight.

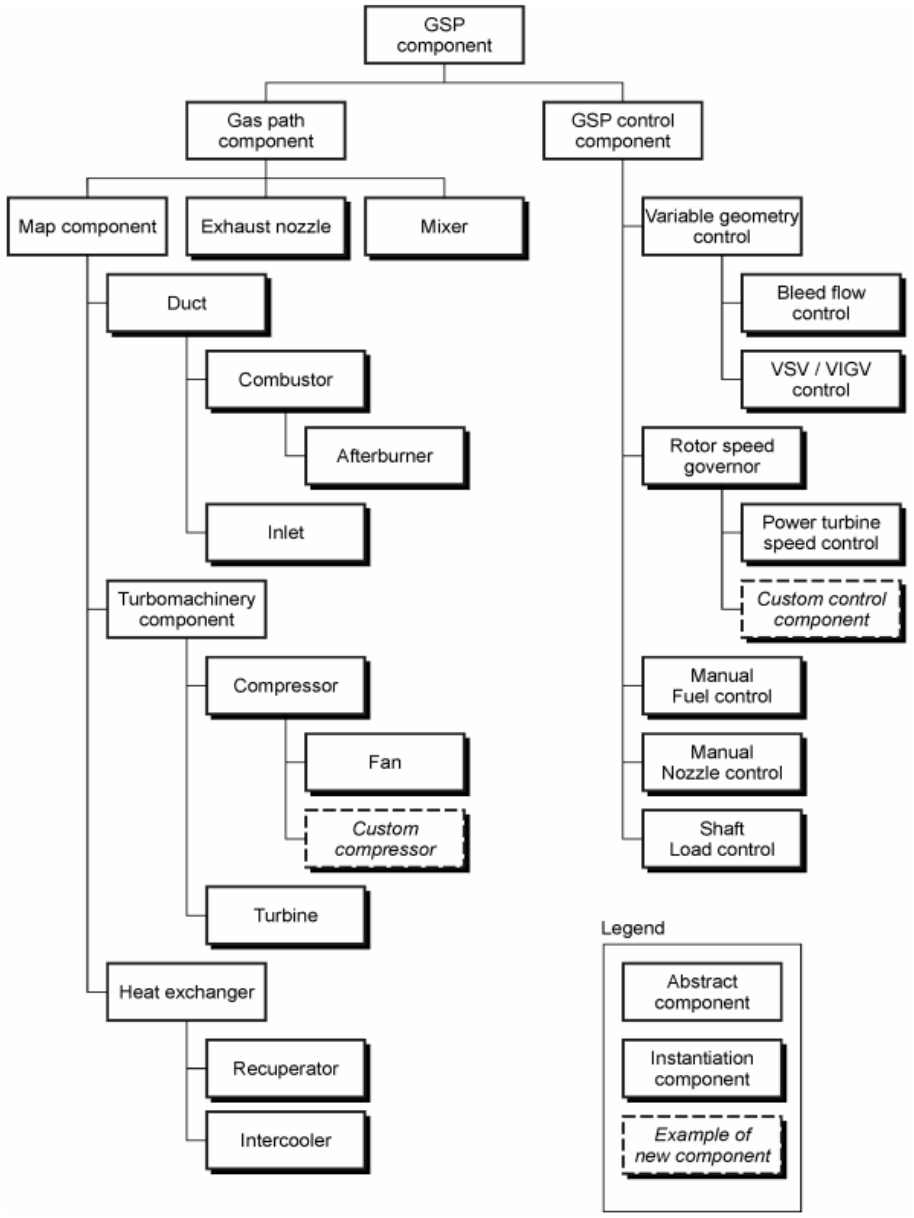

Figure 2.25: Component inheritance architecture. [42]

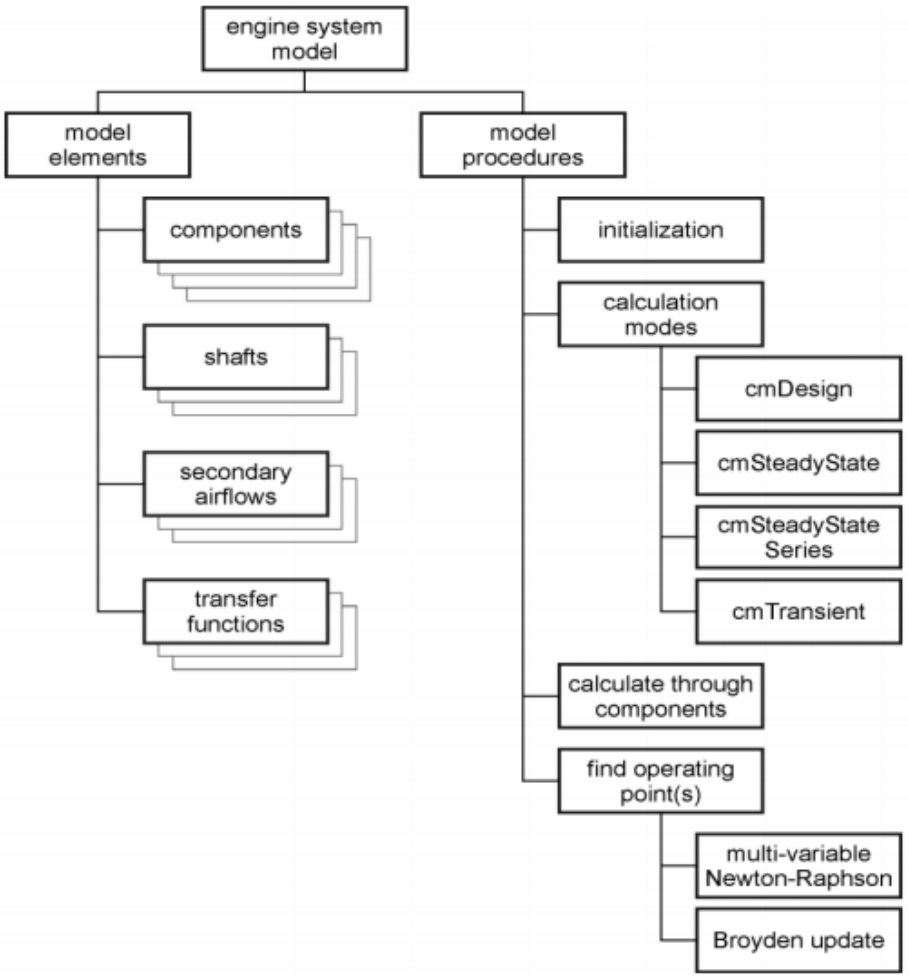

Figure 2.26: Component inheritance architecture. [42]

3

Methodology

A lower TIT is advantageous to the NO_X emissions and a higher OPR is better for the TSFC. This is conflicting since a higher OPR means a higher combustion inlet temperature and this increases the TIT. Introducing new engine architectures can overcome this paradox. The engine architectures that will be discussed here are the ITB and the IC. An ITB helps with lowering the TIT. An IC helps with achieving a higher pressure ratio with lower work. An extra advantage is that an IC provides cooling air at a lower temperature such that less cooling air is needed. To investigate the pros and cons of introducing ITB and intercooling, four engines will be simulated to see if they are beneficial towards the TSFC and the NO_X emissions. These are a conventional engine (baseline), an engine using only an IC (IC-engine), an engine using only an ITB(ITB-engine), and an engine using both an IC and an ITB(IC-ITB-engine). All these engines will be subjected to an on- and off- design performance. The on-design (cruise flight) will be used to model the TSFC during cruise and the off-design simulation will verify if the engine can accomplish the performance requirements at these conditions, and if not, adapt the engine design until the off-design requirements are satisfied. The thrust requirements at different operating conditions are listed in table 3.1.

Table 3.1: Design conditions at various operating conditions

Operating points	Altitude	Mach Number	Thrust Required	Flat rating temperature
Top of climb	11000m	0.85	60kN	ISA+15K
Cruise	11000m	0.85	47kN	/
Hot-day Take-off	0	0	300kN	ISA+25K

3.1. ITB model

An ITB is an element in a gas turbine where fuel is added after the HPT and before the LPT. With the idea of lowering the energy density in the main combustion chamber and thus also lowering the HPT inlet temperature. This might allow for higher pressure ratios since the maximum HPT inlet temperature at hot day take-off stays the same but some of the fuel is added to the ITB which will lower this temperature, lower cooling requirements and a higher specific power of the core. The ITB will be modelled using a constant pressure loss of 3% in the secondary combustion chamber and an energy split fraction chosen (equation 3.1) to be the same as chosen by Yin et al. [18]. This equation consists of the energy going into the ITB defined by the product of the lower heating value (LHV) of the fuel and the mass flow of this fuel (m_f) divided by the total energy going into the system.

$$ITB_f = \frac{LHV_2 \cdot m_{f2}}{LHV_1 \cdot m_{f1} + LHV_2 \cdot m_{f2}} \tag{3.1}$$

In equation 3.1, subscript 1 stands for the main combustion chamber and subscript 2 stands for the ITB. LHV is the lower heating value of the fuel and the m_f stands for the mass of that fuel in kg/s. The used

fuel in both combustion chambers will be Jet-A with an LHV of 42.8 MJ/kg. The ITB energy fraction is how the research will define how much of the total fuel is going to the ITB.

The used fuel Jet-A/A1, JP-8, Avtur for which the following fuel specifications hold. A H/C ratio of 1.9167, an LHV of 42.8 MJ/kg, a Cp at the fuel reference point of 288.15K of 2093 J/kg K.

The constant pressure loss due to mixing and combustion inside the ITB will be a constant 3% for all operating conditions. The combustion efficiency is set to 99.5% which is slightly lower than for the main combustion chamber which operates at 99.7%.

3.2. IC model

An IC in an aero-engine is a heat exchanger placed between the core flow and the bypass flow. In this case, the hot side is cooled between the LPC and the HPC. The cold side of the IC is a fraction of the bypass flow. A passive system will be used in this analysis which means that during all flight phases, the IC will be used.

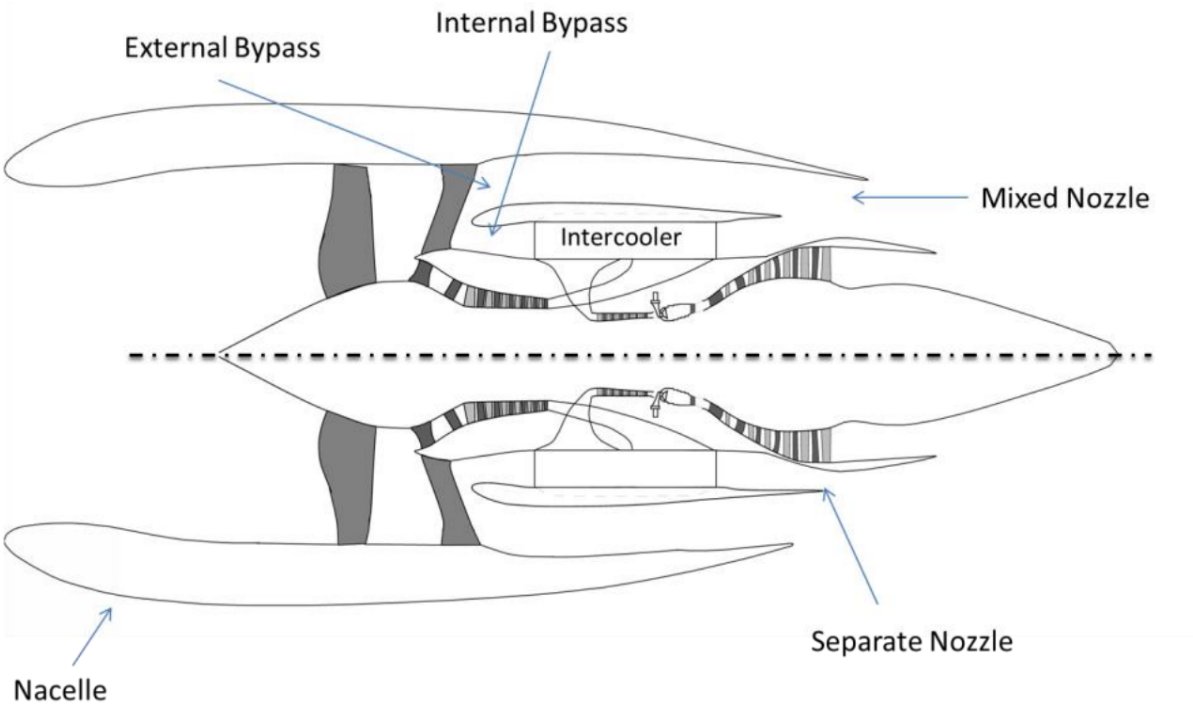

Figure 3.1: Two pass cross-flow heat exchanger [10].

An IC type suited for this purpose is a cross-flow heat exchanger seen in figure 3.1. The hot side will be inside pipes and the cold side will go around these pipes. A split ratio indicates how much of the bypass flow will go through the cross-flow heat exchanger and how much will go around the heat exchanger. An effectiveness of 0.5 is used as the baseline for the IC-engine. This means that 50% of the maximum heat transfer happens. The pressure losses on the cold and hot side are set to 3% for an effectiveness of 0.5 at cruise. This is in line with the existing literature. [6, 7, 7, 9, 10, 25, 44]

The heat exchanger cross-flow is also validated using the method of Zukauskas et al. [45]. and the inside of the tubes is validated by using Dittus-Boelter which is a formula to find the Nusselt number in turbulent pipe flow as shown in equation A.1. This methodology can be seen in Appendix A.

Reynolds analogy is further used to change the pressure losses if the engine goes in other operating modes, such as the sea level static (SLS) ISA+25 take-off condition. Here the heat transfer is different than the heat transfer during cruise (effectiveness is kept constant). The difference in heat transfer has a linear effect on the pressure loss based on Reynolds analogy.

3.3. Cooling model

The following section derives the cooling model. It consists of 2 subsections. One about the cooling mass and one about the polytropic losses in the turbine due to cooling.

3.3.1. Cooling mass required

The used cooling model is based on the work done by Jonsson et al. [33]. The equation giving the model is equation 3.2 and is explained in section 3.

$$\frac{m_c}{m_g} = b\frac{cp_g}{cp_c}\left(\frac{T_g - T_b}{T_b - T_c}\right)^s \tag{3.2}$$

Firstly, the variable parameters of this model are chosen such that they give the same cooling flow requirements as presented by Yin et al.[46] based on the inlet temperatures of the components and varying the parameters b and s. The effect of changing the parameters can be seen in the following figures. In figure 3.2, a b of 0.07 and an s varying between 1 and 2 is shown with a constant coolant temperature of 1040K (which approximates an OPR of 66). In figure 3.3, the effect of a colder flow is shown. It is noticeable that even small differences in a high temperature environment have a high impact on the cooling flow needed.

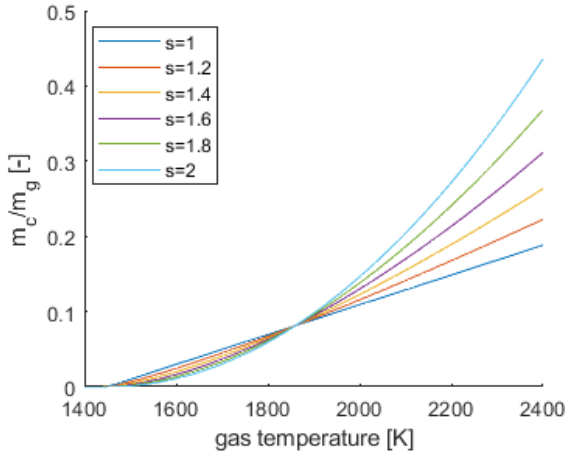

Figure 3.2: m_c over m_g for a constant b of 0.07 and a varying s between 1 and 2

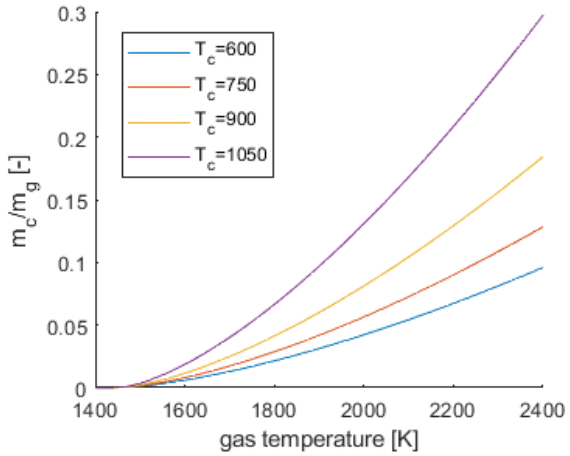

Figure 3.3: m_c over m_g for a constant b of 0.1, a constant s of 1.5 and a varying cooling flow temperature between 600 and 1050K.

Then the parameters b and s are chosen by applying weighted least squares onto the model and data given by [46]. The results of this are a constant s of 1.5 and a b of 0.105 for the stators and a b of 0.07 for the rotors. The fitted data is seen in figure 3.4

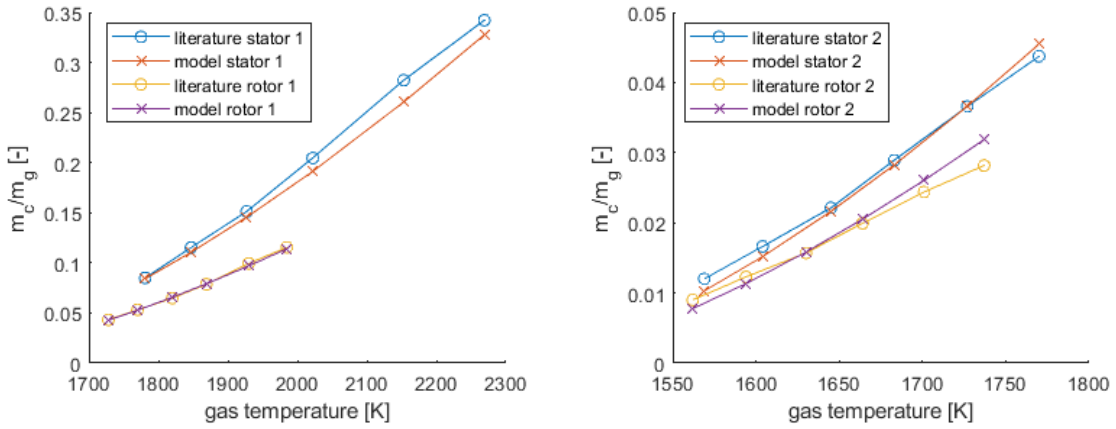

(a) Stator and rotor 1 of HPT.

(b) stator and rotor 2 of HPT.

Figure 3.4: Cooling required for rotor and stator of HPT. Parameters b and s to 0.1 and 1.5 for stators and 0.66 and 1.5 for rotors to match literature [46]

The convective parameter b will be scaled down 25% to account for the cooling improvements possible in future engines. This results in a used b of 0.75 for stators and a b of 0.495 for rotors. The film cooling parameter s is held constant at 1.5.

3.3.2. Efficiency loss factor of turbine cooling

The loss factor is well described by Horlock et al.[32] and by Wilcock et al. [24]. It is a parameter defining how the polytropic turbine efficiencies change when cooling air is added in the turbine. It is defined as cooling mass over gas path mass. Two different loss factors will be used in the report. In the parameter analysis the presented result is for a loss factor of 0.125 to minimize the effect of this parameter and look at the effect the parameters have more clearly. In the on- and off-design sections, the cooling loss factor will be 0.5. This means that the polytropic efficiency will decrease with 0.5% for each added % of cooling mass. This value aligns with previous literature [5]. The loss factor is also investigated. The results are that a high loss factor is most detrimental for cycles that have high TIT and LPT inlet temperature. This is seen in Appendix B

3.4. Engine performance model

The engine performance will be modelled using the Gas Turbine Simulation Program (GSP). All the components will be modelled in the program. The bleed control will be given based on the cooling model just as the pressure loss and temperature change in the IC and the pressure loss and fuel flow in the ITB. Each engine will be optimised to TSFC at cruise with a cruise thrust of 47kN. The minimum thrust at TOC is 60kN and the minimum thrust at SLS ISA+15 will be 300kN. All the components in the model can be seen in figure 3.5. And the stations given are listed in table 3.2. The bleed controls(components 2-4, 6-8) define how much air is bled from the HPC to the stators and rotors that need cooling. Component 5 is used as a thrust control required for off-design performance. The used efficiencies are seen in table 3.3. The bounds for the on/off-design optimization are seen in table 3.4.

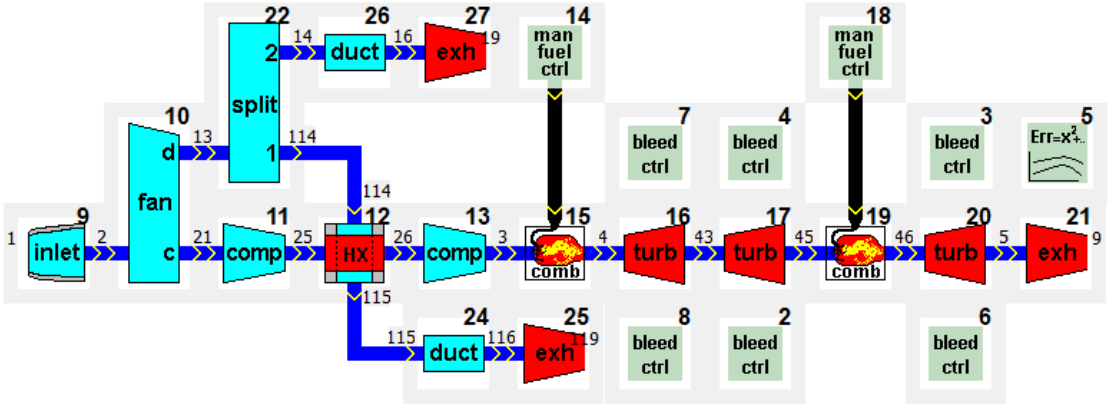

Figure 3.5: Overview of components in intercooled ITB-engine.

Table 3.2: Station numbers used in IC-ITB design in GSP. For the cases were only IC or ITB is used, there is no change in the skipped component.

Core	In	Out	Bypass	In	Out	IC cold side	In	Out
Ambient	0	1						
Inlet	1	2						
Fan core side	2	21	Fan duct side	2	13			
LPC	21	25	Flow Splitter Bypass	13	14	Flow Splitter IC	13	114
IC hot side	25	26	Bypass duct	14	16	IC cold side	114	115
HPC	26	3	Bypass exhaust	16	19	IC duct	115	116
Combustion chamber	3	4				IC exhaust	116	119
HPT stage 1	4	43						
HPT stage 2	43	45						
ITB	45	46						
LPT	46	5						
Core exhaust	5	9						

Table 3.3: Component efficiencies of engine model. Efficiency of HPT and LPT is lower if cooling is required.

Component	Parameter	Notation	Value
Fan	Polytropic efficiency	η_{FAN} [%]	93
LPC	Polytropic efficiency	η_{LPC} [%]	93
HPC	Polytropic efficiency	η_{HPC} [%]	91
Main combustion chamber	Combustion efficiency	η_{comb} [%]	99.7
	Pressure ratio	π_{comb} [-]	0.95
HPT	Uncooled polytropic efficiency	η_{HPT} [%]	93
ITB	Combustion efficiency	η_{ITB} [%]	99.5
	Pressure ratio	$\pi_{ITB}[-]$	0.97
LPT	Uncooled polytropic efficiency	η_{LPT} [%]	92.5
Bypass duct	Relative pressure loss	$\Delta P_{duct}/P_{in}$ [%]	2
LP shaft	Mechanical efficiency	η_{mLPT} [%]	99.5
HP shaft	Mechanical efficiency	η_{mHPT} [%]	99.5

Table 3.4: Engine constraints of on/off-design optimization.

Parameter	constraints
On-Design	
$m_{1_{cruise}}[kg/s]$	517
BPR [-]	5-15
FPR [-]	1.1-2
LPC PR [-]	2-5
HPC PR [-]	4-20
$TT4_{cruise}$ [K]	≤ 1900
OPR_{cruise}	≤ 70
Off-Design	
OPR_{total}	≤ 75
N1 [%]	≤ 106
N2 [%]	≤ 119

The engine model is verified using the known data of the GE90. The available data of GE90 is used as input The inlet air mass flow is varied to match the thrust requirement. Accordingly, the other cycle parameters are iterated. The found parameters at 100% thrust are summarized in table 3.5.

Table 3.5: Results of optimization with known constants of GE90 [47]

Parameter	Known	Model	Δ%
m_1	-	1374kg/s	
BPR	8.33	8.33	
fan PR	-	1.58	
LPC PR	-	1.1	
HPC PR	23	23	
TT4	-	1725K	
m_c/m_{25}	-	0.0917	
w_f Thrust 100% 430kN	3.515	3.515	+0%
w_f Thrust 85% 365kN	2.844	2.876	-1.2%
w_f Thrust 30% 129kN	0.917	1.002	+8.5%
w_f Thrust 7% 30.1kN	0.304	0.296	-2.7%

It is optimised to have the same fuel flow at 100% thrust and then varies the inlet air mass flow, the fan PR, the LPC PR and the TIT to find the given thrust holding in respect the OPR at take-off. The cooling flow is dependent on the temperatures in the turbine and the cooling model. The results for the 30% thrust are 8.5% higher but for the 85% and the 0%, the results are quite good with a difference of -1.23% and -2.7%. The cooling flow of 9.17 % corresponds to the HPC bleed given in the EASA certificate data sheet of 9%. [48]. The model gives good fuel results for the 100% and 85% thrust cases.

3.5. Emissions model

The CO_2 are linear to the TSFC in aero-engines and therefore no model will be used to estimate the CO_2. It follows the TSFC [35]. For the NO_X modelling, multiple correlations are available. one such correlation is from Lewis et al. [39] This correlation rates the NO_X emissions based on the temperature and pressure after combustion. It is shown in equation 3.3. The emission index for NO_X ($EINO_x$) is calculated from the TIT (T_{T4}) and the turbine inlet pressure (P_{T4}). It does not account for temperature rise in the combustion chamber.

$$EINO_x = 2.77 \cdot 10^{-7} \cdot \exp(0.008 T_{T4}) \cdot P_{T4}^{0.5} [gNO_x/kgfuel] \tag{3.3}$$

Equation 3.4 splits this by using the compressor exit temperature (P_{T3}) and the FAR. It also includes a pressure loss component (ΔP) in the equation. 3.5 and divide it by 194. This is a large discrepancy in the dependence on the TIT. It is based upon low NO_X LDI combustion.[49] One problem with this correlation is the fact that it requires a pressure loss value in the combustion chamber. This value is estimated in the current research to be 0.05 for the main combustion and 0.03 for the ITB. This assumed pressure loss is for all engines the same and therefor has no influence on the end result.

$$EINO_x = 1.359 \cdot exp(T_{T3}/194) FAR^{1.69} P_{T3}^{0.595} (\Delta P/P_{T3})^{-0.565} [gNO_x/kgfuel] \tag{3.4}$$

Another way to calculate the NO_X is by using the NO_X severity index (S_{NO_x}) by NASA [50]. It is given by equation 3.5. It is noticeable that the exponent used with the temperature is the same as with equation 3.4. The pressure has a different exponent and they have the water/air ratio (w) which includes the effect of the ambient humidity. The severity parameter then must be multiplied dependent on the combustion method. The variation in the severity parameter is now standardized and independent of which combustion technology used. The severity parameter can be multiplied by a number which gives the estimated NO_X emission index based on figure 3.6. For current turbofan engines, the multiplication factor is 32. This can be reduced by using different combustors. This will not be looked upon and only the severity factor will be used. Conventionally used engines now have a severity factor of 1 at take-off conditions when T3=810K and P3=27bar. The severity can be reduced by using different combustion technologies, different combustion ways (ITB) and by changing the inlet conditions (IC). The relative humidity will be kept constant at 0%, which is the values seen in figure 3.6.

$$S_{NO_x} = \left(\frac{P_{T3}}{2965}\right)^{0.4} exp\left(\frac{T_{T3} - 826}{194} + \frac{6.29 - 100w}{53.2}\right) [gNO_x/kgfuel] \tag{3.5}$$

Equation 3.4 will be adapted to a severity factor since equation 3.5 has no FAR or TT4 included. The pressure loss component is removed since this is combustion depended and assumed constant. This forms equation 3.6. For the new scaling, it was assumed that all conventional engines had a FAR 0.03 (equivalence ratio of 0.45).

$$EINO_x = 1.043 \cdot exp(T_{T3}/194) FAR^{1.69} P_{T3}^{0.595} [gNO_x/kgfuel] \tag{3.6}$$

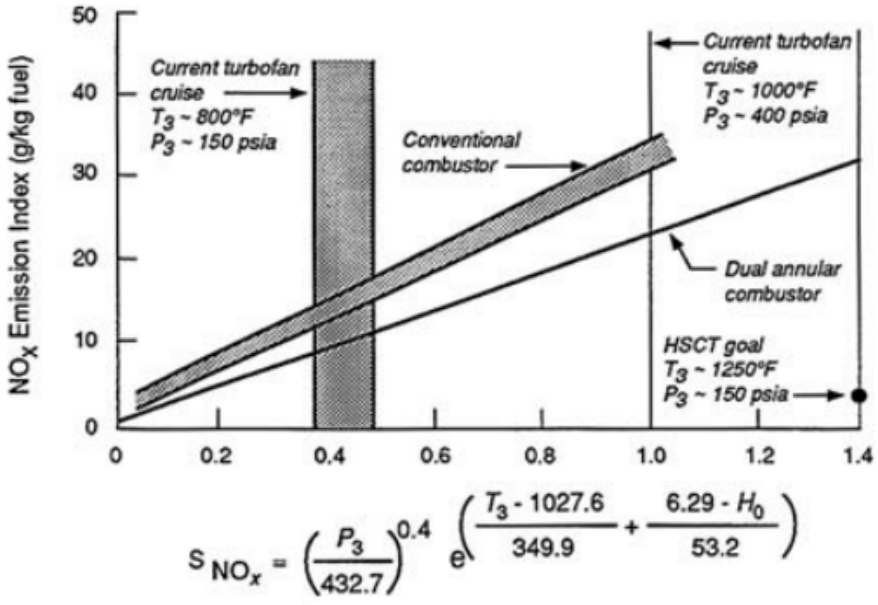

Figure 3.6: NO_X emissions versus severity index for current and future engines.(T and P in non SI units)[50]

The scale of the figure is changed compared to the original one in figure 3.6. The new correlation

gives lower $EISNO_x$ results for older low pressure cycles and approximates newer cycles good. The results based upon existing cycles is seen in table 3.6. The results show the difference between the NO_X severity factor by equation 3.5 and the results from the adapted severity factor based on equation 3.6. This shows that the new method has good correlation with the old method while it includes a FAR and is thus more suited to novel cycles.

Table 3.6: Results on $EISNO_X$ for given parameters and the difference with the new approximation.

	1 (graph)	2 (graph)	3 (LEAP)	4 (LEAP)	4[5]
TT3 [K]	700	811	830	730	1050
PT3 [K]	10.34	27.6	33.7	11.8	66
$EISNO_X$	0.38	1	1.2	0.47	4.9
$EISNO_X$ new	0.28	0.87	1.1	0.37	5.0

For the ITB, the Sullivan's correlation is used.[51] This approximates the NO_X emissions for reheated engine cycles based on the fuel flow split, the exit temperatures of the combustion chambers and the stoichiometric fuel-to-air ratio (FAR_s). It is seen in equation 3.7. NO_X is the newly calculated emission value. NO_{X0} is the NO_X emission if all the fuel were added into the main combustion chamber. The equation further uses a fuel split ratio (y) seen in equation 3.8, the vitiated air mass ratio (α) seen in equation 3.9. Subscripts 1 and 2 signify the combustion chambers. $\Delta TIT = TIT_{LPT} - TIT_{HPT}$, b=1.5 and c=250K.

$$\frac{NO_X}{NO_{X0}} = y^b + (1-y)^b exp\left(\frac{\Delta TIT}{c} - 8.1\alpha\right) \tag{3.7}$$

$$y = \frac{FAR_1}{FAR_1 + FAR_2} \tag{3.8}$$

$$\alpha = \frac{FAR(1 + FAR_s)}{FAR_s - FAR} \tag{3.9}$$

3.6. Exergy

Exergy, or the maximum available work in a state different from a dead (ambient) state will be used to identify the losses in the system. It will be used to compare the component performance in the different configurations. This method allows to quantify what benefits are present in each architecture from a fuel economy viewpoint. The methodology used will closely follow the methodology used by Clarke and Horlock [52]. It combines the first law of thermodynamics, conservation of energy with the second law of thermodynamics, entropy cannot decrease and will only stay constant for a reversible process. Each component can now be seen individually where it changes the state and thus the available work and it also changes the entropy if the process is irreversible.

To derive the equations, first, a steady flow regime with no kinetic energy is assumed. This is seen in figure 3.7. This figure shows as inlet the inlet mass flow times the specific enthalpy of the inlet flow. The outputs are the output mass flow times the specific enthalpy of the output flow and shaft power and heat going out of the system. The equation that follows from figure 3.7 is equation 3.10. The mass flows ($\dot{m}_i$) multiplied by the specific enthalpy (h_i) going in the system are on the left side and on the right side are the mass flows ($\dot{m}_i$) multiplied by the specific enthalpy (h_i) going out the system and the shaft power (P_S) and the rate of heat flow (q_i).

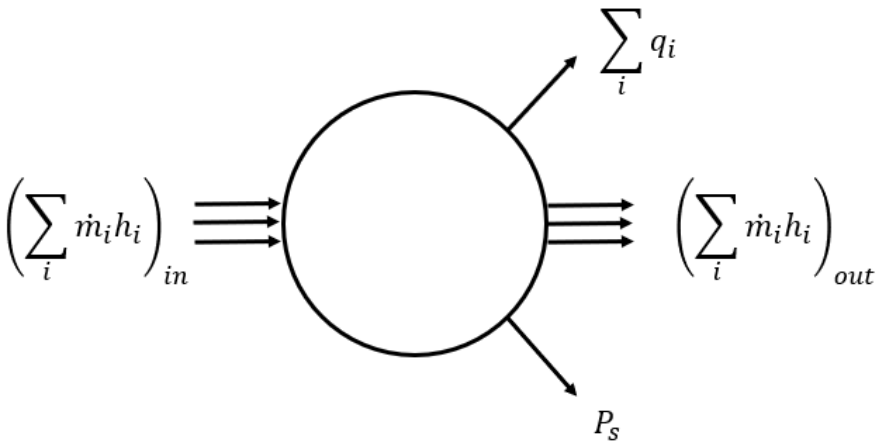

Figure 3.7: Exergy balance for a system without kinetic energy.

$$\left(\sum_i \dot{m}_i h_i\right)_{\text{IN}} = P_{\text{s}} + \left(\sum_i q_i\right) + \left(\sum_i \dot{m}_i h_i\right)_{\text{out}} \tag{3.10}$$

The maximum amount of work that can now be extracted from this system is found by combining the first and second law in equation 3.11. b in this equation is defined as $h - T_\infty s$ and is known as the steady flow availability.

$$\left(\sum_i \dot{m}_i b_i\right)_{\text{in}} \geqslant P_{\text{s}} + \left(\sum_i q_i \frac{T_i - T_\infty}{T_i}\right) + \left(\sum_i \dot{m}_i b_i\right)_{\text{out}} \tag{3.11}$$

Enthalpy and steady flow availability can be changed with the total property if there is kinetic energy in the system. The forces inside the system do not provide an energy component since the control surface is static.

There are multiple velocity datums possible in an engine, relative to the engine or relative to the ground. Relative to the engine will be noted as V and relative to the earth will be noted as C. The speed of the engine is seen as U and thus C=U-V.

Including the kinetic energy in equations 3.10 and 3.11 gives equations 3.12 and 3.13.

$$\left(\sum_i \dot{m}_i h_{0i}\right)_{\text{IN}} = P_{\text{s}} + \left(\sum_i q_i\right) + \left(\sum_i \dot{m}_i h_{0i}\right)_{\text{out}} \tag{3.12}$$

$$\left(\sum_i \dot{m}_i b_{0i}\right)_{\text{in}} \geqslant P_{\text{s}} + \left(\sum_i q_i^{T_i} \frac{-T_\infty}{T_i}\right) + \left(\sum_i \dot{m}_i b_{0i}\right)_{\text{out}} \tag{3.13}$$

If the system relative to the earth is used, an extra component P_T is needed which includes the translation power. This includes the change in speed between all the flows and the pressure differences that pass through the control surface. Total enthalpy and availability will now be inclusive of the kinetic energy of the speed as seen in figure 3.8. This shows an adapted version of figure 3.7 including a speed of the system (U) and thus a thrust power component (P_T) as output.

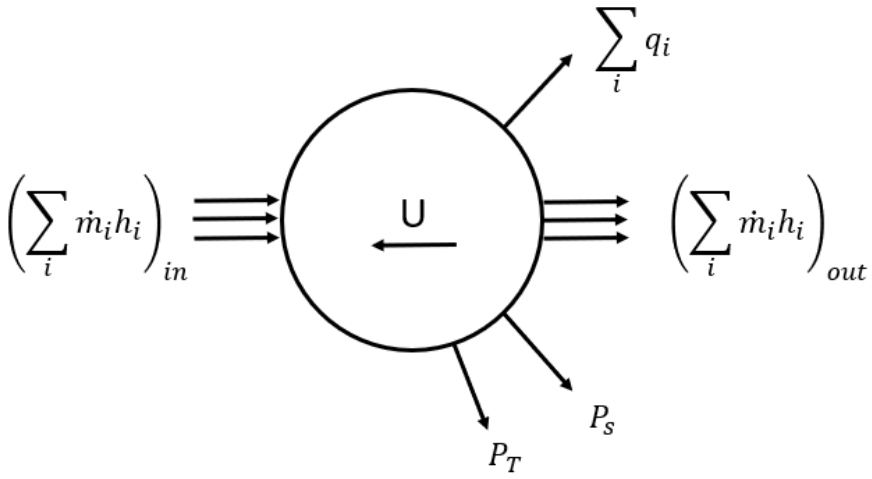

Figure 3.8: Exergy balance for system with kinetic energy.

This changes equations 3.12 and 3.13 to equations 3.14 and 3.15, which were derived by Clarke and Horlock for a single constituent flow [52]. The inequality is now the lost power in the component. The thrust power can be defined in terms of the speed of the system as seen in equation 3.16. Which derives to equation 3.17 when C is replaced by U-V.

$$\left(\sum_i \dot{m}_i h_{0i}\right)_{\text{in}} = P_{\text{S}} + P_{\text{T}} + \left(\sum_i q_i\right) + \left(\sum_i \dot{m}_i h_{0i}\right)_{\text{out}} \tag{3.14}$$

$$\left(\sum_i \dot{m}_i b_{0i}\right)_{\text{in}} \geqslant P_{\text{S}} + P_{\text{T}} + \left(\sum_i q_i^{T_i} \frac{-T_\infty}{T_i}\right) + \left(\sum_i \dot{m}_i b_{0i}\right)_{\text{out}} \tag{3.15}$$

$$\left[\sum_i \dot{m}_i \left(\frac{C_i^2}{2} - \frac{V_i^2}{2}\right)\right]_{IN} = P_T + \left[\sum_i \dot{m}_i \left(\frac{C_i^2}{2} - \frac{V_i^2}{2}\right)\right]_{OUT} \tag{3.16}$$

$$P_T = \frac{U}{2}\left(\left(\sum_i \dot{m}_i \left(U - 2V_i\right)\right)_{in} - \left(\sum_i \dot{m}_i \left(U - 2V_i\right)\right)_{\text{out}}\right) \tag{3.17}$$

Maximum thrust power means that all processes should be reversible. No power is extracted out of the system through the shaft. The heat transfer happens at the ambient condition and all outgoing availability is 0. The available exergy in a fuel is not known exactly but is estimated. The work done on this has been performed by Baehr [53]. It estimates by calculating the work extracted in a reversible combustion for the given fuel as seen in figure 3.9. The reversible work (W_{rev}) is defined in equation 3.18. Which also uses a mass flow (m_i), specific enthalpy (h), specific entropy (s) and the ambient temperature (T_∞).

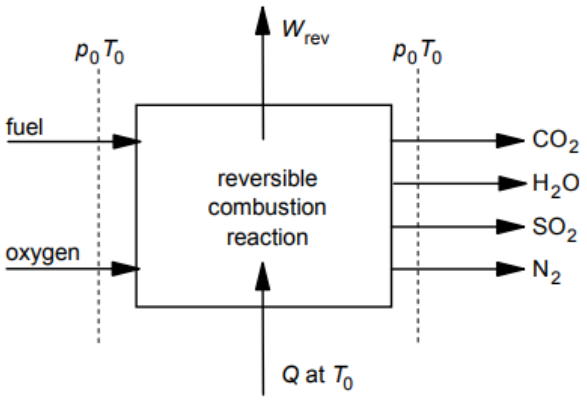

Figure 3.9: Reversible combustion reaction according to Baehr. [54]

$$W_{rev} = \left(\sum_i \dot{m}_i h_i\right)_{out} - \left(\sum_i \dot{m}_i h_i\right)_{in} - T_\infty \left(\left(\sum_i \dot{m}_i s_i\right)_{out} - \left(\sum_i \dot{m}_i s_i\right)_{in}\right) \tag{3.18}$$

The enthalpy change in this equation is equal to the enthalpy change by combustion (ΔH_{0_R}) and the entropy change (ΔS_{0_R}) is also because the combustion. Equation 3.18 is now rewritten as equation 3.19 where the reaction happens at constant temperature T_0.

$$W_{rev} = -\Delta H_{0_R} + T_0 \Delta S_{0_R} \tag{3.19}$$

Equation 3.19 can now be expressed in terms of the constituents in the reaction as seen in equation 3.20. It is noted that all specific exergies (ε) are given for the inlet and outlet condition which is equal to the environment. Since the heat transfer happens at a constant ambient temperature, the exergy of this is 0. The final term in this equation is seen in equation 3.21. Combining equation 3.19 and 3.20 gives equation 3.22.

$$m_f \varepsilon_{f_0} + m_{O_2} \varepsilon_{O_{2_0}} = W_{rev} + \sum_{products} m_i \varepsilon_{i_0} \tag{3.20}$$

$$\sum_{products} m_i \varepsilon_{i_0} = m_{CO_2} \cdot \varepsilon_{CO_{2_0}} + m_{H_2O} \cdot \varepsilon_{H_2O_0} \tag{3.21}$$

$$m_f \varepsilon_f = -\Delta h_{0_R} + T_0 \Delta S_{0_R} + \sum_{products} m_i \varepsilon_{i_0} - m_{O_2} \varepsilon_{O_{2_0}} \tag{3.22}$$

Since the enthalpy rise in the equation is equal to the HHV, this can be substituted. The entropy in the reaction can be seen in equation 3.23 and the exergy of the products - the exergy of oxygen is included in the model by Baehr.

$$\Delta S_{0_R} = m_{CO_2} \cdot \varepsilon_{CO_{2_0}} + m_{H_2O} \cdot \varepsilon_{H_2O_0} - m_{O_2} \varepsilon_{O_{2_0}} \tag{3.23}$$

The exergy at these conditions is calculated already by Baehr and it was estimated that the exergy of the fuel is 1.059 times higher than the LHV of the fuel, in this case kerosene as seen in table 3.7. This is an approximation since the chemical composition is not exactly known. Baehr fixed this by estimating the entropy of the fuel based on entropies of known pure substances. The entry conditions of the fuel are the same as the tests conducted by Baehr and for deviations, enthalpy and entropy changes are incorporated to match real conditions.

Table 3.7: Exergetic content of fuel based on Baehr environment. [53]

Fuel		petrol	kerosine	diesel oil	fuel oil [general]	fuel oil [light]	fuel oil [medium]	fuel oil [heavy]
mass fractions								
C	[-]	0.855	0.859	0.857	0.844	0.855	0.853	0.849
H	[-]	0.145	0.140	0.134	0.138	0.125	0.116	0.106
O	[-]	0.000	0.000	0.000	0.013	0.008	0.003	0.005
N	[-]	0.000	0.000	0.000	0.000	0.000	0.003	0.005
S	[-]	0.001	0.001	0.009	0.005	0.012	0.025	0.035
total	[-]	1.000	1.000	1.000	1.000	1.000	1.000	1.000
HHV_f	[MJ/kg]	46.50	46.50	45.40	42.00	44.80	43.30	42.30
LHV_F	[MJ/kg]	43.35	43.44	42.48	38.99	42.07	40.77	39.99
Baehr-I								
ε_f	[MJ/kg]	45.96	45.99	45.00	41.55	44.50	43.17	42.33
f_{ε_f}	[-]	1.060	1.059	1.060	1.066	1.058	1.059	1.059

The used calculation to calculate the loss factor is the balance equation with the inequality filled in as seen in equation 3.24. This is done for each component individually. Then, the lost energy in each component can be compared with each other when divided by the total chemical exergy going in the system as seen in equation 3.25. This gives the specific lost exergy (L^*). L^*+$P_T{}^*$ equal to 1.

$$\left(\sum_i \dot{m}_i b_{0i}\right)_{\text{in}} = P_{\text{S}} + P_{\text{T}} + \left(\sum_i q_i \frac{T_i - T_\infty}{T_i}\right) + \left(\sum_i \dot{m}_i b_{0i}\right)_{\text{out}} + L \tag{3.24}$$

$$L^* = \frac{\sum L}{\dot{m}_f \varepsilon_f} \tag{3.25}$$

4

Parameter Analysis

Before the optimization is done, an analysis is performed to see what the impact of parameters is on the TSFC. This is to find the sensitivity of the parameters on the optimization. As a centre point, the conventional engine described by Yin et al. is used[5]. From this engine all design parameters are varied to see the influence on different performance parameters. The design parameters are listed in table 4.1. This analysis does not include any off-design criteria. Also, the influence of the cooling model parameters and the loss factor on the turbine efficiency dependent on the cooling is investigated. The loss factor is not a design parameter but does have an impact on the results.

Table 4.1: Variable parameters of parameter analysis

Parameter	Range
BPR [-]	5-25
Fan PR [-]	1-1.8
LPC PR [-]	2-15
HPC PR [-]	5-30
TT4 [K]	1400-2700
e [-]	0-1
IC Δp_{hot} [%]	0-0.2
IC Δp_{cold} [%]	0-0.2
Split ratio [-]	0-1
ITB fraction [-]	0-0.5
loss factor [-]	0-0.625

Unless otherwise stated, during the parameter analysis, the design parameters in table4.2 are kept constant to the given value.

4.1. Bypass ratio

The effect of the BPR on the TSFC and other performance parameters will be described in this section. The BPR is changed from 5 to 25. This has a huge impact on all the performance parameters as can be seen in figure 4.1. In figure 4.1a, the thrust drops when the BPR increases for all 4 engine architectures. A higher BPR means less air through the core cycle and more air through the bypass. The propulsive efficiency will increase while the average exit speed of the flow will be lower, thus a lower thrust. The highest thrust is seen for the engine with both an ITB and an IC because the core for this configuration has the highest power density since it has additional fuel in the main combustion chamber and more fuel in the ITB. Figure 4.1b shows that increasing the BPR lowers the TSFC until an optimum is reached. When it goes up further, an infeasible engine is found (more power going to the shaft than possible). It looks like the conventional engine is the most efficient in this figure but that is only at the given parameters which were optimized for a conventional engine. The trend is for all engines the same and it is also noticeable that the changed architectures can all handle a larger

Table 4.2: Constant variables of parameter analysis

Parameter	Constant
BPR [-]	15
Fan PR [-]	1.44
LPC PR [-]	5
HPC PR [-]	9.7
TT4 [K]	1900
e [-]	0.5
IC Δp_{hot} [%]	0.05
IC Δp_{cold} [%]	0.05
Split ratio [-]	0.1
ITB fraction [-]	0.2
loss factor [-]	0.125

BPR which is logical since the energy density of the core is higher. As can be seen in figure 4.1c, the BPR has no effect on the cooling air of a specifIC-engine and thus also no effect on the poly-tropic efficiencies in the turbine. In figure 4.1d, the NO_X emission index in g/kg (fuel) is presented. The BPR has no influence on the NO_X emission index since the core parameters stay the same. The only difference is the IC which gives a lower entry temperature and the ITB which burns at a lower pressure and temperature. The lower entry temperature lowers the NO_X emissions. In figure 4.1e, the total NO_X content in grams can be seen for the engine configurations. At first glance, it looks like the benefit of the lower entry temperature of the IC is more beneficial than the extra combustion chamber for the ITB. This is not definite since the parameters were optimized for a conventional engine. Both the IC and the ITB will probably have lower TITs. The ITB-engine has the same main combustion chamber as the conventional engine. The only difference is that the $EINO_X$ is higher because more fuel is used compared to the conventional engine since the ITB operates at a lower thermal efficiency. The Sullivan factor cannot counteract the added fuel to the system.

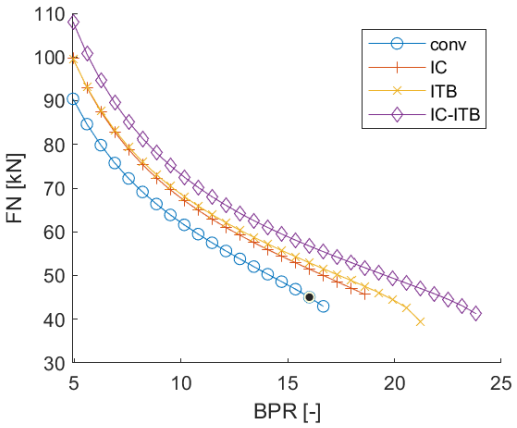

(a) Thrust for varying BPR.

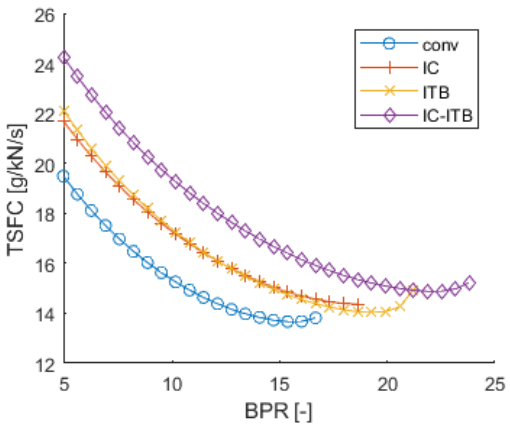

(b) TSFC for varying BPR.

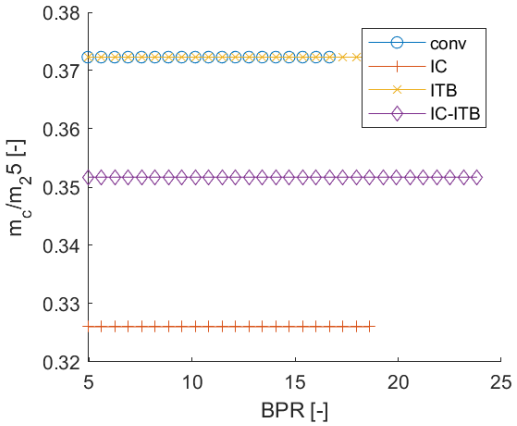

(c) Cooling air for changing BPR.

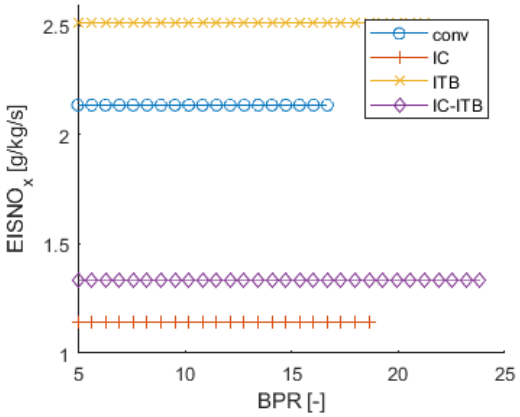

(d) $EISNO_X$ per kg fuel for varying BPR.

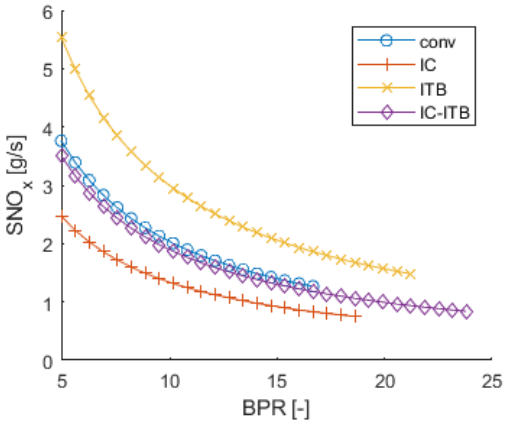

(e) Total NO_X in grams for varying BPR.

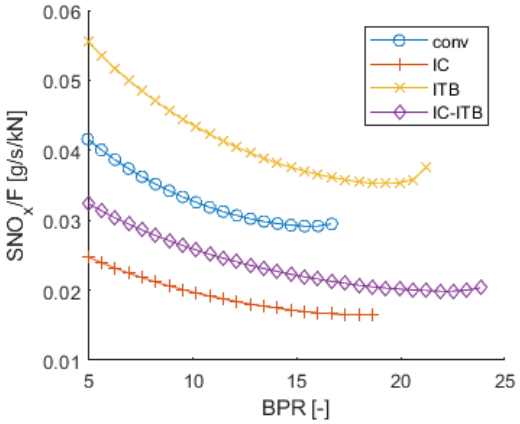

(f) NO_X per kg fuel per kN for varying BPR.

Figure 4.1: Effect of changing BPR.

4.2. Fan bypass pressure ratio

The effect of the FPR on the TSFC and other performance parameters will be described in this section. In figure 4.2a, The thrust of the engine increases with a higher FPR. This holds until the required power to the shaft is too high. Then the core will not deliver thrust and stall. This gives an infeasible engine which can be seen for high values of the FPR. The conventional engine stalls first which shows that the other architectures are more resilient. In figure 4.2b, a higher FPR means a lower TSFC, this is because a higher propulsive efficiency is reached when more power goes to the bypass instead of

the core cycle. The total cooling air is seen in figure 4.2c. The cooling air is constant for all cases except the IC because a higher FPR means a higher temperature in the bypass which means a higher cooling temperature and thus more cooling needed. This is not seen in the IC-ITB since the lower HPC exit temperature means more fuel is needed in the main combustion chamber to reach the required temperature. Then the constant energy fraction means that this also increases the fuel content in the ITB. The HPT will therefore follow the cooling flow of the IC, but the ITB exit temperature is higher and thus extra cooling is needed in the LPT. This evens out the cooling requirements for this configuration. Figure 4.2d shows the emission index for NO_X. The IC-engine has the lowest NO_X emission index. The engines containing an IC are also the only ones seeing a difference in the index for varying FPR. In figure 4.2e. It is seen that the IC shows the lowest total NO_X. The ITB configuration uses more fuel, the thrust is higher, and the NO_X is higher. When each engine is optimized to the same thrust, this might show different results.

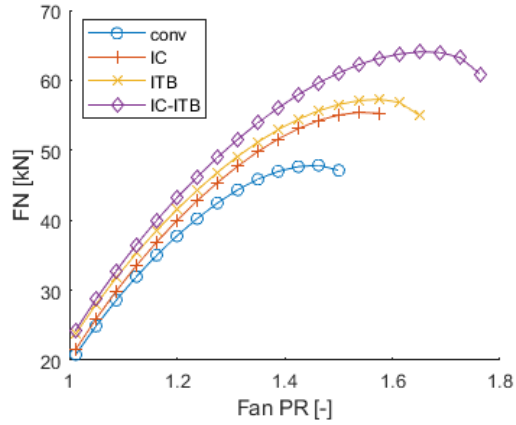

(a) Thrust to FPR.

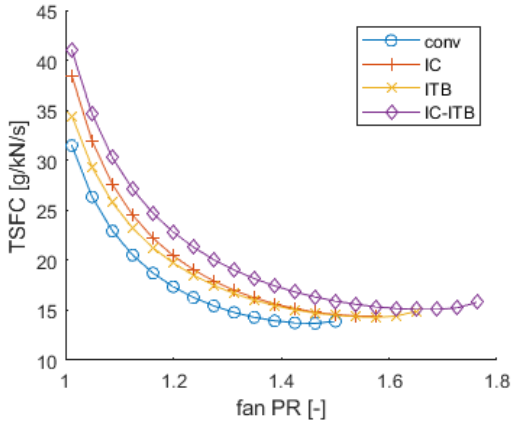

(b) TSFC to FPR.

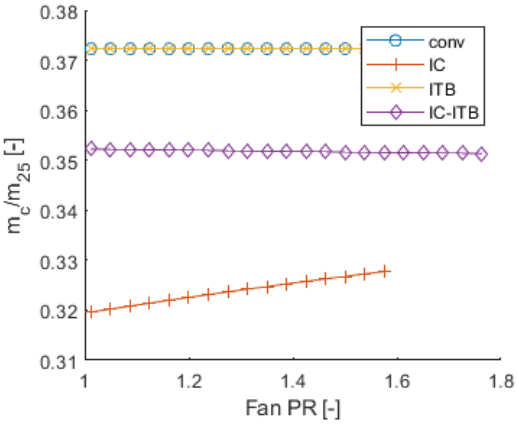

(c) Cooling air to FPR.

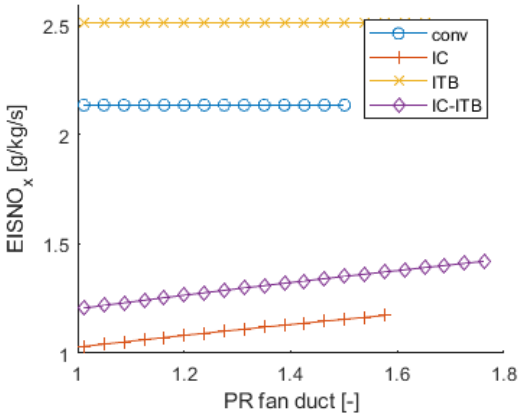

(d) $EISNO_X$ per kg fuel to FPR.

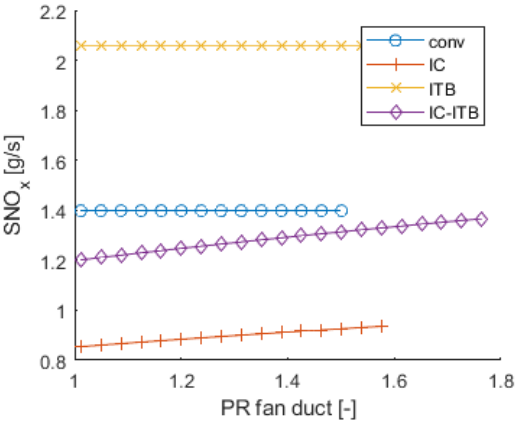

(e) total NO_X to FPR.

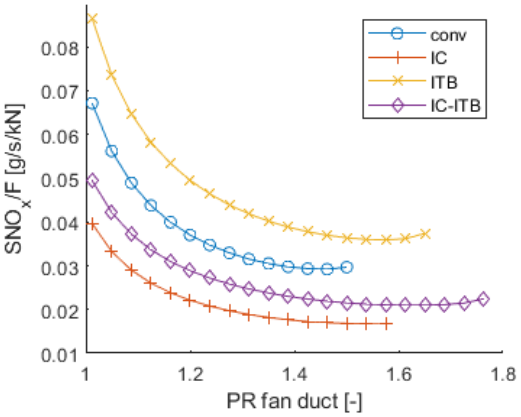

(f) total NO_X per kN to FPR.

Figure 4.2: Effects of changing the FPR.

4.3. low pressure ratio

Figure 4.3a shows that the temperature reduction in the IC becomes higher for an increasing pressure ratio since more heat can be taken out by the bypass flow since the temperature difference is larger and the maximum extractable heat is not reached. In figure 4.3b, it is shown that the heat taken out in the IC is not linear with the heat going out of the HPC. a Delta T of -40K aligns with a difference in TT3 of -90K and a delta T of -140K aligns with a difference in TT3 of -250K which means that even small temperature changes in the IC can decrease the maximum temperature in the turbine significantly. In

figure 4.4a the thrust variation for the low pressure ratio can be seen. Since the TIT is kept constant, a higher pressure ratio means less fuel into the combustion chamber to reach this constant burner exit temperature. The 2 configurations that contain an IC are less impacted by this since they take away some of the heat added in the low. Figure 4.4b shows that for the optimized conventional cycle, the optimum is found at an LPC pressure ratio of 5.5 (upper bound of 5 during optimization). The cooling requirements increase with an increase in the LPC pressure ratio since the cooling air goes to a higher temperature. For the cases that have an IC, this happens slower since more heat can be taken out for a given effectiveness. Both ITB total cooling air lowers for low LPC pressure ratios. The reason is that for a low LPC pressure ratio, the power going into the HPC is less. This means that less heat goes out in the HPT and thus the temperature in the ITB is higher. In figure 4.4e it can be seen that again the IC-engine gives the lowest $EINO_X$, but they all have the same trend of: a higher LPC pressure ratio means more NO_X.

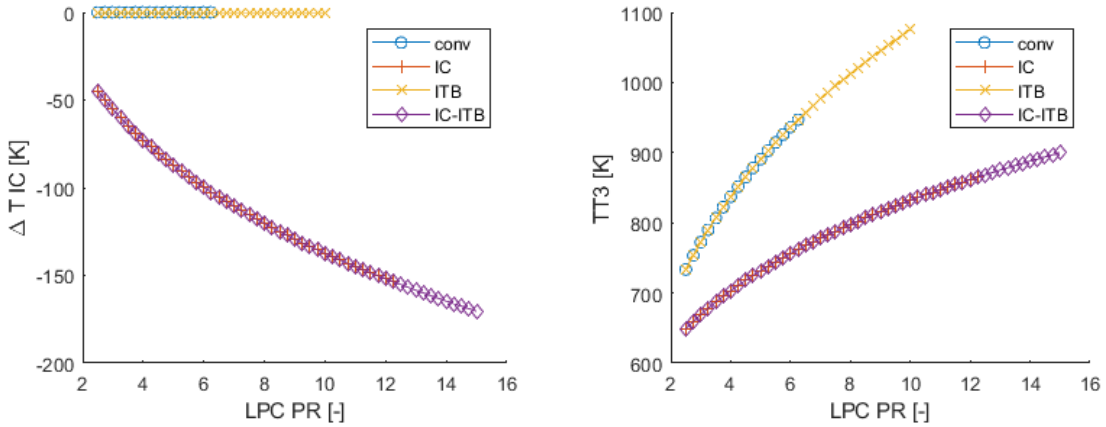

(a) ΔT in IC for varying LPC PR.

(b) ΔT in TT3 for varying LPC PR.

Figure 4.3: Temperature differences before the combustion for varying LPC pressure ratio.

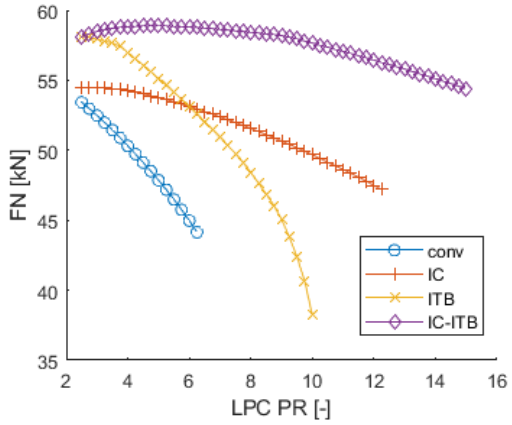

(a) Thrust to PR LPC.

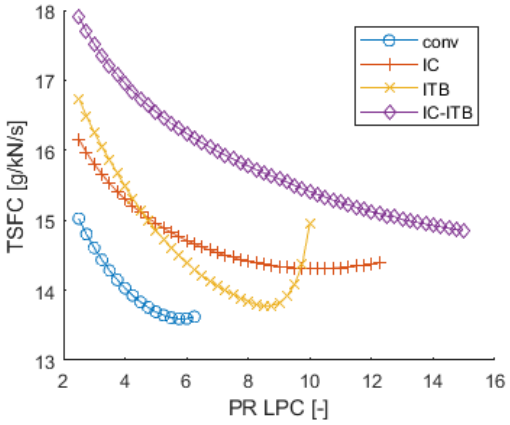

(b) TSFC to PR LPC.

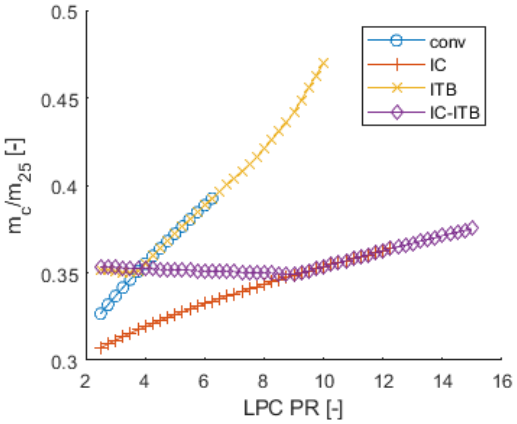

(c) Cooling air to PR LPC.

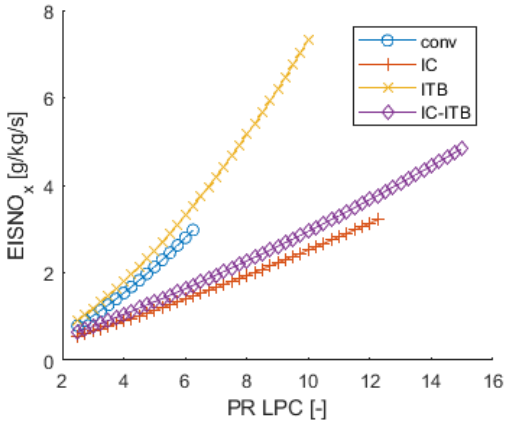

(d) $EISNO_X$ per kg fuel to PR LPC.

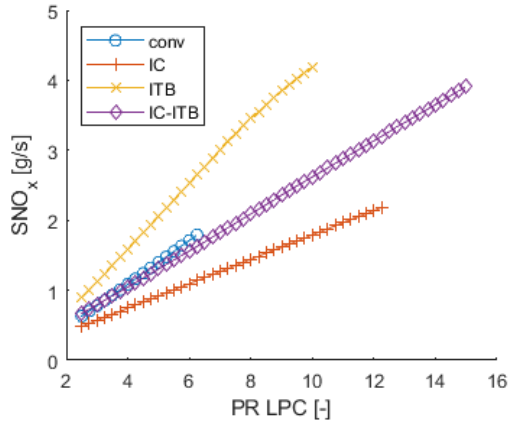

(e) Total NO_X to PR LPC.

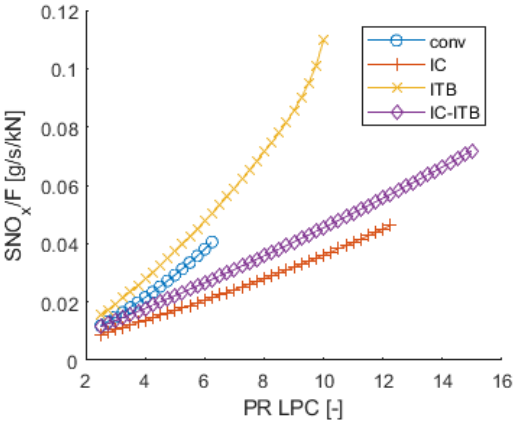

(f) Total NO_X per kN to PR LPC.

Figure 4.4: Effect of changing low pressure ratio.

4.4. HPC pressure ratio

Figures 4.5a and 4.5b show that a higher pressure ratio decreases the total delivered thrust and decreases the TSFC. The NO_X production is lowest for the IC-engine and the lowest EINOX is also for the IC and increases for an increased pressure ratio. Thus, higher pressure ratios benefit the non-conventional cycles more than the conventional cycles.

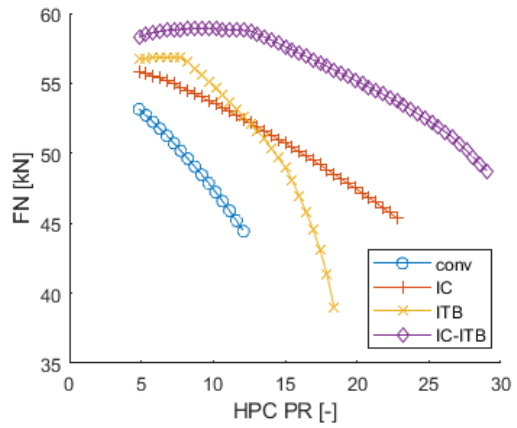

(a) Thrust to PR HPC.

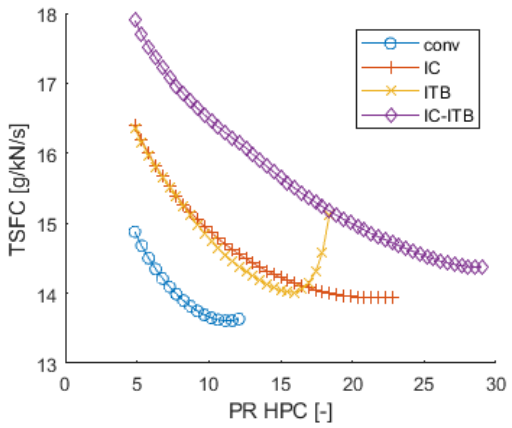

(b) TSFC to PR HPC.

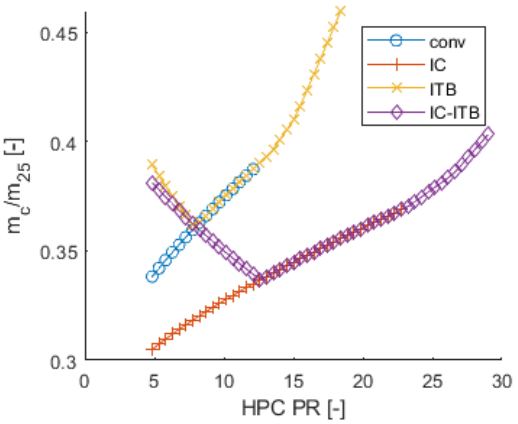

(c) Cooling air to PR HPC.

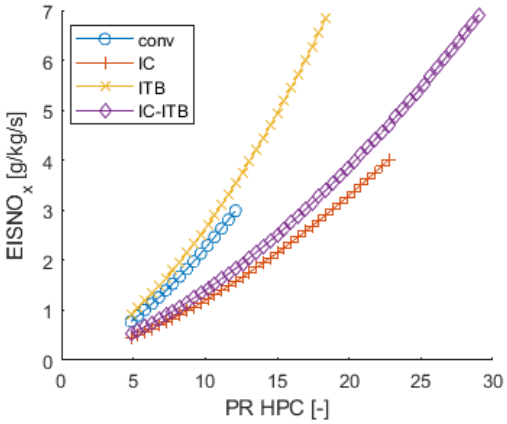

(d) $EISNO_X$ per kg fuel to PR HPC.

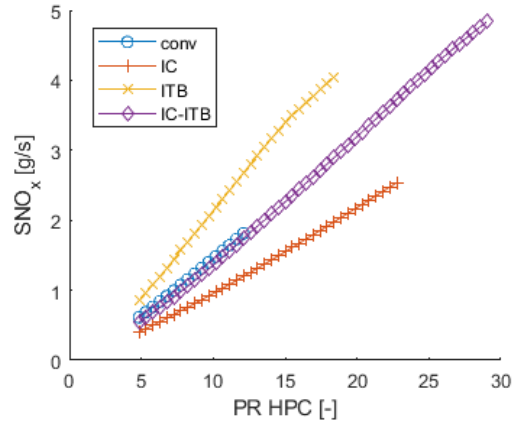

(e) Total NO_X to PR HPC.

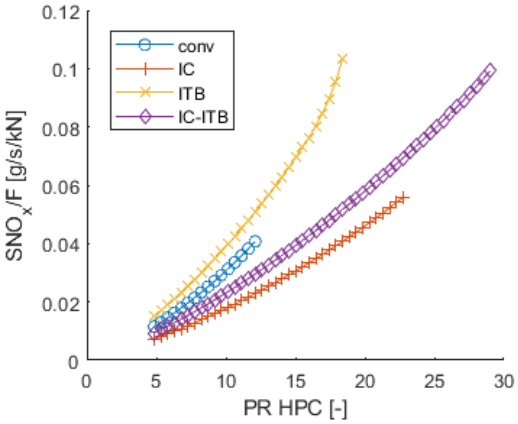

(f) Total NO_X per kN to PR HPC.

Figure 4.5: Effect of changing HPC pressure ratio.

4.5. Turbine inlet temperature

For the parameter analysis of the TIT, all architectures have an optimum that is dependent on the total cooling air needed. If the cooling air requirements become too high, the thrust goes down and the TSFC goes up. The effect of the IC is not very noticeable in figure 4.6c since the scale is large but for a TT4 of 2200K, the difference between conventional cooling and IC cooling is 0.45 and 0.55. A more realistic TT4 is however in the range of 1900K or lower. In figure 4.6d, the NO_X emission index is presented. It is noticeable that this is not a linear relation but it is not as exponential as initially thought.

In figure 4.6e the NO_X increases for higher TITs. This is mainly because the NO_X correlation is based on inlet conditions and FAR which increases linear with increased TT4 for constant inlet conditions.

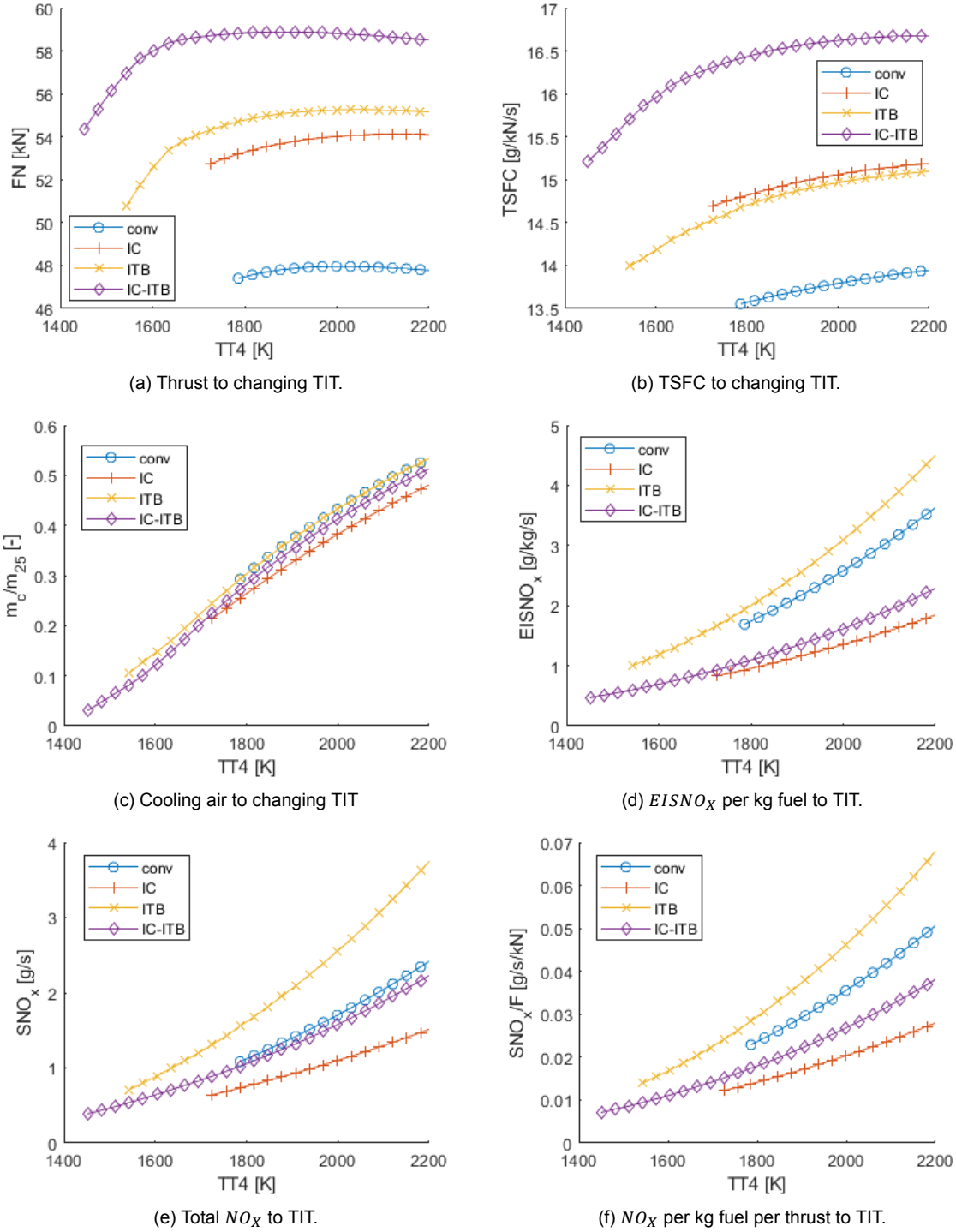

(a) Thrust to changing TIT.

(b) TSFC to changing TIT.

(c) Cooling air to changing TIT

(d) $EISNO_X$ per kg fuel to TIT.

(e) Total NO_X to TIT.

(f) NO_X per kg fuel per thrust to TIT.

Figure 4.6: Effect of changing TIT.

4.6. IC effectiveness

It can be seen in figure 4.7 that increasing the effectiveness increases both the thrust delivered and the TSFC when all the other parameters are kept the same. The reason for this is the added fuel in the combustion chamber becomes more when the LPC air is cooled since the HPC exit temperature is

lower. It can also be seen that the IC-ITB configuration levels the cooling requirements from a certain effectiveness. An ITB energy fraction of 0.2 results that there is an increase in fuel in the ITB and thus more cooling is needed in the LPT. This means that for an optimized IC-ITB, the temperature in the main combustion chamber will be a lot lower than for the other architectures. In figure 4.7f the temperature change in the IC on the hot and cold side is shown. For a cross flow IC, the heat taken out of the core flow only increases the temperature in the bypass flow by a minimal amount. A small IC will be able to do the trick. As seen in figure 4.7e, the NO_X becomes higher for the IC-ITB-engine as the effectiveness becomes higher. This is because the TIT stays the same. More fuel is needed to reach this temperature which also increases the fuel used in the ITB since the energy fraction stays the same.

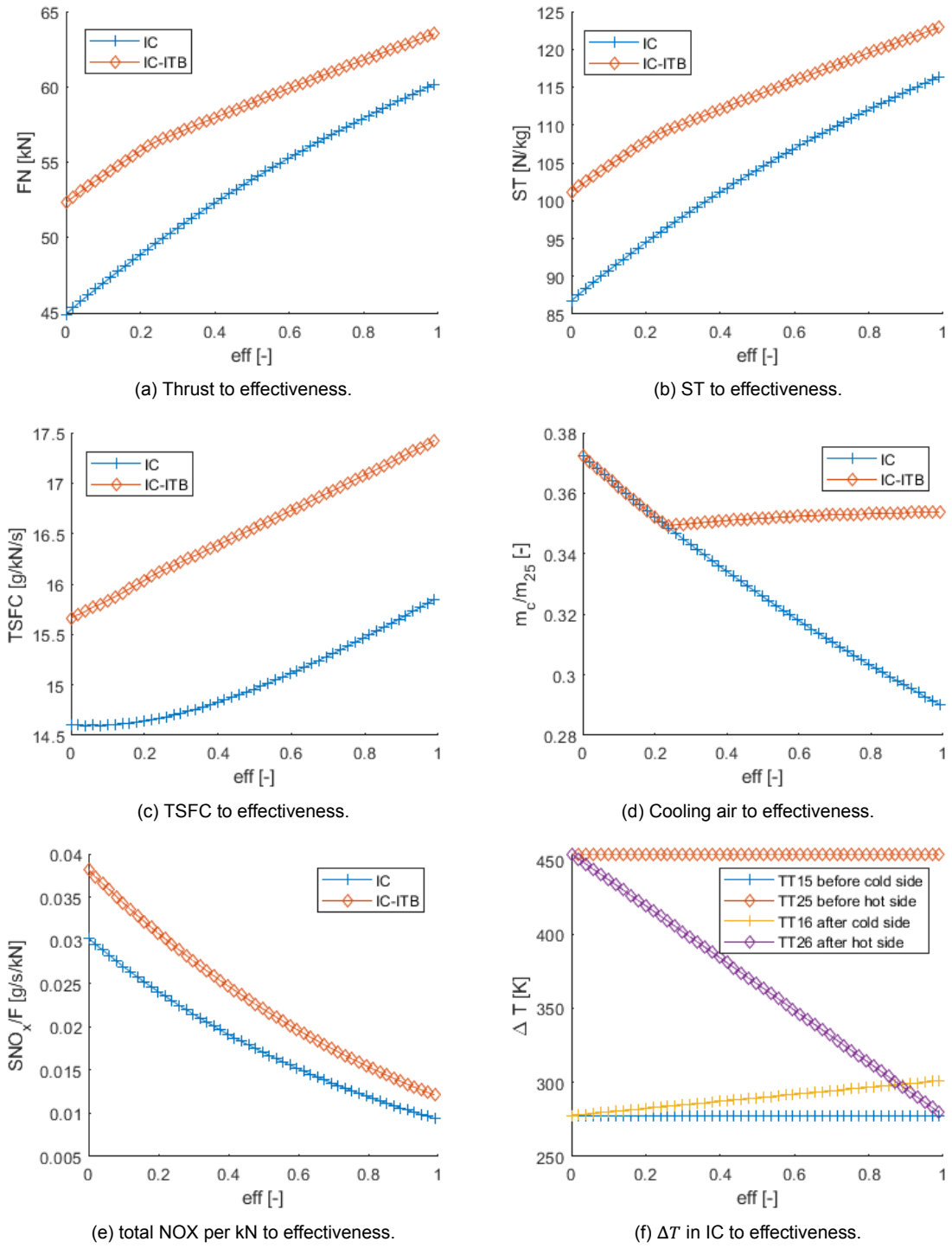

(a) Thrust to effectiveness.

(b) ST to effectiveness.

(c) TSFC to effectiveness.

(d) Cooling air to effectiveness.

(e) total NOX per kN to effectiveness.

(f) ΔT in IC to effectiveness.

Figure 4.7: Effect of changing effectiveness.

4.7. IC pressure loss

In figure 4.8 the effect of the pressure loss on both the hot and the cold side of the IC are shown. The values are the same for the case where the pressure loss is 5% It is noticeable that the pressure loss on the cold side is much more influential to the performance of the aero-engine. A pressure loss difference of 15% on the core side has an influence of 2.4% on the TSFC and 2.2% on the thrust while the same pressure loss on the cold side has an influence of 14.8% on the TSFC and 16.6% on the thrust. This shows immediately that for the IC, it will favour a low pressure loss on the cold side while the pressure

loss on the hot side is not that influential. The low pressure side has more air than the high pressure side. Since the baseline case has a high BPR, and 10% of the bypass flow goes trough the IC, The bypass is more sensitive to pressure losses.

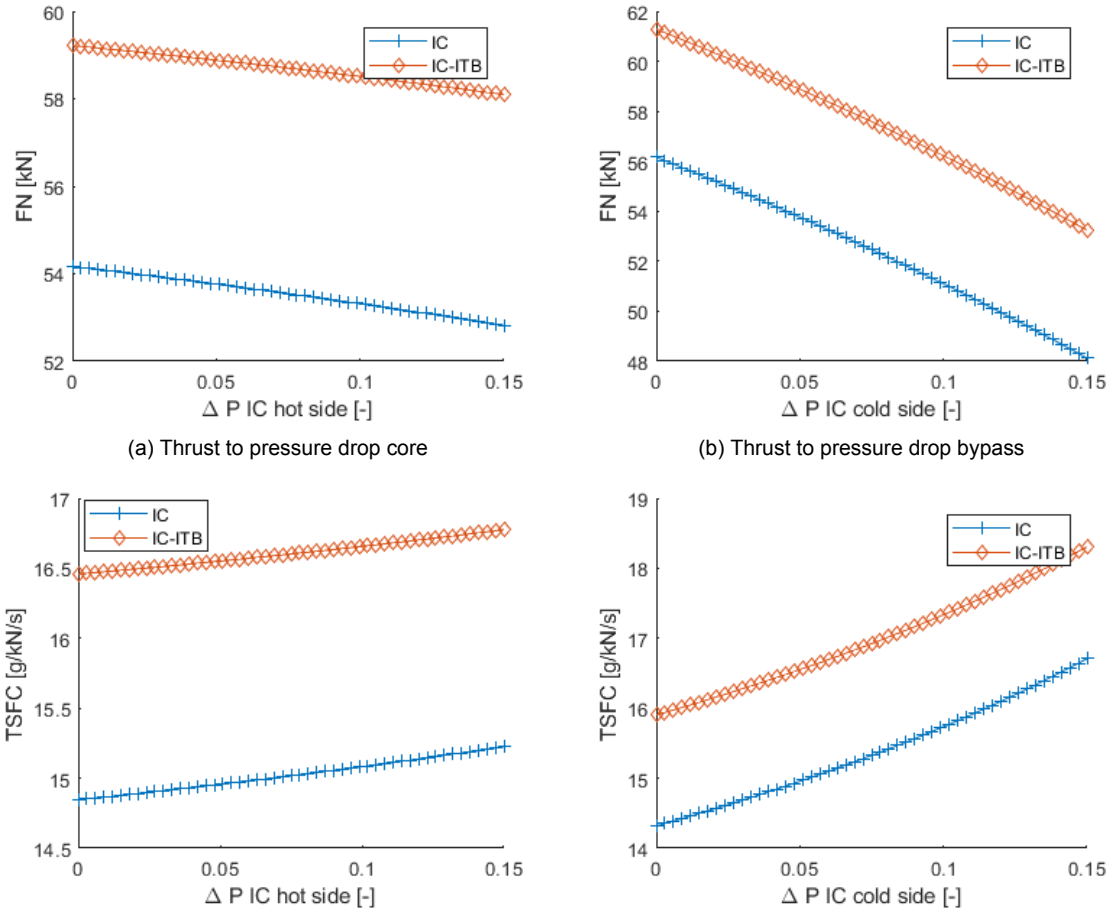

(a) Thrust to pressure drop core

(b) Thrust to pressure drop bypass

(c) TSFC to pressure drop core

(d) TSFC to pressure drop bypass

Figure 4.8: Effect of pressure drop in IC.

4.8. Bypass split ratio

The influence of the split ratio of the bypass flow is shown in figure 4.9. A split ratio of 0.1 means that 10% of the flow goes through the cold side of the IC and 0.9 means that 90% of the flow goes through the cold side IC. It is seen that when a minimal amount of flow goes through the cold side of the IC, the TSFC is optimal. The least amount of air goes trough the cold side of the IC for constant pressure loss. This configuration also shows the highest thrust, again because the least amount of flow is influenced by the pressure loss. The temperature rise in the cold side(TT16) of the IC is higher for low split ratio since less air is available to store the heat from the core side for a constant effectiveness.

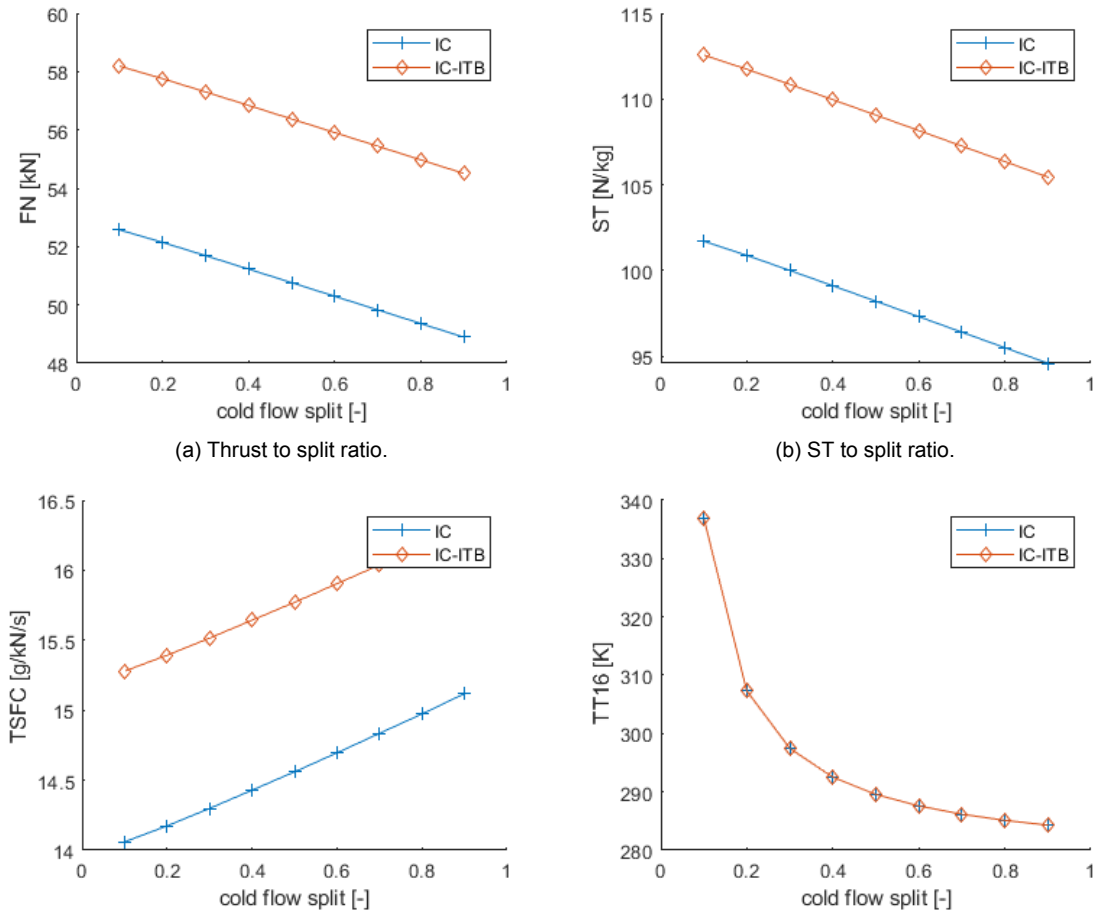

(a) Thrust to split ratio.

(b) ST to split ratio.

(c) TSFC to split ratio.

(d) TT16 to split ratio.

Figure 4.9: Effect of split ratio on engine performance.

4.9. ITB energy fraction

The ITB energy fraction stands for how much of the energy in the fuel goes to the ITB, since the same fuel is used in main combustion chamber and ITB in all configurations, this is also a mass split. In figure 4.10, it is seen that for low values of fuel split, there is no cooling required in the LPT because the LPT inlet temperature do not go above the cooling threshold. When this threshold is reached (0.15 for IC-ITB and 0.25 for ITB), the cooling required counteracts the thrust increase while the TSFC keeps going up. For very high values of ITB split, the temperature in the ITB becomes higher than the temperature in the main combustion chamber and thus the NO_X in the engine starts to increase exponentially. It can be concluded that while high fuel split values are theoretically possible, they will increase the TSFC and increase the NO_X emissions when keeping TT4 constant. This effect is more noticeable in the IC-ITB-engine since the amount of fuel used is also larger.

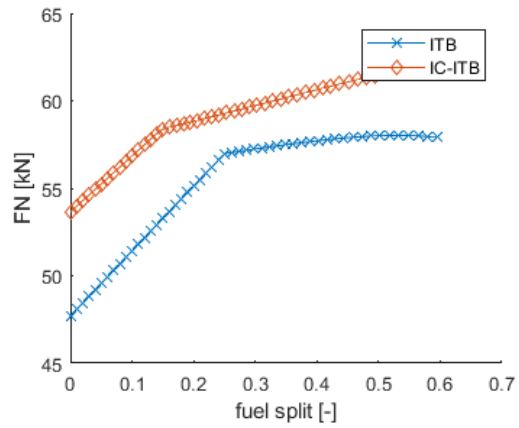

(a) Thrust to ITB ff.

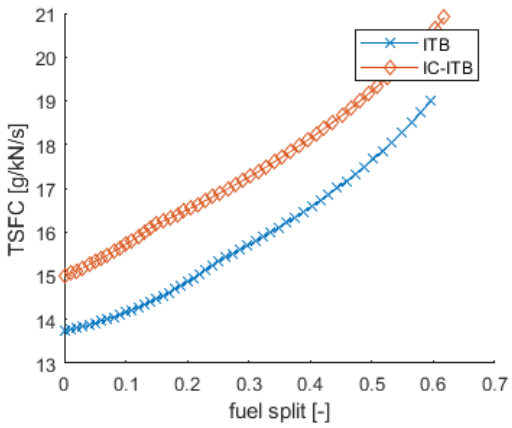

(b) TSFC to ITB ff.

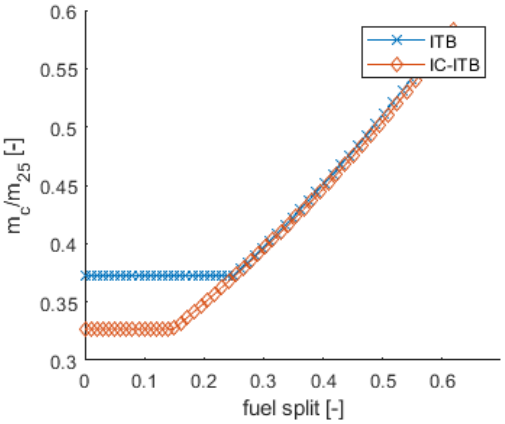

(c) Cooling air to ITB ff.

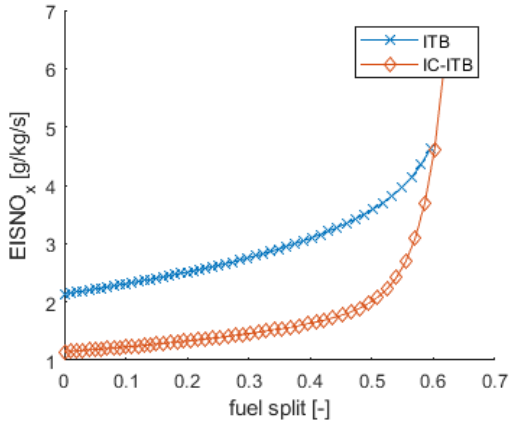

(d) NO_X per kg fuel to ITB ff.

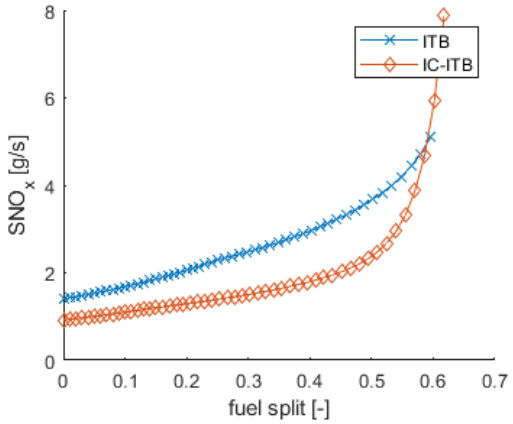

(e) total NO_X to ITB ff.

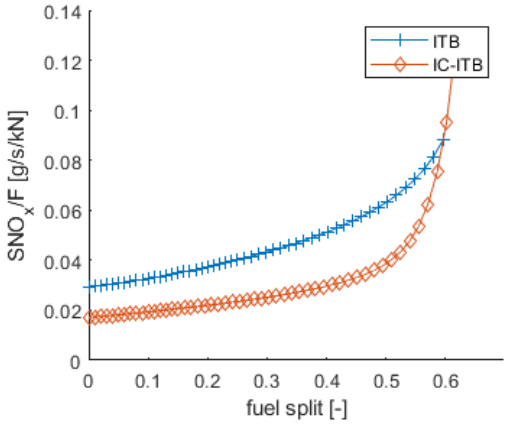

(f) total NO_X per kN to ITB ff.

Figure 4.10: Effect of changing the ITB energy fraction.

4.10. summary parameter analysis

It is noticeable in the parameter analysis that it started for a optimized conventional engine. The parameters all go to the optimum or the bounds for this conventional engine. It is also directly visible that all the architectures using IC and IC-ITB will have lower TITs when the OPR is limited to 70 since they can easily reach the thrust requirements. At first glance it seems that the IC-engine is better to reduce NO_X emissions during cruise.

5

On-Design optimization

In this chapter, the findings of the on-design performance of the 4 engines will be analysed and reported. The on-design performance is taken at cruise altitude of 11000m. Also, the cruise speed is 0.85 Mach and the cruise thrust is 47kN. The matching cooling system is created using off-design performance for take-off at ISA SLS +25K as seen in table 5.1. All the engines will use a loss factor of 0.5 based on literature.[32] 2 different cooling models are used. Both models align with previous literature. The first model has higher cooling requirements and aligns with [5]. and the second model is 25% more efficient and aligns with the GE90 validation and Jonsson et al.[33]. The first cooling model will be defined as model 1 and the second cooling model will be defined as model 2. The methodology is described in Chapter3.

Table 5.1: Design conditions at various operating conditions

Operating points	Altitude	Mach Number	Thrust Required	Flat rating temperature
Cruise	11000m	0.85	47kN	/
Hot-day Take-off	0	0	300kN	ISA+25K

5.1. Conventional Engine

First, the optimization is performed on a conventional configuration. This is done for both cooling models. The design parameters of the 2 found optimal conventional engines within the design space are summarized in table 5.2. The effect the cooling has on the TSFC of the engines is immediately visible and as expected. Less turbine cooling results in a more efficient engine since the core can be hotter for the same amount of cooling and thus a more thermodynamic efficient engine is achieved. This translates into a more energetic core and a higher BPR. A 25% better cooling system results in a 1% more fuel efficient engine.

Table 5.2: Summarized design variables for both cooling models in a conventional architecture

	model 1	model 2
$m_1[kg/s]$	517	517
BPR [-]	12.98	12.06
OPR [-]	70	66.7
FPR [-]	1.446	1.446
LPC PR [-]	5	5
HPC PR [-]	9.681	9.206
TT4 cruise [K]	1626	1585
TT4 SLS ISA+25 [K]	1985	1938
HPT m_c/m_{25} [%]	22.47	23.26
LPT m_c/m_{25} [%]	0	0
TSFC [kg/kN/s]	13.50	13.63
$EISNO_X$ cruise [g/kg]	1.15	0.97
$EISNO_X$ ISA SLS [g/kg]	5.00	4.19

5.2. Intercooled Engine

The intercooled engine is summarized in table 5.3 and table 5.4 for both cooling models. The effectiveness is increased from 10% to 90%. It is seen that the higher the effectiveness of the IC, the higher the efficiency of the aero-engine. It is also beneficial for the NO_X emissions both in cruise and take-off in comparison to the conventional engine. The increased pressure drop for a higher effectiveness is less impactful than the benefit of a higher effectiveness. It is seen that the intercooled engine favours a higher HPC PR and a lower LPC PR for an increasing effectiveness. Once the HPC PR limit is reached, there is no added benefit for the TSFC. This is logical since the pressure loss is percentual, thus having it at a lower pressure means less absolute pressure loss. For the combined cycle, only an effectiveness of 0.3, 0.5 and 0.7 will be investigated. The flow split in the IC is always kept the same at 10% of the bypass flow.

Table 5.3: Summarized design variables for cooling model 1 in an intercooled architecture. The columns are the varying effectivenesses from 0.1-0.9

model 1 10% IC flow split	conv	e=0.1	e=0.2	e=0.3	e=0.4	e=0.5	e=0.6	e=0.7	e=0.8	e=0.9
$m_1[kg/s]$	517	517	517	517	517	517	517	517	517	517
BPR [-]	12.98	13.73	14.62	15	15	15	15	15	15	15
OPR [-]	70	70	70	70	70	70	70	70	70	70
FPR [-]	1.45	1.44	1.44	1.44	1.44	1.44	1.44	1.44	1.44	1.44
LPC PR [-]	5	4.37	4.26	4.01	3.20	3.00	2.85	2.54	2.55	2.57
HPC PR [-]	9.68	11.16	11.53	12.33	15.53	16.69	17.71	20	20	20
TT4 cruise [K]	1626	1601	1616	1595	1572	1541	1515	1508	1479	1452
TT4 SLS ISA+25 [K]	1985	1959	1985	1967	1945	1916	1893	1894	1867	1845
HPT m_c/m_{25} [%]	22.47	19.46	19.40	17.43	15.92	14.04	12.57	12.38	10.85	9.57
LPT m_c/m_{25} [%]	0	0	0	0	0	0	0	0	0	0
dT25 cruise [K]	0	-15.7	-30.8	-43.9	-45.25	-55.4	-62.8	-70.5	-73.9	-83.8
dT25 SLS ISA+25 [K]	0	-19.0	-37.2	-53.1	-54.8	-67.2	-76.2	-85.5	-89.6	-101.6
dP25 cruise [-]	0	0.006	0.012	0.018	0.024	0.030	0.036	0.042	0.048	0.054
dP SLS ISA+25 [-]	0	0.017	0.034	0.052	0.068	0.086	0.103	0.120	0.137	0.154
TSFC $[g/kN/s]$	13.50	13.46	13.44	13.42	13.39	13.38	13.37	13.35	13.35	13.35
SNO_X cruise [g/kg]	1.15	1.13	0.95	0.83	0.76	0.67	0.60	0.58	0.50	0.44
SNO_X ISA SLS [g/kg]	5.00	4.82	4.29	3.78	3.55	3.17	2.86	2.82	2.46	2.18

Table 5.4: Summarized design variables for cooling model 2 in an intercooled architecture. The columns are the varying effectivenesses from 0.1-0.9

model 2 10% IC flow split	conv	e=0.1	e=0.2	e=0.3	e=0.4	e=0.5	e=0.6	e=0.7	e=0.8	e=0.9
$m_1[kg/s]$	517	517	517	517	517	517	517	517	517	517
BPR [-]	12.06	12.85	13.54	14.34	14.58	15	15	15	15	15
OPR [-]	66.7	70	70	70	70	70	70	70	70	70
FPR [-]	1.45	1.44	1.44	1.44	1.44	1.44	1.44	1.44	1.44	1.44
LPC PR [-]	5	4.38	4.33	4.16	3.29	3.19	3.00	2.80	2.66	2.57
HPC PR [-]	9.2	11.14	11.35	11.90	15.14	15.71	16.78	18.10	19.16	20
TT4 cruise [K]	1585	1600	1595	1609	1602	1594	1557	1532	1509	1488
TT4 SLS ISA+25 [K]	1938	1958	1960	1986	1984	1982	1946	1923	1906	1891
HPT m_c/m_{25} [%]	23.26	23.35	22.53	22.01	21.26	20.26	17.83	16.32	15.07	14.00
LPT m_c/m_{25} [%]	0	0	0	0	0	0	0	0	0	0
dT25 cruise [K]	0	-15.7	-31.2	-45.3	-48.7	-59.0	-66.6	-72.1	-77.7	-83.8
dT25 SLS ISA+25 [K]	0	-19.0	-37.8	-54.8	-59.0	-71.6	-80.8	-87.4	-94.3	-101.6
dP IC cruise [-]	0	0.006	0.012	0.018	0.024	0.03	0.036	0.042	0.048	0.054
dP IC SLS ISA+25 [-]	0	0.017	0.034	0.052	0.069	0.086	0.103	0.120	0.137	0.154
TSFC [g/kN/s]	13.63	13.59	13.56	13.54	13.50	13.47	13.44	13.43	13.41	13.4
SNO_X cruise [g/kg]	0.97	0.99	0.94	0.86	0.80	0.75	0.67	0.59	0.54	0.48
SNO_X ISA SLS [g/kg]	4.19	4.47	4.24	3.93	3.71	3.52	3.15	2.82	2.60	2.39

In figure 5.1 the summarized results for both cooling models for the IC are presented. It can be seen in figure 5.1a that model 1 is more efficient over the whole line as expected. The maximum temperature in both models reaches 1950K and becomes lower once the maximum BPR is reached. This means that a higher BPR is more important than having more efficient turbines. The SNO_X for both cruise and take-off are similar since the inlet conditions of the combustion chamber are the same. The cooling regiment only has a small impact on the NO_X emissions. Less cooling means more air in the combustion chamber thus a lower maximum temperature, but it also means a higher BPR which in turn decreases the air in the main combustion chamber.

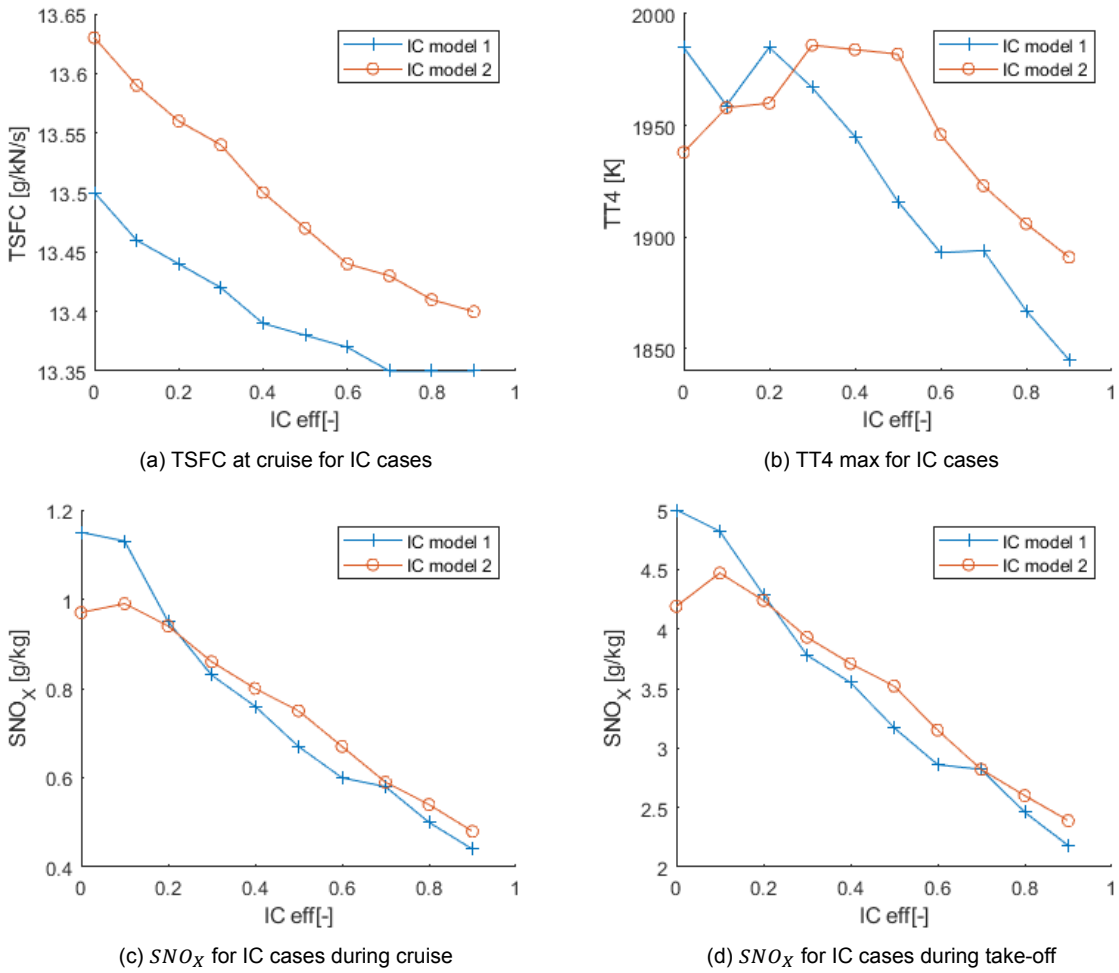

(a) TSFC at cruise for IC cases

(b) TT4 max for IC cases

(c) SNO_X for IC cases during cruise

(d) SNO_X for IC cases during take-off

Figure 5.1: Results of different cooling models on the performance parameters of the intercooled engine.

5.3. Inter-turbine-burning Engine

Optimizing the on-design cycle for an ITB-engine will be split in 2 optimizations. One will look at the results when the ITB is always operated over the entire flight mission, and the other will look at the effect when the ITB is only used during take-off.

5.3.1. ITB during cruise and take-off

Firstly, the results for cooling model one are shown in table 5.5. The ITB-engine is optimized with respect to the ITB energy fraction from 0% to 40%. It is noticeable that the ITB is always less efficient than the conventional engine for this configuration. The added benefit of lowering the maximum turbine temperature that ITB has, does not weigh in the drawbacks of the lower thermal efficiency and the pressure drop.

Table 5.5: Summarized design variables for cooling model 1 in an inter-burner architecture where the inter-burner has a constant fuel split. The columns are the varying ITB energy fraction from 0.05-0.4

model 1	conv	ITB05	ITB10	ITB15	ITB20	ITB25	ITB30	ITB35	ITB40
$m_1[kg/s]$	517	517	517	517	517	517	517	517	517
BPR [-]	12.98	13.54	14.08	14.55	15	15	15	15	15
OPR [-]	70	70	70	70	70	70	70	70	70
FPR [-]	1.45	1.45	1.45	1.45	1.45	1.45	1.45	1.45	1.45
LPC PR [-]	5	5	5	5	5	5	5	5	5
HPC PR [-]	9.68	9.67	9.67	9.67	9.67	9.67	9.67	9.67	9.67
TT4 cruise [K]	1626	1608	1594	1571	1547	1491	1442	1396	1356
TT4 SLS ISA+25 [K]	1985	1964	1948	1922	1895	1828	1769	1714	1666
HPT m_c/m_{25} [%]	22.47	21.32	20.52	19.12	17.65	14.08	10.96	8.21	5.92
LPT m_c/m_{25} [%]	0	0	0	0.05	0.29	0.37	0.48	0.61	0.79
TSFC [g/kN/s]	13.50	13.68	13.76	13.85	13.97	14.08	14.21	14.37	14.56
SNO_X cruise [g/kg]	1.15	1.13	1.11	1.10	1.03	0.88	0.77	0.66	0.56
SNO_X ISA SLS [g/kg]	5.00	5.09	5.02	4.98	4.68	4.05	3.42	3.01	2.60

In table 5.6, the results for the second cooling model are shown. Overall, this gives a higher TSFC for all engines, but the same trend is visible. It is only beneficial for the TSFC in very low fuel split fraction of 0.05. These models also show that the BPR does not go to 15 when the amount of cooling flow required is higher. For both models, the pressure loss added cannot overcome by having the ITB advantages. It is less efficient than the conventional engine, but it does add benefits for high ITB ratios in terms of the NO_X emissions.

Table 5.6: Summarized design variables for cooling model 2 in an inter-burner architecture where the inter-burner has a constant fuel split. The columns are the varying ITB energy fraction from 0.05-0.4

model 2	conv	ITB05	ITB10	ITB15	ITB20	ITB25	ITB30	ITB35	ITB40
$m_1[kg/s]$	517	517	517	517	517	517	517	517	517
BPR [-]	12.06	12.66	12.98	13.37	13.75	13.92	14.08	14.15	14.20
OPR [-]	66.7	66.9	68.5	70	70	70	70	70	70
FPR [-]	1.45	1.44	1.45	1.45	1.45	1.45	1.45	1.45	1.45
LPC PR [-]	5	5	5	5	5	5	5	5	5
HPC PR [-]	9.2	9.22	9.45	9.67	9.67	9.67	9.67	9.67	9.67
TT4 cruise [K]	1585	1572	1559	1542	1507	1459	1416	1372	1334
TT4 SLS ISA+25 [K]	1938	1922	1907	1888	1846	1787	1737	1684	1639
HPT m_c/m_{25} [%]	23.26	22.3	21.87	20.98	18.45	14.89	11.77	8.57	6.11
LPT m_c/m_{25} [%	0	0	0	0	0	0	0.09	0.20	0.41
TSFC [g/kN/s]	13.63	13.82	13.90	13.97	14.05	14.15	14.27	14.40	14.60
SNO_X cruise [g/kg]	0.97	0.96	0.99	1.00	0.92	0.80	0.70	0.60	0.52
SNO_X ISA SLS [g/kg]	4.19	4.33	4.49	4.58	4.21	3.71	3.30	2.81	2.47

5.3.2. ITB only active during take-off

No ITB in cruise but ITB in take-off is investigated. During cruise, the core air flow goes through the ITB, but no fuel is added, the same pressure loss in the ITB of 3% is used since the turbulent elements are still necessary during take-off. The results for cooling model 1 are visible in table 5.7. and for cooling model 2 in table 5.8. The results for both cooling models are similar. The results are now better than for when the ITB runs during cruise. When the ITB is only active during take-off operations, the thermal efficiency during cruise is higher. The ITB during take-off also lowers the TIT which reduces the cooling requirements and increases the core efficiency. The most optimal ITB fuel fraction found now is 0.15. This results in a TSFC decrease of 1.8%. The better TSFC is already substantial for small ITB fractions and diminishes for ITB fractions higher than the optimum of 0.15. Because not burning ITB in cruise and only using it in take-off conditions has effects on the cycle. The ITB has an exponential effect on

both the OPR and the BPR of the engine. For an increasing ITB ratio during take-off, it is observed that the OPR becomes lower and the BPR becomes higher during take-off operations. As seen from the fact that the design BPR becomes lower for increasing ITB energy fraction. Two effects are noticeable in the cycle. First, the pressure ratio during take-off becomes lower for higher ITB energy fraction. This has the effect of reduced cooling requirements. Secondly the increasing BPR during take-off means less air going through the core which increases the temperature rise in the core. This increases the maximum temperature in the core during take-off and results in more cooling required. An optimum fuel split fraction of 0.15 is found for the design. The NO_X reduction in comparison to the conventional engine lies between 13% for the smallest ITB fraction to 75% for the highest ITB fraction. The ITB fraction that offers the best TSFC has a 32.6% reduction in the NO_X emissions during take-off. During cruise it only reduces the NO_X emissions by 7%. Mostly from the lower FAR due to less cooling.

Table 5.7: Summarized design variables for cooling model 1 in an inter-burner architecture where the inter-burner has a constant fuel split during take-off and no ITB burning during cruise. The columns are the varying ITB energy fraction from 0.05-0.4

model 1 no ITB cruise	conv	ITB05	ITB10	ITB15	ITB20	ITB25	ITB30	ITB35	ITB40
$m_1[kg/s]$	517	517	517	517	517	517	517	517	517
BPR [-]	12.98	13.82	14.04	14.04	13.51	12.9	12.02	11.12	10.23
OPR [-]	70	70	70	70	70	70	70	70	70
FPR [-]	1.45	1.45	1.46	1.46	1.46	1.46	1.47	1.47	1.48
LPC PR [-]	5	5	5	5	4.87	4.66	4.48	4.27	4.08
HPC PR [-]	9.68	9.62	9.6	9.6	9.82	10.27	10.66	11.13	11.63
TT4 cruise [K]	1626	1620	1615	1598	1551	1512	1463	1420	1378
TT4 SLS ISA+25 [K]	1985	1929	1901	1862	1795	1747	1690	1638	1593
HPT m_c/m_{25} [%]	22.47	18.39	16.7	14.6	11.02	8.52	5.87	3.75	2.24
LPT m_c/m_{25} [%]	0	0	0	0.05	0.07	0.22	0.30	0.43	0.66
TSFC [g/kN/s]	13.50	13.49	13.45	13.42	13.43	13.46	13.52	13.61	13.75
SNO_X cruise [g/kg]	1.15	1.13	1.13	1.07	0.94	0.84	0.73	0.63	0.54
SNO_X ISA SLS [g/kg]	5.00	4.39	3.85	3.37	2.72	2.32	1.89	1.53	1.23

Table 5.8: Summarized design variables for cooling model 2 in an inter-burner architecture where the inter-burner has a constant fuel split during take-off and no ITB burning during cruise. The columns are the varying ITB energy fraction from 0.05-0.4

model 2 no ITB cruise	conv	ITB05	ITB10	ITB15	ITB20	ITB25	ITB30	ITB35	ITB40
$m_1[kg/s]$	517	517	517	517	517	517	517	517	517
BPR [-]	12.06	12.79	13.11	13.40	13.22	12.50	11.75	10.79	9.9
OPR [-]	66.7	70	70	70	70	70	70	70	70
FPR [-]	1.45	1.46	1.46	1.46	1.46	1.46	1.47	1.47	1.48
LPC PR [-]	5	5	5	5	4.93	4.7	4.55	4.38	4.23
HPC PR [-]	9.21	9.62	9.61	9.6	9.70	10.17	10.47	10.86	11.19
TT4 cruise [-]	1585	1597	1597	1560	1567	1509	1459	1409	1372
TT4 SLS ISA+25 [-]	1938	1903	1879	1865	1813	1742	1677	1620	1581
HPT m_c/m_{25} [%]	23.26	20.62	19.06	17.95	14.68	10.44	6.85	4.08	2.59
LPT m_c/m_{25} [%]	0	0	0	0	0.05	0.09	0.16	0.26	0.65
TSFC [g/kN/s]	13.63	13.60	13.55	13.52	13.50	13.51	13.55	13.63	13.78
SNO_X cruise [g/kg]	0.97	1.07	1.07	1.07	1.00	0.83	0.69	0.60	0.53
SNO_X ISA SLS [g/kg]	4.19	4.20	3.89	3.40	2.82	2.26	1.77	1.45	1.17

5.3.3. ITB comparison

In figure 5.2, the summary is seen for both the ITB cases, when the ITB is always working and when the ITB only works during take-off. It is seen in figure 5.2a that the ITB-engine prerformance improves in both cases when the cooling model is most efficient (model 1) and the TSFC is lower when the ITB

only works during take-off. An optimum TSFC is found for an ITB fraction of 0.15 and 0.2 for model 1 and model 2, respectively. The maximum temperatures are also lower when the ITB only works during take-off. The NO_X emissions for cruise condition are lowest when the ITB is running during cruise, which is logical cause this adds the Sullivan correlation. The NO_X emissions during take-off are lowest when the ITB only works during take-off. Since the case where the ITB only works during take-off is much more fuel efficient than the other case, only this case will be further investigated and combined with the IC to see the combined effect.

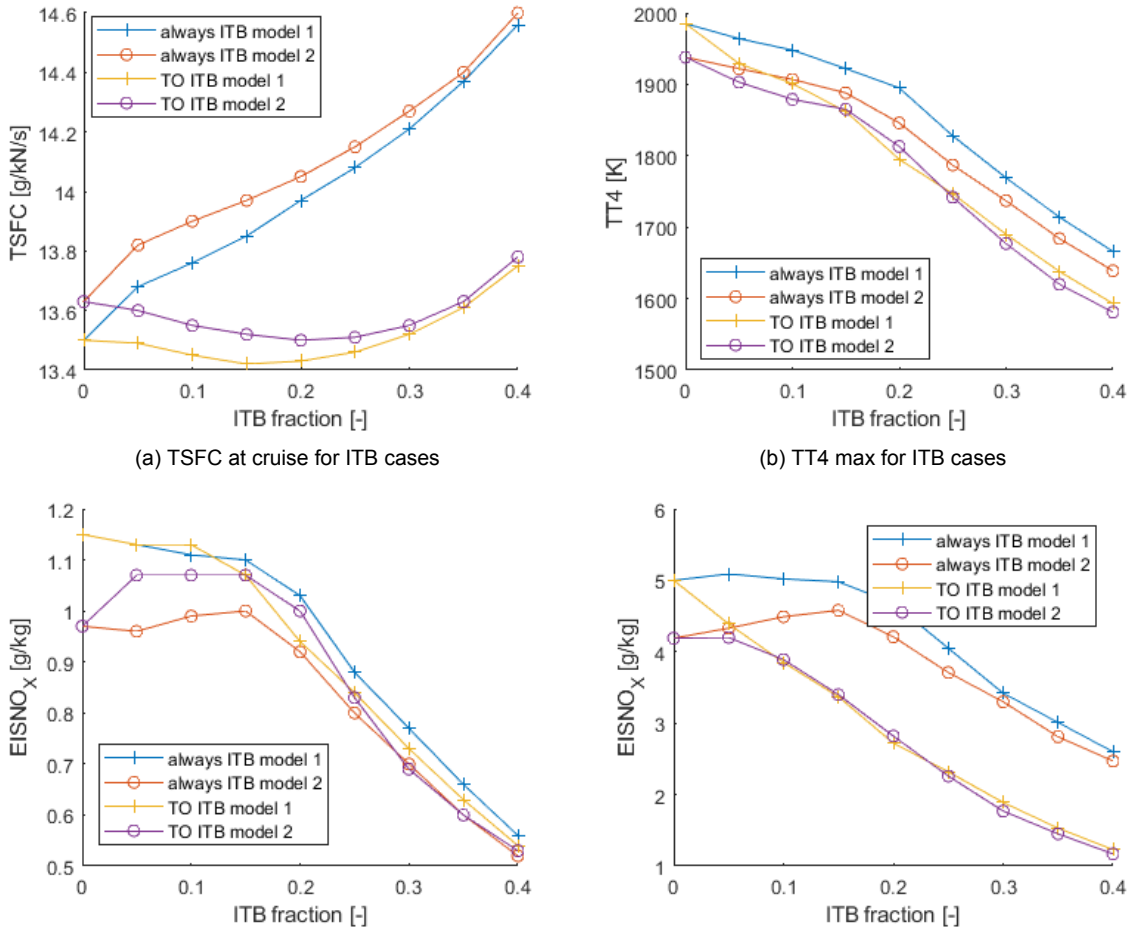

(a) TSFC at cruise for ITB cases

(b) TT4 max for ITB cases

(c) SNO_X for ITB cases during cruise

(d) SNO_X for ITB cases during take-off

Figure 5.2: Effect of different cooling models on both ITB configurations. One where the ITB is always burning fuel and one where the ITB only burns fuel during hot day take-off.

5.4. Engine with both IC and inter-turbine-burner

Combining the 2 architectures creates an engine with both an IC and an ITB. It is investigated if they have a positive effect on the performance and the emissions of an aero-engine. The engines are made for ITB fuel fractions ranging from 0.05 to 0.25 and this is done for a varying IC effectiveness of 0.3, 0.5 and 0.7. This is done for both cooling models. The results for cooling model 1 are seen in tables 5.9, 5.10, and 5.11 and the engines for cooling model 2 are summarized in tables 5.12,5.13 and 5.14. The effect is again present that both the IC and the ITB increase the maximum BPR and lower the necessary cooling. Since the ITB also increases the BPR during take-off condition while lowering the pressure ratio at the same time, an optimum ITB fuel fraction is found for the IC-ITB-engines. The TSFC and the SNO_X values are seen in figure5.3 and 5.4 for model 1 and in figure 5.5 and 5.6 for model 2. The data to create the mesh is shown as the red lines in the figures. The conventional engine is located at an ITB fuel fraction and effectiveness of 0. In cooling model 1, it is seen that an ITB never showed better TSFC than an IC once it reached an effectiveness of 0.3. The IC-ITB is only more

beneficial if a low effectiveness is used in the IC. Once a high enough effectiveness is reached in the IC, the IC-ITB will have a worse TSFC compared to only an IC. The NO_X emissions during cruise are influenced by the ITB only when no IC is present. Once an IC is present in the architecture, the ITB has little impact in the cruise NO_X emissions. Both IC and ITB show good NO_X reduction in comparison to the conventional engine. For take-off, the ITB has a larger impact on the emissions then the IC. For a varying fuel fraction between 0 and 0.25, the engines using an ITB all reach a NO_X reduction of more than 50%. The IC-engine also reaches this, but only for very high effectiveness. In model 2, the same results are seen for the TSFC, a reduction to the conventional engine and a lower TSFC for the pure intercooled engine. The NO_X reduction during cruise is again mainly created by the IC. The reason that the cruise emissions for the ITB-engine are larger is because the ITB allows for a higher BPR and a higher pressure ratio which increases the FAR and P_{T3}. The NO_X reductions during take-off are again dominated by the ITB. For all ITB-engines, again a reduction of 50% is achievable for fuel fractions higher than 0.25. The IC reduces it by a maximum of 40% for high effectiveness which is still a great reduction.

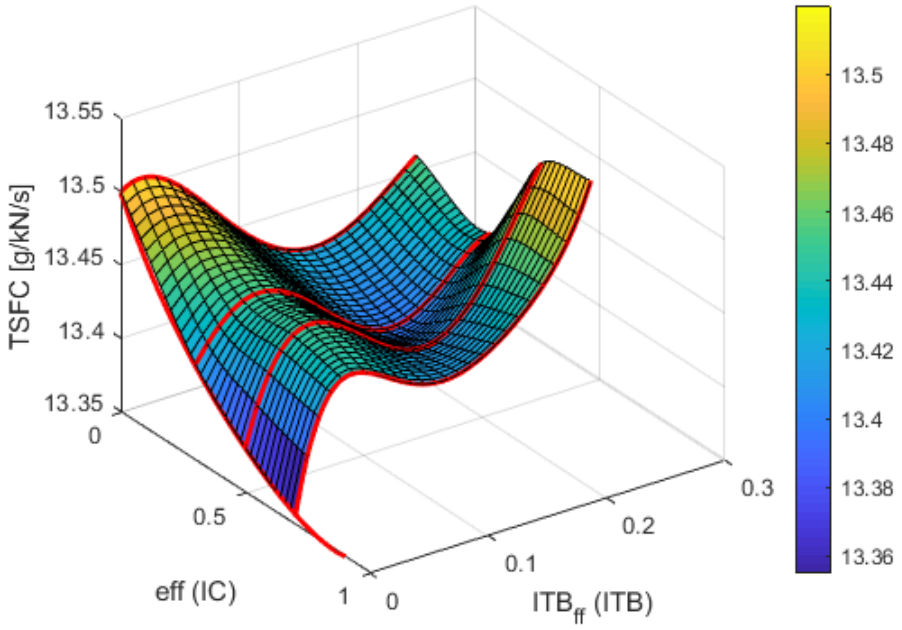

Figure 5.3: TSFC comparison for all architectures for cooling model 1. Conventional engine in the left corner. Increasing effectiveness follows the eff(IC) line and increasing ITB energy fraction follows the ITB line. Low ITB fractions have increased TSFC to counteract ITB pressure loss. High ITB fractions have increased TSFC from lower thermal efficiency. increased IC effectiveness decreases TSFC.

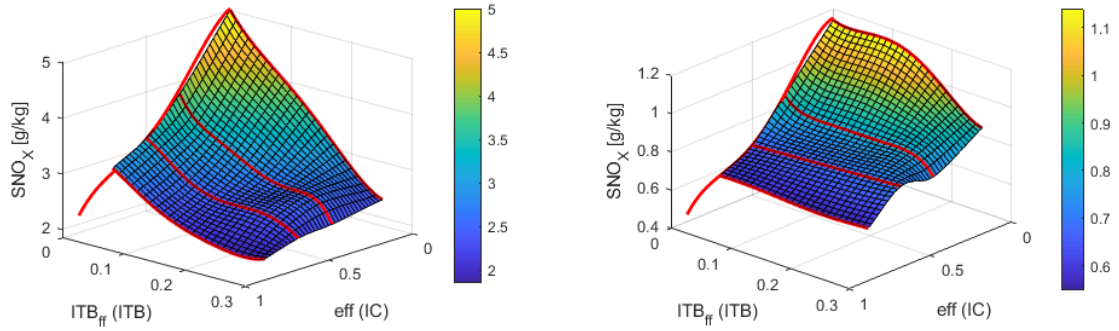

(a) SNO_X comparison for all architectures during take-off.

(b) SNO_X comparison for all architectures during cruise.

Figure 5.4: Comparison of NO_X emissions for all architectures for cooling model 1. Conventional engine located in top corner (yellow region). Increased IC effectiveness follows the eff (IC) line and increased ITB energy fraction follows the ITB line.

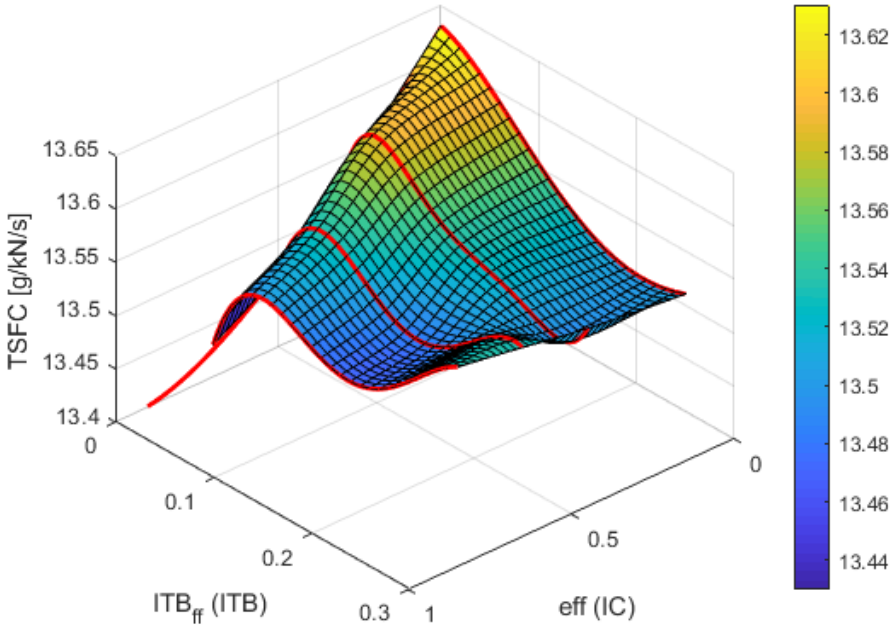

Figure 5.5: TSFC comparison for all architectures for cooling model 2. Conventional engine in the top corner. Increasing effectiveness follows the eff(IC) line and increasing ITB energy fraction follows the ITB line. Low ITB fractions have increased TSFC to counteract ITB pressure loss. High ITB fractions have increased TSFC from lower thermal efficiency. increased IC effectiveness decreases TSFC.

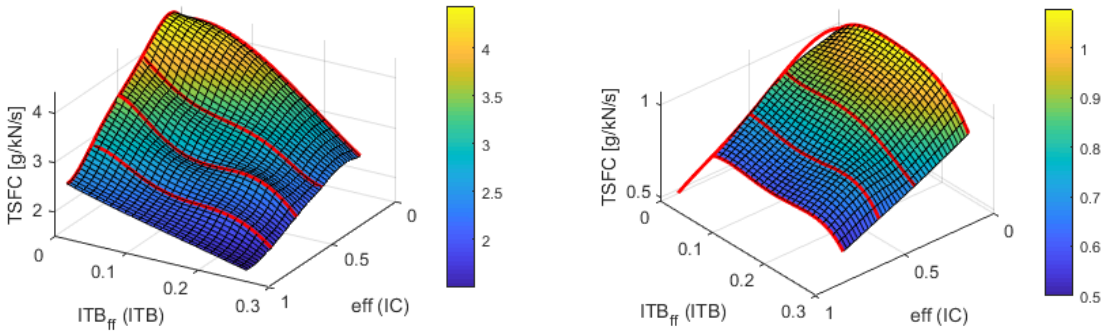

(a) SNO_X comparison for all architectures during take-off.

(b) SNO_X comparison for all architectures during cruise.

Figure 5.6: Comparison of NO_X emissions for all architectures for cooling model 2. Conventional engine located in top corner (yellow region). Increased IC effectiveness follows the eff (IC) line and increased ITB energy fraction follows the ITB line.

Table 5.9: Cooling model 1 on a combined engine with effectiveness of 0.3.

model 1 IC10% eff30	conv	IC	ITB05	ITB10	ITB15	ITB20	ITB25
$m_1[kg/s]$	517	517	517	517	517	517	517
BPR [-]	12.98	15	15	15	15	15	14.04
OPR [-]	70	70	70	70	70	70	70
FPR [-]	1.45	1.44	1.44	1.45	1.45	1.45	1.46
LPC PR [-]	5	4.01	3.72	3.66	3.08	2.94	2.79
HPC PR [-]	9.68	12.33	13.28	13.46	15.95	16.66	17.48
TT4 cruise [-]	1626	1595	1560	1546	1552	1545	1497
TT4 SLS ISA+25 [-]	1985	1967	1870	1830	1826	1803	1743
HPT m_c/m_{25} [%]	22.47	17.43	12.51	10.7	10.56	9.47	7.00
LPT m_c/m_{25} [%]	0	0	0	0	0	0.14	0.19
dT cruise [K]	0	-42.9	-41.1	-40.5	-34.3	-32.6	-30.8
dT SLS ISA+25 [K]	0	-53.1	-47.6	-46.5	-38.7	-36.3	-33.6
dP cruise [-]	0	0.018	0.018	0.018	0.018	0.018	0.018
dP SLS ISA+25 [-]	0	0.052	0.051	0.050	0.048	0.046	0.044
TSFC [g/kN/s]	13.50	13.42	13.45	13.43	13.40	13.41	13.44
SNO_X cruise [g/kg]	1.15	0.83	0.78	0.75	0.78	0.78	0.69
SNO_X ISA SLS [g/kg]	5.00	3.78	3.12	2.67	2.67	2.59	2.16

Table 5.10: Cooling model 1 on a combined engine with effectiveness of 0.5.

model 1 IC10% eff50	conv	IC	ITB05	ITB10	ITB15	ITB20	ITB25
$m_1[kg/s]$	517	517	517	517	517	517	517
BPR [-]	12.98	15	15	15	15	15	15
OPR [-]	70	70	70	70	70	70	70
FPR [-]	1.45	1.44	1.44	1.44	1.45	1.46	1.47
LPC PR [-]	5	3.00	2.88	2.84	2.49	2.48	2.46
HPC PR [-]	9.68	16.69	17.38	17.58	20	20	20
TT4 cruise [K]	1626	1541	1535	1524	1536	1534	1538
TT4 SLS ISA+25 [K]	1985	1916	1886	1850	1852	1837	1834
HPT m_c/m_{25} [%]	22.47	14.04	12.39	10.84	11.07	10.29	9.97
LPT m_c/m_{25} [%]	0	0	0	0	0.01	0.29	0.91
dT cruise [K]	0	-55.4	-53.0	-52.2	-44.8	-44.6	-44.3
dT SLS ISA+25 [K]	0	-67.2	-61.5	-60.0	-50.4	-49.4	-48.2
dP cruise [-]	0	0.03	0.03	0.03	0.03	0.03	0.03
dP SLS ISA+25 [-]	0	0.086	0.083	0.081	0.078	0.075	0.072
TSFC [g/kN/s]	13.50	13.38	13.45	13.43	13.41	13.44	13.51
SNO_X cruise [g/kg]	1.15	0.67	0.67	0.65	0.70	0.70	0.71
SNO_X ISA SLS [g/kg]	5.00	3.17	2.75	2.42	2.39	2.36	2.25

Table 5.11: Cooling model 1 on a combined engine with effectiveness of 0.7.

model 1 IC10% eff70	conv	IC	ITB05	ITB10	ITB15	ITB20	ITB25
$m_1[kg/s]$	517	517	517	517	517	517	517
BPR [-]	12.98	15	15	15	15	15	15
OPR [-]	70	70	70	70	70	70	70
FPR [-]	1.45	1.44	1.45	1.45	1.45	1.45	1.46
LPC PR [-]	5	2.54	2.53	2.53	2.53	2.51	2.50
HPC PR [-]	9.68	20	20	20	20	20	20
TT4 cruise [K]	1626	1508	1502	1493	1487	1488	1494
TT4 SLS ISA+25 [K]	1985	1894	1866	1837	1818	1806	1804
HPT m_c/m_{25} [%]	22.47	12.38	10.91	9.75	8.93	8.41	8.18
LPT m_c/m_{25} [%]	0	0	0	0	0.03	0.35	0.97
dT cruise [K]	0	-62.8	-64.0	-63.9	-63.8	-63.5	-63.1
dT SLS ISA+25 [K]	0	-85.5	-73.8	-73.0	-72.0	-70.5	-68.7
dP cruise [-]	0	0.042	0.042	0.042	0.042	0.042	0.042
dP SLS ISA+25 [-]	0	0.120	0.115	0.113	0.110	0.106	0.101
TSFC [g/kN/s]	13.50	13.35	13.44	13.42	13.42	13.45	13.52
SNO_X cruise [g/kg]	1.15	0.58	0.57	0.56	0.55	0.55	0.56
SNO_X ISA SLS [g/kg]	5.00	2.82	2.44	2.14	1.96	1.86	1.92

Table 5.12: Cooling model 2 on a combined engine with effectiveness of 0.3.

model 2 IC10% eff30	conv	IC	ITB05	ITB10	ITB15	ITB20	ITB25
$m_1[kg/s]$	517	517	517	517	517	517	517
BPR [-]	12.06	14.34	14.63	15	15	14.18	13.47
OPR [-]	66.7	70	70	70	70	70	70
FPR [-]	1.45	1.44	1.45	1.45	1.46	1.46	1.46
LPC PR [-]	5	4.16	4.02	3.94	3.61	2.97	2.81
HPC PR [-]	9.21	11.90	12.26	12.47	13.54	16.48	17.33
TT4 cruise [K]	1585	1609	1597	1604	1596	1543	1495
TT4 SLS ISA+25 [K]	1938	1986	1935	1919	1891	1824	1761
HPT m_c/m_{25} [%]	23.26	22.01	18.69	17.77	16.27	12.94	9.70
LPT m_c/m_{25} [%]	0	0	0	0.12	0.15	0.07	0.15
dT cruise [K]	0	-45.3	-44.0	-43.3	-40.1	-33.0	-31.1
dT SLS ISA+25 [K]	0	-54.8	-51.4	-50.2	-45.9	-37.0	-34.2
dP cruise [-]	0	0.018	0.018	0.018	0.018	0.018	0.018
dP SLS ISA+25 [-]	0	0.052	0.050	0.049	0.048	0.046	0.044
TSFC [g/kN/s]	13.63	13.54	13.58	13.54	13.52	13.50	13.52
SNO_X cruise [g/kg]	0.97	0.86	0.84	0.86	0.85	0.77	0.68
SNO_X ISA SLS [g/kg]	4.19	3.93	3.37	3.08	2.90	2.53	2.15

Table 5.13: Cooling model 2 on a combined engine with effectiveness of 0.5.

model 2 IC10% eff50	conv	IC	ITB05	ITB10	ITB15	ITB20	ITB25
$m_1[kg/s]$	517	517	517	517	517	517	517
BPR [-]	12.06	15	15	15	15	15	13.58
OPR [-]	66.7	70	70	70	70	70	70
FPR [-]	1.45	1.44	1.45	1.45	1.45	1.46	1.46
LPC PR [-]	5	3.19	3.10	3.04	2.78	2.73	2.47
HPC PR [-]	9.21	15.71	16.08	16.40	17.87	18.09	20
TT4 cruise [K]	1585	1594	1570	1554	1555	1551	1468
TT4 SLS ISA+25 [K]	1938	1982	1925	1886	1870	1847	1754
HPT m_c/m_{25} [%]	23.26	20.26	16.94	15.01	14.29	13.06	8.80
LPT m_c/m_{25} [%]	0	0	0	0	0.03	0.36	0.19
dT cruise [K]	0	-59.0	-57.5	-56.3	-51.1	-50.11	-44.5
dT SLS ISA+25 [K]	0	-71.6	-66.9	-64.9	-57.9	-55.9	-48.4
dP cruise [-]	0	0.03	0.03	0.03	0.03	0.03	0.03
dP SLS ISA+25 [-]	0	0.086	0.083	0.082	0.079	0.076	0.072
TSFC [g/kN/s]	13.63	13.47	13.53	13.50	13.48	13.51	13.52
SNO_X cruise [g/kg]	0.97	0.75	0.71	0.69	0.71	0.71	0.59
SNO_X ISA SLS [g/kg]	4.19	3.52	3.00	2.58	2.52	2.43	1.89

Table 5.14: Cooling model 2 on a combined engine with effectiveness of 0.7.

model 2 IC10% eff70	conv	IC	ITB05	ITB10	ITB15	ITB20	ITB25
$m_1[kg/s]$	517	517	517	517	517	517	517
BPR [-]	12.06	15	15	15	15	15	13.99
OPR [-]	66.7	70	70	70	70	70	70
FPR [-]	1.45	1.44	1.44	1.45	1.45	1.46	1.46
LPC PR [-]	5	2.80	2.69	2.65	2.52	2.51	2.50
HPC PR [-]	9.21	18.10	18.79	19.06	20	20	20
TT4 cruise [K]	1585	1532	1531	1517	1518	1517	1449
TT4 SLS ISA+25 [K]	1938	1923	1905	1866	1851	1836	1748
HPT m_c/m_{25} [%]	23.26	16.32	15.14	13.30	12.70	11.85	7.92
LPT m_c/m_{25} [%]	0	0	0	0	0.04	0.44	0.45
dT cruise [K]	0	-72.1	-69.0	-67.7	-63.7	-63.4	-63.3
dT SLS ISA+25 [K]	0	-87.4	-79.9	-77.6	-71.8	-70.3	-68.9
dP cruise [-]	0	0.042	0.042	0.042	0.042	0.042	0.042
dP SLS ISA+25 [-]	0	0.120	0.116	0.113	0.110	0.106	0.101
TSFC [g/kN/s]	13.63	13.43	13.50	13.48	13.47	13.50	13.54
SNO_X cruise [g/kg]	0.97	0.59	0.60	0.58	0.59	0.59	0.50
SNO_X ISA SLS [g/kg]	4.19	2.82	2.56	2.24	2.14	2.03	1.61

6

off-design

For the off-design analysis, the TOC ISA+15 is added with a required thrust of 60kN. All engines had the same issue that this condition could not be met by any configuration since spool speed 1 goes to 106% before the required thrust is reached. In this section, analysis will be conducted with respect to the operating limits at off-design conditions

6.1. Conventional

The results for the conventional engine are reported in table 6.1. Since the cooling is rated at the SLS ISA+25 condition, this is also the flat rated temperature. It is noticeable that the conventional engine with a design PR of 70 has a standardized emission index that is 3 times higher than the standardized emission index for LEAP(1.1 in take-off and 0.37 in cruise). It is already noticeable that any measure to optimize the TSFC has a negative effect on the NO_X emissions for a conventional cycle.

Table 6.1: Summarized results for conventional engine

Parameters conventional	Design 55kN	Cruise 47kN	TOC ISA+15 60kN	TO 300kN	SLS ISA+25 300kN
W1 [kg/s]	517	498.09	511.61	1196.64	1147.39
BPR [-]	11.62	12.13	11.37	11.88	11.89
OPR [-]	70	63.89	74.25	60.67	60.48
Fan PR [-]	1.52	1.46	1.57	1.43	1.43
LPC PR [-]	5	4.83	5.1	4.55	4.56
HPC PR [-]	9.18	9.08	9.3	9.3	9.26
TT4 [K]	1614	1568	1758	1808	1939
HPT m_c/m_{25}[%]	19.08	19.08	19.08	19.08	19.08
LPT m_c/m_{25}[%]	0	0	0	0	0
N1 [%]	100	96.03	106	98.56	102.7
N2 [%]	100	98.25	104.58	105.44	109.43
TSFC [g/kN/s]	13.54	13.84	14.04	6.57	6.93
$EISNO_X$ [g/kg]	1.12	0.88	2.08	4.05	6.93

6.2. ITB

Adding an ITB is already known to reduce the maximum temperature in the engine by replacing some of the fuel of the main combustion chamber to a second combustion chamber after the HPT. It is noticeable in the results that this shift is not necessary during TOC. The N1 spool speed limits the TOC condition and the ITB does not reduce this. One other aspect is that the temperature limit during take-off SLS ISA does not reach the maximum temperature of SLS ISA+25 when no fuel is added to the ITB. A choice between a slightly worse TSFC in ground operations or a reduction in NO_X emissions is created. The cases presented are the cases for which during SLS ISA+25 an ITB energy fraction of 0.1,0.15 and

0.3 is used for the design of the cooling system. This gives a representation along the optimized result and a view on what happens for high ITB energy fractions. It is noticeable that for the ITB10 case seen in table 6.2, the flat rated temperature is the designed temperature while no cooling is needed inside the LPT. This is because the optimizer chose the maximum LPT temperature to be 1450K, the exact temperature for which no cooling is needed. A higher ITB fraction than 0.1 will require cooling in the LPT and it is therefore not possible to increase the flat rated temperature of the ITB10 case. This effect of reducing the NO_X emissions during take-off is noticeable for all ITB-engines. A choice can be made on how much fuel is burned in the ITB. The fuel from the main combustion chamber can be sent to the ITB if the TT46 maximum is not exceeded. This can significantly reduce the NO_X emission during take-off operations that are not constrained by inlet temperature such as for the ISA+0 condition. In the ITB-engine with a design ITB energy fraction of 0.1, The LPT limiting temperature is not yet reached (lower than 1450K). A higher energy fraction is thus possible. This temperature limit is reached for an energy fraction of 0.23 on this engine configuration. This does lower the TIT and has an effect on the emissions and the TSFC. The reduced NO_X emissions however are now 58% lower for an increase in TSFC of 6.5% during take-off at ISA+0. In contrary to no fuel in the ITB during SLS ISA+0 which minimizes the TSFC during this condition.

Table 6.2: Summarized results for ITB with design flat rated fuel split of 0.10

Parameters ITB10	Design 55kN	Cruise 47kN	TOC ISA+15 60kN	TO no ITB ISA 300kN	TO ITB10 ISA 300kN	TO ITBmax ISA 300kN	TO ISA+25 300kN
W1 [kg/s]	517	498.77	512.57	1197.78	1196.32	1192.57	1147.22
BPR [-]	12.47	13.03	12.2	12.75	13.08	14.09	13.09
OPR [-]	70	63.79	74.25	60.57	57.71	52.76	57.58
Fan PR [-]	1.52	1.45	1.57	1.43	1.43	1.44	1.43
LPC PR [-]	4.91	4.75	5.01	4.47	4.88	5.43	4.89
HPC PR [-]	9.34	9.24	9.45	9.46	8.24	6.76	8.21
TT4 [K]	1875	1745	1766	1576	1623	1696	1817
TT46 [K]	1157	1123	1268	1312	1347	1450	1450
HPTm_c/m_{25}[%]	14.92	14.92	14.92	14.92	14.92	14.92	14.92
LPTm_c/m_{25}[%]	0	0	0	0	0	0	0
N1 [%]	100	95.96	106	98.46	98.43	98.38	102.57
N2 [%]	100	98.17	104.57	105.44	98.05	90.8	101.81
TSFC [g/kN/s]	13.52	13.82	14.03	6.56	6.67	6.99	7.04
$EISNO_X$ [g/kg]	1.14	0.9	2.13	4.14	3.23	2.72	5.51

The optimal TSFC for on-design was found for the case were the cooling system is designed for an ITB fraction of 0.15. The results for an ITB fraction of 0.15 for off-design are shown in table 6.3. A higher ITB configuration shows lower NO_X emissions and lower TSFC during all phases except SLS ISA+25. The cooling requirements in the HPT are lower but in the LPT, the cooling requirements are higher to fulfil the hot day take-off requirement. The optimiser chooses a lower BPR for this case than for the case where ITB fraction is 0.1. The reason for this can be seen in the take-off limitation. The OPR for this case during take-off is lower but the BPR is higher. This is an interesting relation following from increasing the ITB fraction noticed already in the on-design performance. The pressure ratio will go down and the bypass ratio will go up. This is also noticeable in table 6.3 between the ISA+0 conditions. The ITB fraction goes from 0 to the limited maximum. During this transition, the NO_X emission reduce. The BPR increases and the OPR reduces.

Table 6.3: Summarized results for ITB with design flat rated fuel split of 0.15

Parameters ITB15	Design 55kN	Cruise 47kN	TOC ISA+15 60kN	TO no ITB ISA 300kN	TO ITB15 ISA 300kN	TO ITBmax ISA 300kN	TO ISA+25 300kN
W1 [kg/s]	517	498.83	512.56	1198	1195.42	1191.55	1146.29
BPR [-]	12.41	12.97	12.14	12.68	13.29	14.39	13.32
OPR [-]	70	63.8	74.25	60.58	56.16	51.26	55.91
Fan PR [-]	1.52	1.45	1.56	1.43	1.43	1.44	1.43
LPC PR [-]	4.88	4.71	4.98	4.44	5.06	5.53	5.08
HPC PR [-]	9.42	9.31	9.54	9.53	7.74	6.46	7.68
TT4 [K]	1598	1552	1740	1787	1698	1662	1824
TT46 [K]	1152	1118	1263	1305	1369	1480	1481
HPT $m_c/m_{25}[\%]$	12.06	12.06	12.06	12.06	12.06	12.06	12.06
LPT $m_c/m_{25}[\%]$	0.07	0.07	0.07	0.07	0.07	0.07	0.07
N1 [%]	100	95.97	106	98.5	98.46	98.41	102.6
N2 [%]	100	98.15	104.58	105.4	95.31	89.09	98.76
TSFC [g/kN/s]	13.49	13.79	14	6.54	6.74	7.08	7.12
$EISNO_X$ [g/kg]	1.07	0.84	1.99	3.86	2.81	2.44	4.76

The following presented case is for an ITB fraction of 0.3. This is the optimal take-off energy fraction. The fact that the engine has to be overdesigned (higher cruise thrust) resulted in a higher take-off energy fraction. The results are presented in table 6.4. Everything between 0.15 and 0.3 follows a consistent trend. A slightly better TSFC and lower NO_X emissions. The design BPR is again lower and during TO, it is seen that a higher ITB energy fraction increases the BPR and lowers the OPR. This has the effect that the cooling temperature is lower, but the core becomes more powerful and requires more cooling. This shows that a higher ITB energy fraction is better for engines with a higher design specific thrust. The case where the design ITB fraction is 0.4 is not presented since the TSFC for this case increased to a cruise TSFC of 13.98 (+1.5%).

Table 6.4: Summarized results for ITB with design flat rated fuel split of 0.30

Parameters ITB30	Design 55kN	Cruise 47kN	TOC ISA+15 60kN	TO no ITB ISA 300kN	TO ITB30 ISA 300kN	TO ITBmax ISA 300kN	TO ISA+25 300kN
W1 [kg/s]	517	498.97	512.55	1198.45	1190.6	1187.14	1141.86
BPR [-]	11.55	12.07	11.3	11.78	13.7	14.85	13.68
OPR [-]	70	63.82	74.25	60.65	50.07	45.99	50.09
Fan PR [-]	1.52	1.45	1.56	1.43	1.43	1.44	1.43
LPC PR [-]	4.52	4.38	4.61	4.12	5.21	5.46	5.2
HPC PR [-]	10.2	10.06	10.33	10.28	6.7	5.86	6.71
TT4 [K]	1510	1466	1646	1686	1565	1547	1683
TT46 [K]	1104	1070	1212	1248	1448	1559	1559
HPT $m_c/m_{25}[\%]$	4.47	4.47	4.47	4.47	4.47	4.47	4.47
LPT $m_c/m_{25}[\%]$	0.31	0.31	0.31	0.31	0.31	0.31	0.31
N1 [%]	100	96	106	98.61	98.52	98.5	102.67
N2 [%]	100	98.05	104.64	105.37	87.93	83.84	91.47
TSFC [g/kN/s]	13.48	13.77	13.98	6.52	7.17	7.5	7.56
$EISNO_X$ [g/kg]	0.84	0.65	1.57	3	1.79	1.62	3.04

6.2.1. results

The optimal case for ITB-engines is the case with an ITB energy fraction of 0.3. An reduction in the TSFC of 0.6% and a decrease in NO_X emissions from 26% in cruise to 60% at take-off compared to the conventional engine. This is a significant improvement to the on-design results. A higher specific

thrust is more beneficial for ITB architecture.

6.3. IC

The modified results for the IC based upon the TOC ISA+25 condition will be presented in this section. The only presented results will be the case for an effectiveness of 0.3,0.5 and 0.7. This is done to see if the results follow the same trend, namely a higher effectiveness is better despite the scaling pressure losses. It is noticeable that the NO_X emissions are lower than for the on-design engine. An increase in specific thrust decreases the NO_X emissions for the engine during cruise.

In table 6.5, the results will be presented for the IC with an effectiveness of 0.3. This case is followed by the case with an effectiveness of 0.5 seen in table 6.6. It shows that a higher effectiveness is still beneficial to reduce the NO_X emissions and the TSFC for a given specific thrust. Lastly, the case for an effectiveness of 0.7 is shown. Again, the TSFC and the NO_X emissions are better for the higher effectiveness as seen in table 6.7

Table 6.5: Summarized results for IC with an effectiveness of 0.3

Parameters IC30	Design 55kN	Cruise 47kN	TOC ISA+15 60kN	TO ISA 300kN	TO ISA+25 300kN
W1 [kg/s]	517	499	514	1198	1148
BPR [-]	14.25	14.93	13.91	14.56	14.58
OPR [-]	70.03	63.75	74.75	61.01	60.82
Fan PR [-]	1.52	1.45	1.57	1.44	1.44
LPC PR [-]	2.97	2.9	3.03	2.8	2.81
HPC PR [-]	15.78	15.43	16.08	15.92	15.81
TT4 [K]	1711	1665	1868	1934	2074
HPT $m_c/m_{25}[\%]$	21.09	21.09	21.09	21.09	21.09
LPT $m_c/m_{25}[\%]$	0	0	0	0	0
N1 [%]	100.01	95.96	106	98.76	102.91
N2 [%]	100.02	97.84	104.91	106.17	110.16
TSFC [g/kN/s]	13.5	13.78	13.98	6.59	6.95
$EISNO_X$ [g/kg]	1.16	0.93	2.14	4.38	7.35

Table 6.6: Summarized results for IC with an effectiveness of 0.5

Parameters IC50	Design 55kN	Cruise 47kN	TOC ISA+15 60kN	TO ISA 300kN	TO ISA+25 300kN
W1 [kg/s]	517	499	513	1197	1148
BPR [-]	14.69	15.4	14.34	15.01	15.04
OPR [-]	70	63.68	74.74	61.14	60.93
Fan PR [-]	1.52	1.45	1.56	1.44	1.44
LPC PR [-]	2.84	2.79	2.89	2.74	2.76
HPC PR [-]	16.73	16.27	17.09	16.8	16.65
TT4 [K]	1669	1625	1823	1897	2035
HPT $m_c/m_{25}[\%]$	18.09	18.09	18.09	18.09	18.09
LPT $m_c/m_{25}[\%]$	0	0	0	0	0
N1 [%]	100	95.96	106	99.01	103.18
N2 [%]	100	97.68	104.93	106.39	110.23
TSFC [g/kN/s]	13.43	13.73	13.94	6.6	6.96
$EISNO_X$ [g/kg]	0.92	0.74	1.68	3.54	5.86

Table 6.7: Summarized results for IC with an effectiveness of 0.7

Parameters IC70	Design 55kN	Cruise 47kN	TOC ISA+15 60kN	TO ISA 300kN	TO ISA+25 300kN
W1 [kg/s]	517	499	513	1196	1147
BPR [-]	14.93	15.67	14.57	15.28	15.31
OPR [-]	70	63.64	74.74	61.23	61.04
Fan PR [-]	1.52	1.45	1.56	1.44	1.44
LPC PR [-]	2.63	2.59	2.67	2.58	2.6
HPC PR [-]	18.31	17.72	18.73	18.39	18.21
TT4 [K]	1634	1593	1785	1870	2007
HPT m_c/m_{25}[%]	16.1	16.1	16.1	16.1	16.1
LPT m_c/m_{25}[%]	0	0	0	0	0
N1 [%]	100	95.97	106.25	99.14	103.34
N2 [%]	100	97.57	104.94	106.74	110.57
TSFC [g/kN/s]	13.4	13.72	13.9	6.62	6.98
$EISNO_X$ [g/kg]	0.76	0.62	1.37	3.01	4.92

6.4. IC and ITB

In this section, the combined cycle results will be presented. For all the intercooled cycles, the best ITB results are given. This is to evaluate whether an ITB and an IC benefit from each other. The results for the combined cycle with an effectiveness of 0.3 had an optimal ITB energy fraction of 0.25. This is seen in table 6.8. The cruise TSFC is slightly lower than for the IC alone by 0.2%. The real difference lies in the NO_X emissions. At hot day take-off, a reduction of 55% is achieved and during cruise a reduction of 34% is achieved. At take-off, the ITB offers an extra degree of freedom when the temperature limits are not reached. A choice can be made to reduce to NO_X between 34% and 57% based on how much fuel is added into the ITB. This reduces the NO_X emissions immensely compared to the intercooled engine. It is also an improvement compared to the ITB-engine since both the NO_X emissions and TSFC are also improved considering the optimal ITB case.

Table 6.8: Summarized results for combined cycle with effectiveness of 0.3 and ITB energy fraction of 0.25.

Parameters IC30ITB25	Design 55kN	Cruise 47kN	TOC ISA+15 60kN	TO no ITB ISA 300kN	TO ITB25 ISA 300kN	TO ITBmax ISA 300kN	TO ISA+25 300kN
W1 [kg/s]	517	499	513	1198	1190	1187	1141
BPR [-]	12.86	13.46	12.57	13.1	15.45	16.73	15.46
OPR [-]	70	63.72	74.6	61.07	50.62	46.83	50.55
Fan PR [-]	1.52	1.45	1.56	1.43	1.44	1.44	1.44
LPC PR [-]	2.62	2.57	2.67	2.47	2.97	3.09	2.98
HPC PR [-]	17.93	17.48	18.3	18.02	12.34	11.03	12.37
TT4 [K]	1530	1488	1672	1726	1658	1661	1786
TT46 [K]	1083	1052	1192	1238	1461	1578	1579
HPT m_c/m_{25}[%]	5.83	5.83	5.83	5.83	5.83	5.83	5.83
LPT m_c/m_{25}[%]	0.47	0.47	0.47	0.47	0.47	0.47	0.47
N1 [%]	100	95.99	106.17	98.87	98.73	98.74	102.92
N2 [%]	100	97.74	104.94	106.17	89.36	85.75	93.14
TSFC [g/kN/s]	13.45	13.75	13.95	6.56	7.24	7.56	7.65
$EISNO_X$ [g/kg]	0.76	0.61	1.42	2.88	1.97	1.87	3.32

The results for an effectiveness of 0.5 came to an optimal ITB energy fraction of 0.25 and is presented in table 6.9. The results follow the trend of the combined cycle with an effectiveness of 0.3. Small impact on the TSFC but big impact on the NO_X emissions, though smaller. During cruise, a reduction of 26% is achieved compared to the intercooled case and during take-off a reduction between

25% and 52% is accomplished based on how much fuel is added into the ITB.

Table 6.9: Summarized results for combined cycle with effectiveness of 0.5 and ITB energy fraction of 0.25.

Parameters IC50ITB25	Design 55kN	Cruise 47kN	TOC ISA+15 60kN	TO no ITB ISA 300kN	TO ITB25 ISA 300kN	TO ITBmax ISA 300kN	TO ISA+25 300kN
W1 [kg/s]	517	499	513	1197	1189	1186	1140
BPR [-]	13.25	13.88	12.94	13.5	16.15	17.46	16.16
OPR [-]	70	63.73	74.66	61.25	50.21	46.49	50.12
Fan PR [-]	1.51	1.45	1.56	1.44	1.44	1.44	1.44
LPC PR [-]	2.38	2.34	2.42	2.3	2.71	2.8	2.71
HPC PR [-]	20	19.41	20.45	20.09	13.92	12.46	13.89
TT4 [K]	1520	1480	1661	1727	1668	1670	1794
TT46 [K]	1080	1050	1189	1244	1488	1606	1606
HPT $m_c/m_{25}[\%]$	5.85	5.85	5.85	5.85	5.85	5.85	5.85
LPT $m_c/m_{25}[\%]$	0.18	0.18	0.18	0.18	0.18	0.18	0.18
N1 [%]	100	96.01	106	99.07	98.97	98.95	103.13
N2 [%]	100	97.63	104.97	106.58	89.62	85.89	93.26
TSFC [g/kN/s]	13.45	13.75	13.95	6.6	7.33	7.63	7.73
$EISNO_X$ [g/kg]	0.68	0.55	1.25	2.66	1.82	1.71	3.01

The results for an effectiveness of 0.7 came to an optimal ITB energy fraction of 0.20 and is presented in table 6.9. It is noticeable that for a high effectiveness, the ITB becomes less of an improvement to the TSFC. For the case were effectiveness is 0.7, the combined cycle performs slightly worse than the intercooled cycle by 0.14%. The NO_X reductions are however still achievable. During cruise, a reduction of 18% is found and during take-off a reduction between 19% and 45% is found. This shows that the improvements of adding an ITB to an intercooled engine become less significant for higher intercooled effectiveness. The maximum achievable effectiveness is however not 1 currently. Based upon the previous research by Kyprianidis et al. and Xin Zhao et al.[7, 10], an IC effectiveness of 0.5 is close to what was found by CFD simulations. This is what will be used to compare the cycles. It should be noted that when a higher effectiveness is possible despite a larger pressure loss, this would be beneficial.

Table 6.10: Summarized results for combined cycle with effectiveness of 0.7 and ITB energy fraction of 0.2.

Parameters IC70ITB20	Design 55kN	Cruise 47kN	TOC ISA+15 60kN	TO no ITB ISA 300kN	TO ITB20 ISA 300kN	TO ITBmax ISA 300kN	TO ISA+25 300kN
W1 [kg/s]	517	499	513	1196	1190	1187	1141
BPR [-]	14.02	14.7	13.68	14.31	16.34	17.66	16.35
OPR [-]	70	63.67	74.71	61.33	52.62	48.76	52.57
Fan PR [-]	1.51	1.45	1.56	1.44	1.45	1.45	1.45
LPC PR [-]	2.42	2.39	2.46	2.38	2.71	2.81	2.71
HPC PR [-]	19.93	19.27	20.39	20	15.05	13.44	15.03
TT4 [K]	1530	1490	1671	1749	1689	1693	1817
TT46 [K]	1102	1073	1213	1278	1458	1571	1573
HPT $m_c/m_{25}[\%]$	6.98	6.98	6.98	6.98	6.98	6.98	6.98
LPT $m_c/m_{25}[\%]$	0.18	0.18	0.18	0.18	0.18	0.18	0.18
N1 [%]	100	96	106.21	99.25	99.17	99.14	103.34
N2 [%]	100	97.56	104.94	106.84	92.44	88.23	96.26
TSFC [g/kN/s]	13.43	13.74	13.93	6.63	7.15	7.44	7.54
$EISNO_X$ [g/kg]	0.62	0.51	1.12	2.46	1.75	1.64	2.87

6.5. Comparison

Comparing the conventional engine, the intercooled engine, the ITB-engine and the engine with both an IC and an ITB will be done in this section.

The conventional engine is the baseline used and this engine shows quite high results for NO_X emissions with a TSFC of 13.84 during cruise at 47kN. The maximum temperature in the engine is 1939K and the cooling extracted from the HPC accounts for 19.08% of the mass going in. The optimal engine for an ITB is found for the fuel split ratio of 0.3. This engine shows a reduction of the TSFC of 0.5%, 26% reduction for the NO_X emissions for the cruise condition and a reduction during take-off between 26% and 60%.

The used effectiveness for comparison is the effectiveness of 0.5 as stated previously since this is closest to a real achievable intercooled engine. This engine shows a reduction towards the conventional engine for the TSFC of 0.8% and a reduction for the NO_X emissions during cruise of 16% and 14% during take-off. The intercooled engine shows better results than the optimal ITB-engine for fuel economy. It also reduces the NO_X emissions more during cruise but less during take-off.

The combined cycle is the most efficient cycle with a constant effectiveness of 0.5 and an ITB fuel fraction of 0.25. It shows a TSFC reduction of 0.7% as compared to the conventional engine. No improvement is seen compared to the intercooled engine. The NO_X emissions do differ a lot. During cruise, a reduction of 37% is found and during take-off a reduction between 34% and 58% is found compared to the conventional engine. An improvement compared to both the intercooled and ITB-engines. The results for cruise condition are visible in table 6.11 and the results for take-off are visible in table 6.12. The engines having an ITB have 2 results for take-off. The first result is the design ITB energy fraction and the second result is the maximum ITB energy fraction without exceeding the LPT temperature limit of 1450K. The first value is no fuel to the ITB (optimal TSFC) and the second value is the maximum amount of fuel to the ITB such that TT46 does not go higher then TT46 during hot day take-off (optimal NO_X emissions).

Table 6.11: Cruise comparison of TSFC and NO_X emissions.

parameter	cruise		Δ	
	TSFC [g/kN/s]	$EISNO_X$[g/kg]	TSFC [Δ%]	$EISNO_X$ [Δ%]
Conventional	13.84	0.88	0%	0%
ITB30	13.77	0.65	-0.5%	-26%
IC50	13.73	0.74	-0.8%	-16%
IC50ITB25	13.75	0.55	-0.7%	-38%

Table 6.12: Take-off comparison of TSFC and NO_X emissions.

parameter	Take-off ISA+0		Δ	
	TSFC [g/kN/s]	$EISNO_X$[g/kg]	TSFC [Δ%]	$EISNO_X$ [Δ%]
Conventional	6.57	4.05	0%	0%
ITB30	6.52	3	-0.8%	-26%
	7.5	1.62	+14%	-60%
IC50	6.6	3.54	+0.5%	-13%
IC50ITB25	6.6	2.66	+0.5%	-34%
	7.63	1.71	+16%	-58%

7

Exergy Analysis

To analyse where all the individual component losses in the engine are, an exergy analysis is performed on the different cycles. The optimal ITB-engine will be compared with the ITB15 engine. The IC50 engine will be compared with both the IC30 and IC70 engine and lastly the conventional engine, the ITB30, the IC50 and the IC50ITB25 engine will be compared since they are the optimal designs for the specific architecture. The conventional engine is used as baseline to compare. The methodology is explained in Chapter 3.

7.1. ITB

The exergy analysis is performed on both the cruise condition and the take-off condition at ISA+25. Since the speed of the engine is 0 during the take-off condition, the thrust power is 0. This shows as extra loss in both the cold exhaust and the hot exhaust. The results for cruise flight are presented in figure 7.1. The results for SLS ISA+25 are visible in figure 7.2. c_1 is the main combustion chamber, c_2 is the ITB, cd is the cold duct and $cold_e$ is the cold exhaust. It is noticeable that the ITB shifts the losses during operation. Adding an ITB means less cooling is needed in the system. More air must be compressed to the maximum pressure (cooling air for later stages in the turbine is extracted at lower temperatures). Because less air is extracted for cooling, the losses in the HPC are higher. In return less cooling is needed and the losses in the HPT are lower. The losses in the main combustion chamber also become larger for a higher ITB fraction during take-off. The only difference here is how much air goes through the combustion chamber and how much air goes around it. It is more beneficial to heat the air to a higher temperature with less air instead of a lower temperature with more air. The cold and hot exhaust are both more beneficial for the ITB cycle and no changes for the fan.

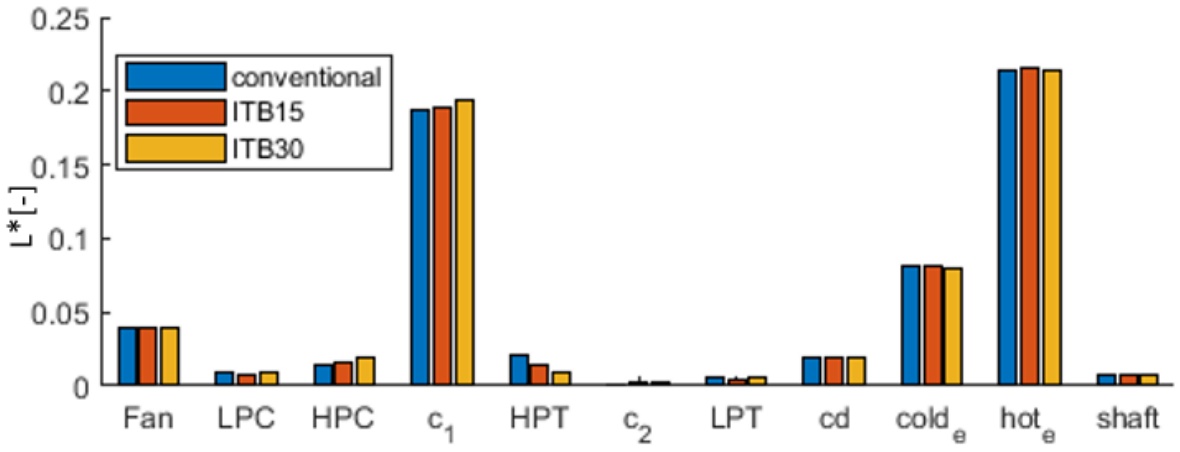

Figure 7.1: Exergy destroyed in each component for the ITB configuration during cruise.

During take-off condition, the losses of the main combustion chamber are now split towards the ITB combustion chamber. This in turn lowers the losses in the cold exhaust and increases the losses in the hot exhaust which is as expected. More fuel is added to the system in total and this translates to a higher enthalpy at the end of the cycle.

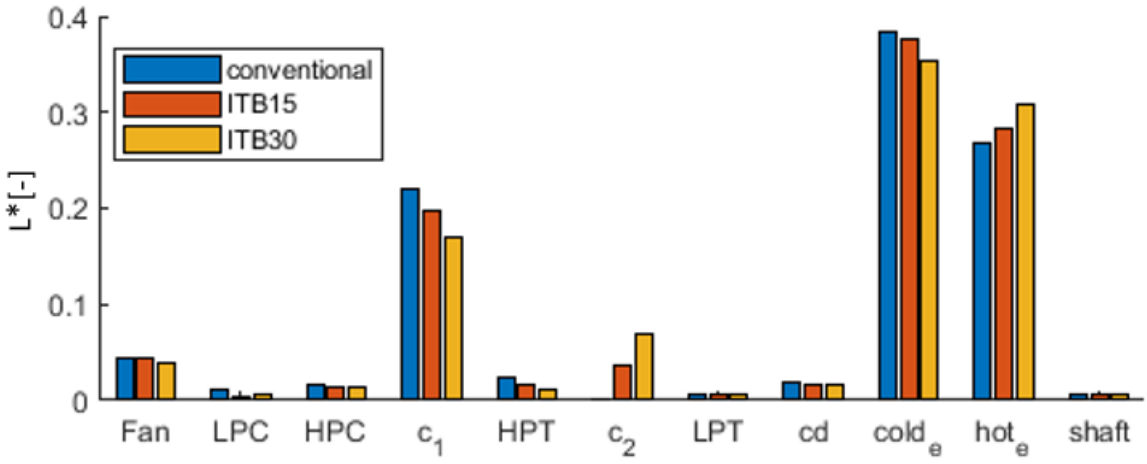

Figure 7.2: Exergy destroyed in each component for the ITB configuration during hot day take-off.

7.2. IC

The results for the IC during cruise are presented in figure 7.3 and during take-off are presented in figure 7.4. The same trend is seen as for the ITB in the combustion chamber because of the cooling. More losses are expected in the combustion chamber for a higher effectiveness. A higher effectiveness also increases the losses in the IC. An effect of the IC configuration was that a higher effectiveness increased the pressure ratio of the HPC and reduced the pressure ratio of the LPC. Therefore, the LPC losses are almost completely gone. The HPC losses are larger despite that the compression happens at a lower temperature since the pressure ratio is larger. The combined losses during compression are lower. In the HPT the effect of reduced cooling is visible. The pressure ratio in the HPT is higher for the intercooled cases but the losses for the highest effectiveness are almost equal to what is lost in the conventional HPT. This is also observed in the LPT. The losses are reduced while most of the power of the LPT goes to the unchanged fan. The cold duct and the intercooled duct (icd) have an almost constant loss. The loss in the cold exhaust is lower for the intercooled cases since some of the air that normally goes through the cold duct now goes through the intercooled duct. The losses in the intercooled exhaust increase for a higher effectiveness since the air comes out at a higher enthalpy. The losses in the hot exhaust are significantly lower for a higher effectiveness and the losses in the shaft also reduce since less power must go through the shaft.

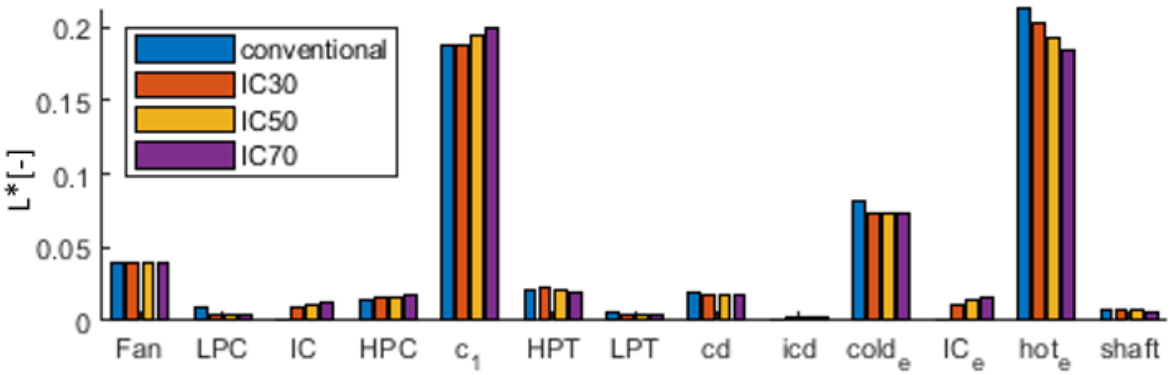

Figure 7.3: Exergy destroyed in each component for the intercooled configuration during cruise.

Similar results are seen during take-off. This is because the constant effectiveness in all operations.

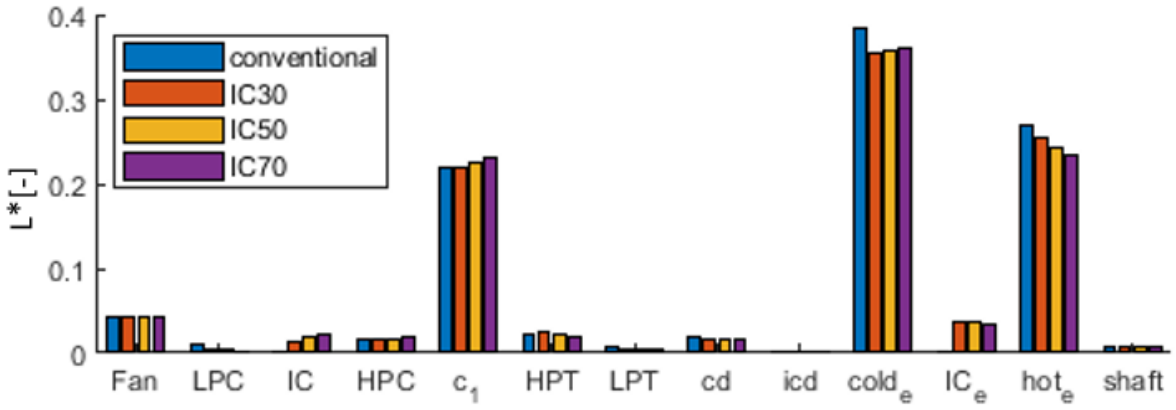

Figure 7.4: Exergy destroyed in each component for the intercooled configuration during hot day take-off.

7.3. Combined

In the combined cycle it is seen that both architectures add the losses in the combustion chamber in figure 7.5 and figure 7.6. The combined cycle has slightly lower losses inside the IC since the BPR is higher. Addition of the ITB is seen to reduce the losses in the HPT significantly. The IC lowers the losses in the exhaust more than the ITB. The combined cycle needs least power in the shaft. Most of the shaft power reduction is from the more efficient compression from the IC but the ITB also reduces the shaft power by increasing the BPR.

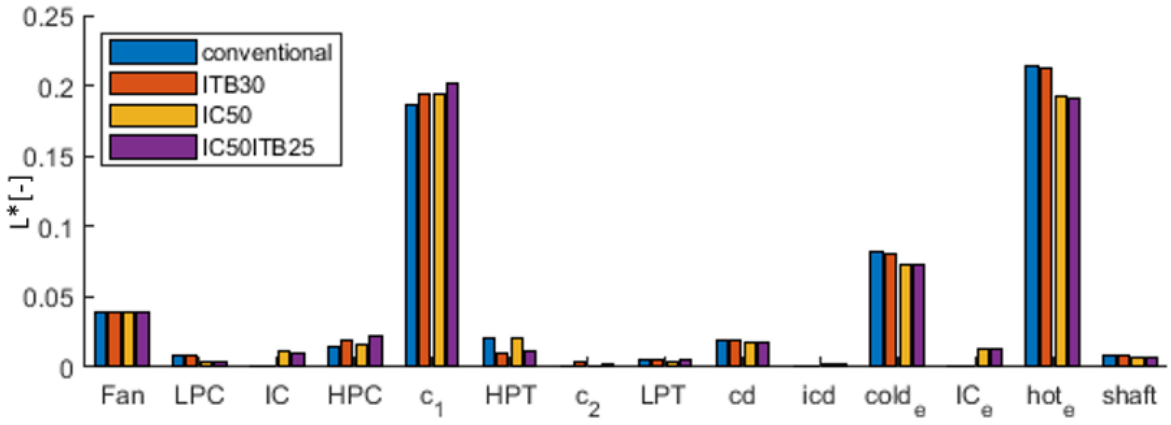

Figure 7.5: Exergy destroyed in each component for all configurations during cruise.

The same trend is seen during take-off with the difference that the ITB now consumes fuel and this is seen in the ITB combustion chamber. This increases the losses in the hot exhaust since this increases the enthalpy at the end of the cycle.

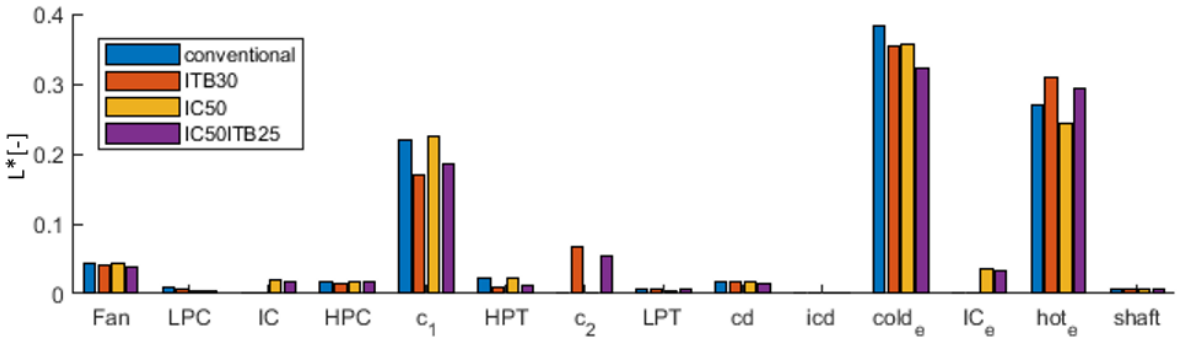

Figure 7.6: Exergy destroyed in each component for all configurations during hot day take-off.

The main benefits that are given by intercooling an engine with respect to the TSFC are in the compressor. The lower temperature at the HPC inlet lowers the power needed and this reduces the associated losses. It also reduces the temperature after the combustion chamber, and this is visible at the exhaust where less power is lost due to it being unusable. The benefits of the ITB with respect to the exergy are that it reduces the cooling needs and reduces the lost power due to this during cruise. During take-off or when the ITB is burning fuel, it increases the TSFC and this is mainly from exergy lost in the core exhaust. A benefit that cannot be seen in the exergy analysis is the extra degree of freedom in operation at sea level conditions. In figure 7.7 the comparison to the conventional is presented for cruise and in figure 7.8 this is done for take-off.

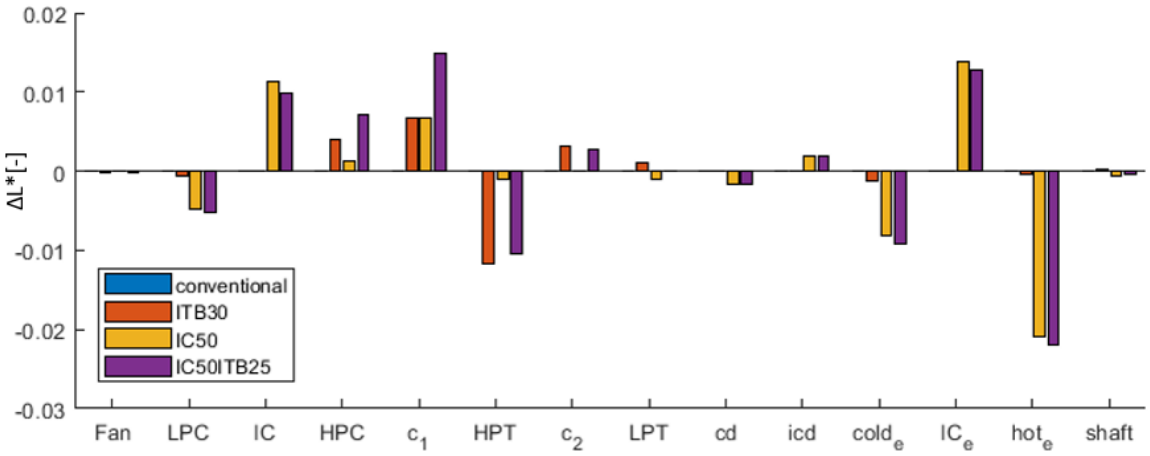

Figure 7.7: Exergy destroyed in each component compared to the conventional engine during cruise.

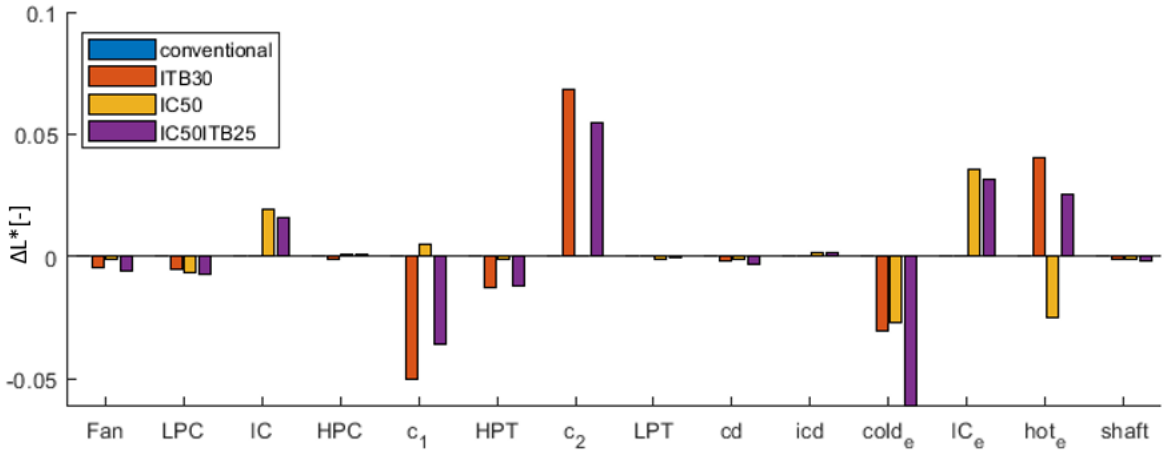

Figure 7.8: Exergy destroyed in each component compared to the conventional engine during take-off.

8

Conclusions

This chapter makes conclusions on the results presented in the thesis.

Firstly, the parameter analysis shows that it is important to keep the cooling flows rather small. If this is fulfilled, it is best to maximize the pressure ratio and the BPR. An intercooler allows for higher pressure ratio while keeping the compressor exit temperature low and an ITB allows to keep the TIT low which both benefit cooling. For the IC-engine, the cold side pressure loss is more detrimental for the TSFC as the hot side pressure loss. The reason for this is because there is a higher mass flow going through the cold side. If the mass through the cold side is reduced, the heat transfer becomes limited by the cold side instead of the hot side.

In the on-design optimization, it is seen that a 25% reduced cooling mass flow results in a 1% more fuel efficient baseline engine. For the IC-engine, it is 0.7% more efficient. For the ITB-engine this results in a 0.8% more efficient engine. For the IC-ITB engine, it results in a 0.6% more efficient engine. This shows that cooling efficiency is more important for the conventional engine and becomes less impactful as the IC and ITB architectures are added. The on-design optimization also shows that an ITB-engine where the ITB burns all the time (take-off and cruise) is less efficient than an ITB-engine where the ITB burns only during take-off. An ITB should thus only be used as a method to change take-off behaviour since it is too detrimental for the TSFC during cruise.

In the on-design optimization, the NO_X emissions are also investigated. This shows a reduction of all novel cycles compared to the baseline engine. An ITB engine lowers the NO_X emissions more during take-off. An IC engine lowers the NO_X emissions more during cruise. Combining the cycle into the IC-ITB engine lowers the NO_X emissions even more but not by the same degree as only an ITB or an IC. This is seen on both cooling models.

8.1. Off-Design conclusion

The off-design optimization delivers quantifiable results since this is an engine that accounts for more operating conditions. This showed that all the engines in the on-design optimization needed to be changed to meet the off-design conditions. Where design thrust for the on-design engines was equal to the cruise thrust (47kN),the off-design conditions changed the design thrust to 55kN for all engine architectures. This was since the limiting factor was the low pressure spool speed. This was limited to 106% (100%=design N1). An IC and an ITB had no influence on N1 and had the same new design thrust as the baseline engine. This new baseline engine was 2.5% less TSFC efficient. Mainly because the BPR was lower. Following from this is a larger core which reduces the temperatures for quasi the same fuel flow (2.5% more). Thus the NO_X emissions during cruise were 25% better than for the on-design engine from this as well. The IC-engine used for comparing is the engine with an effectiveness of 0.5. This engine had a 2.6% higher TSFC than its on-design counterpart. This also had lower NO_X emissions. The ITB-engine used for comparing is the most efficient ITB-engine. Namely with an ITB energy fraction of 0.3. This is different than the optimal energy fraction for the previous on-design iteration which had an optimal energy fraction of 0.15. A design ST that is higher thus results in a higher optimal energy fraction. Compared to its previous on-design counterpart, the TSFC was 2.5% higher during cruise. The IC-ITB engine has an effectiveness of 0.5 and an ITB energy fraction of 0.25,

which shows that combining the 2 diminishes the effects of the ITB. The IC-ITB engine has also a 2.5% increased TSFC compared to its optimal on-design counterpart.

Comparing the off-design engines to the baseline engine which has a TSFC of 13.84, the IC engine had a TSFC that was 0.8% lower, the ITB engine had a TSFC that was 0.5% lower and the IC-ITB engine had a TSFC that was 0.7% lower. The most efficient engine is thus the IC-engine. The effect that the IC and the ITB have on each other for the TSFC is thus not beneficial since both influence the temperatures of the core cycle. The positive effect both cycles have is larger for higher temperatures and combining them is thus not efficient for the TSFC.

The baseline engine had a higher standardized NO_X emission than LEAP. Mainly because it has a higher pressure ratio and a higher turbine inlet temperature which are both important key parameters for estimating the NO_X emissions. It was 2.2 times higher during cruise and 3.7 times higher during take-off. This shows that improving the cycle for minimal TSFC has a negative effect on the NO_X emissions. All new architectures improve this behaviour though. The IC engine lowers the NO_X emissions by 16% during cruise and 13% during take-off compared to the baseline engine. The ITB engine lowers the NO_X emissions by 26% during cruise and up to 60% during take-off compared to the baseline engine. The IC-ITB engine lowers the NO_X emissions by 38% during cruise and up to 58% during take-off compared to the baseline engine. This is take-off reduction seen in the ITB-engine and the IC-ITB engine is from increasing the ITB energy fraction during ISA SLS+0 above the design ITB energy fraction. This is possible since the design ITB energy fraction is based upon the SLS ISA+25 condition. The ISA SLS+0 condition has a lower air inlet temperature. This lowers the overall temperature in the engine. The maximum temperature limits are however still in place. The maximum LPT inlet temperature is still 1450K. The ITB energy fraction can be higher in the ISA SLS+0 condition up until it reaches this 1450K. This results in an increased TSFC during take-off (15%) and reduced NO_X emissions. The ITB energy fraction can also be lowered in this condition up until the maximum TIT temperature is reached. This results in reduced NO_X emissions of -26% for the ITB-engine and -34% for the IC-ITB engine compared to the baseline engine. This does decrease the TSFC such that it is -0.8% lower during take-off for the ITB engine compared to the baseline engine. and 0.5% higher during take-off for the IC-ITB engine compared to the baseline engine. The IC engine has a 0.5% increased TSFC compared to the baseline engine during take-off at ISA+0.

In the exergy analysis it is seen that the components which lose the most exergy are: the fan, the combustion chambers and the exhausts. A bit lower but still noteworthy are the compressors and the turbines. The component which losses the least is the shaft. In cruise flight, the different architectures have almost no influence in the losses in the fan. The IC-engine and the IC-ITB engine lower the losses in the LPC. This is mainly because these architectures lower the LPC pressure ratio and increase the HPC pressure ratio. The IC has losses from the pressure losses. Lowering these can be important to increase the benefit of an IC engine. In the HPC it is seen that the ITB has an increased loss compared to the conventional and the IC also has an increased loss but smaller. The IC-ITB engine adds these losses. The reason is that less cooling means a larger portion of the HPC mass flow is compressed to the maximum pressure (bleed flows for later stages in the turbine). This effect is lower on the IC-engine since this engine increases the BPR more than the ITB engine. In the combustion chamber, the new architectures increase the losses. This is added for the IC-ITB engine. The losses in the HPT are reduced most for the ITB-engine and the IC-ITB engine. The ITB reduces the cooling flow most thus the efficiency is highest. Then until the exhaust there are almost no significant differences in losses. The IC-engine and the IC-ITB engine reduces the losses in the cold exhaust but the losses in the Intercooled exhaust are higher than the reduction since heat is added to this part. The reduction of losses in the hot exhaust is high for the IC-engine and the IC-ITB engine. During take-off, almost the same thing happens. Except, the ITB-engine and the IC-ITB engine shift losses from the main combustion chamber to the ITB which is less efficient. The ITB increases the losses in the hot-exhaust and reduces the loses in the cold exhaust which it did not do during cruise (not burning) and reduces the losses in the cold exhaust. This is because now the core cycle delivers more thrust and thus the bypass needs to deliver less thrust. Adding all the results, it follows that both cycles have net positive effect compared to the baseline engine for the TSFC. The ITB improves the HPT most and is negative for the combustion chambers and the IC improves the hot exhaust significantly while adding losses in the IC from the heat transfer and thus also in the exhaust of the IC.

8.2. Research questions

Then to look at the research questions:

1. Is the proposed architecture better from an emission viewpoint?
    - The CO_2 emissions are lower in all new architectures but best when only using an IC.
    - The NO_X emissions are lower in all new architectures but decrease significantly more for the IC-ITB engine.
2. Is the proposed architecture better from a fuel economy viewpoint?
    - The same as for the CO_2 emissions, it is better for all new architectures but best for the IC engine with a 0.1% margin.
3. What is the maximum temperature in the engine?
    - The maximum TIT in the conventional engine is 1939K during hot day take-off, 1683K for the ITB-engine, 2035K for the IC-engine and 1794K for the IC-ITB engine. The IC engine reaches a hotter TIT by 96K compared to the baseline engine. The maximum TIT in the ITB-engine is 256K lower than for the baseline engine and the maximum TIT in the IC-ITB engine is 145K lower compared to the baseline engine. The addition of an ITB decreases the maximum TIT and the addition of an IC increases the maximum TIT. The effect of the ITB is larger.
4. What are the design and operational challenges?
    - Adding an IC is a challenge since the IC needs to be fitted in the bypass. The pressure losses need to be minimized while the heat transfer needs to be maximized. The IC discussed here is a passive component. Adding an ITB is adding a new segment in between the HPT and the LPT. This will make the engine longer and could reduce reliability since it is a component that has active elements in it (fuel pump).m TIT and the addition of an IC increases the maximum TIT. The effect of the ITB is larger.

The fuel reductions found for both the IC-engine and the ITB-engine were not as large as found in the literature. The TSFC for these 2 cycles matched the literature but the found TSFC for the conventional was lower. The difference in the conventional engine is a lower BPR (11.62) compared to different literature and this gave a lower TSFC. [5–18]

If only the TSFC matters, the IC-engine is the preferred engine. But NO_X emissions are also of great importance now and this shifts the favour to the IC-ITB engine. The ITB has an extremely positive impact on the NO_X emissions. It reduces the emissions compared to the IC-engine by 27% during cruise and up to 52% during take-off. This for an increase in TSFC of 0.1%. This engine also has lower maximum temperatures which can be beneficial for design choices.

9

Recommendations

This chapter includes the recommendations based on the results and on possible improvements for future work.

9.1. Recommendations from results

The research objective was to find advantages and disadvantages of an engine architecture using intercooling and inter-turbine burning and make recommendations based on the findings by simulating and optimizing the jet engine with the use of the Gas Turbine Simulation program (GSP). The model found that for the current design limitations, the IC-ITB engine was favourable. If only the TSFC matters, the IC-engine is the preferred engine. But NO_X emissions are also of great importance now and this shifts the favour to the IC-ITB engine. The ITB has an extremely positive impact on the NO_X emissions. It reduces the emissions compared to the IC-engine by 27% during cruise and up to 52% during take-off. This for an increase in TSFC of 0.1%. This engine also has lower maximum temperatures which can be beneficial for design choices. Disadvantages are the added complexity of the engine in the form of extra components.

9.2. Recommendations from methodology

This section highlights recommendations for future work and points out possible improvements on the current methodology and results.

- Exergy analysis is a handy method to split which component is responsible for which losses. This is an method that offers more insight compared to polytropic efficiencies Since all components have different mass flows and operate at different temperatures.
- Some future model implementations might increase the efficiency of all the cycles. Now, Reynold analogy was used to model the IC. This could be improved by modelling a complete IC in the engine performance model. This could give a better coupling between the heat transfer and the pressure losses.
- The pressure losses in the combustion chamber and the ITB were set constant. This also could be coupled to a combustion model which could better estimate these losses during all operation modes.
- A different fuel type in the ITB might also benefit the emissions more than the used fuel Jet-A. This combined with new combustion techniques could influence the emissions and the pressure loss in the combustion chamber.
- The NO_X emission were modelled based on a correlation, if this was included in a combustion model, the results could differ and more accurate estimation could be given.
- Since this was only a thermodynamical analysis, adding the sizing and weight can greatly improve the accuracy of this study. This would also make the design inlet mass flow a variable and this

could have interesting effects on both the IC and the ITB since both seem to perform better with higher ST. It would also account for the differences in the shaft power since less shaft power could mean a lighter shaft.

- Adding more novel architectures could change the results, for example a recuperator could change the dynamic between all the components and might thus have different results.
- It was not possible in the current design to have the IC split ratio as a design variable since the used code did not allow for this to be set variable in the API. A different method which allows more control on the optimization could allow for the integration of more design variables. The points were the bleed air was extracted (fraction of enthalpy gain) were also not variable in the API, this could have an effect since the pressure ratios were a variable.
- Off-design optimization had to be performed by checking the model to the off-design condition manual. This because the software did not allow to combine an optimized engine in an off-design setting without changing the mode from design mode to steady-state mode. A model which combined this could greatly improve the time needed to reach an optimum.

Bibliography

[1] Atmosfair. Atmosfair emissions calculator, 2018.

[2] EASA. Climate change : Programme of action, 2009.

[3] IATA. Climate change: Three targets and four pillars, 2016.

[4] David Schimel, D. Glover, J. Melack, R. Beer, R. Myneni, Y. Kaufman, C. Justice, and J. Drummond. Atmospheric chemistry and greenhouse gases. 2000.

[5] Feijia Yin and Arvind Gangoli Rao. Off-Design Performance of an Interstage Turbine Burner Turbofan Engine. *Journal of Engineering for Gas Turbines and Power*, 139, 2017.

[6] Konstantinos G. Kyprianidis, Tomas Grönstedt, S. O. T. Ogaji, P. Pilidis, and R. Singh. Assessment of Future Aero-engine Designs With Intercooled and Intercooled Recuperated Cores. *Journal of Engineering for Gas Turbines and Power*, 133(1):011701–011701–10, 2010.

[7] Konstantinos G. Kyprianidis. On Intercooled Turbofan Engines. In Andrew M. Rolt and Vishal Sethi ED1 - Ernesto Benini, editors, *Progress in Gas Turbine Performance*, page Ch. 1. IntechOpen, Rijeka, 2013.

[8] Konstantinos G. Kyprianidis, Andrew M. Rolt, and Tomas Grönstedt. Multidisciplinary Analysis of a Geared Fan Intercooled Core Aero-Engine. *Journal of Engineering for Gas Turbines and Power*, 136(1):011203–011203–11, 2013.

[9] Tomas Grönstedt and Konstantinos Kyprianidis. Optimizing the Operation of the Intercooled Turbofan Engine. *ASME Turbo Expo 2010: Power for Land, Sea, and Air, Glasgow*, 2010.

[10] Xin Zhao, Tomas Grönstedt, and Konstantinos Kyprianidis. Assessment of the performance potential for a two-pass cross flow intercooler for aero engine applications, 2013.

[11] Xin Zhao, Oskar Thulin, and Tomas Grönstedt. First and Second Law Analysis of Intercooled Turbofan Engine. *Journal of Engineering for Gas Turbines and Power*, 138(2):021202–021202–8, 2015.

[12] Dimitris Missirlis, Zinon Vlahostergios, Michael Flouros, Christina Salpingidou, Stefan Donnerhack, A. Goulas, and Kyros Yakinthos. Intercooled recuperated aero engine: development and optimization of innovative heat exchanger concepts. 2016.

[13] Christina Salpingidou, Dimitris Missirlis, Zinon Vlahostergios, Michael Flouros, Stefan Donnerhack, and Kyros Yakinthos. Numerical assessment of the performance of a heat exchanger for a low pressure ratio gas turbine. *Energy*, 164, 2018.

[14] Christina Salpingidou, Zinon Vlahostergios, Dimitris Missirlis, Michael Flouros, Fabian Donus, and Kyros Yakinthos. Investigation and assessment of the performance of various recuperative cycles based on the intercooled recuperation concept. page V003T06A020, 2018.

[15] Christina Salpingidou, Dimitris Missirlis, Zinon Vlahostergios, Michael Flouros, F Donus, and Kyros Yakinthos. Conceptual design study of a geared turbofan and an open rotor aero engine with intercooled recuperated core. *Proceedings of the Institution of Mechanical Engineers, Part G: Journal of Aerospace Engineering*, page 095441001877088, 2018.

[16] Dimitris Missirlis, Zinon Vlahostergios, Michael Flouros, Christina Salpingidou, Stefan Donnerhack, A. Goulas, and Kyros Yakinthos. Optimization of heat exchangers for intercooled recuperated aero engines. *Aerospace*, 4:14, 2017.

[17] Dimitris Missirlis, Zinon Vlahostergios, Michael Flouros, Christina Salpingidou, Stefan Donnerhack, A. Goulas, and Kyros Yakinthos. Intercooled recuperated aero engine: development and optimization of innovative heat exchanger concepts. 2016.

[18] F. Yin and A. Gangoli Rao. Performance analysis of an aero engine with inter-stage turbine burner. *The Aeronautical Journal*, 121(1245):1605–1626, 2017.

[19] NASA. Ideal brayton cycle, 2015.

[20] Hugo Canière, Arnout Willockx, Erik Dick, and Michel De Paepe. Raising cycle efficiency by intercooling in air-cooled gas turbines. *Applied Thermal Engineering*, 26, 2006.

[21] G.P. Systems. Lms100-pa+/pb aeroderivative gas turbine, 2005.

[22] H.I.H. Saravanamuttoo, G.F.C. Rogers, and H. Cohen. *Gas Turbine Theory*. Prentice Hall, 2001.

[23] P.P. Walsh and P. Fletcher. *Gas Turbine Performance*. Wiley, 2008.

[24] R. C. Wilcock, J. B. Young, and J. H. Horlock. The Effect of Turbine Blade Cooling on the Cycle Efficiency of Gas Turbine Power Cycles. *Journal of Engineering for Gas Turbines and Power*, 127(1):109–120, 2005.

[25] Lei Xu and Tomas Grönstedt. Design and Analysis of an Intercooled Turbofan Engine. *Journal of Engineering for Gas Turbines and Power*, 132(11):114503–114503–4, 2010.

[26] Feng Liu and Sirignano William. Turbojet and Turbofan Engine Performance Increases Through Turbine Burners. *Journal of Propulsion and Power - J PROPUL POWER*, 17, 2001.

[27] Gordon Chen, Mike Hoffman, and Roger Davis. Gas-Turbine Performance Improvements Through the Use of Multiple Turbine Interstage Burners. *Session: ABP-3: Turbomachinery - Computational*, 20, 2004.

[28] K H. Liew, C J. Marek, J D. Mattingly, Egel Urip, and Song-Lin Yang. Performance Cycle Analysis of Turbofan Engine with Interstage Turbine Burner. *Journal of Propulsion and power*, 22, 2006.

[29] Cantera. *Cantera Documentation: Reactors and Reactors Network*, 2018. Available from:http://www.cantera.org/docs/sphinx/html/reactors.html [cited 2019 June].

[30] S.A. Shakariyants. *Generic methods for aero-engine exhaust emission prediction*. PhD thesis, TU Delft, 2008.

[31] S Honnet, K Seshadri, Ulrich Niemann, and Norbert Peters. A surrogate fuel for kerosene. *Proceedings of the Combustion Institute*, 32:485–492, 2009.

[32] J. H. Horlock, D. T. Watson, and T. V. Jones. Limitations on Gas Turbine Performance Imposed by Large Turbine Cooling Flows. *Journal of Engineering for Gas Turbines and Power*, 123(3):487–494, 2001.

[33] Maria Jonsson, Olav Bolland, Dominikus Bücker, and Mike Rost. Gas turbine cooling model for evaluation of novel cycles, 2005.

[34] Nicolas E. Antoine and Ilan M. Kroo. Aircraft Optimization for Minimal Environmental Impact. *Journal of Aircraft*, 41(4):790–797, 2004.

[35] Arthur H. (Arthur Henry) Lefebvre and Dilip R Ballal. *Gas turbine combustion : alternative fuels and emissions*. Boca Raton, FL : CRC Press, 3rd ed edition, 2010. ”A CRC title.”.

[36] James R. Maughan, Andrew Luts, and Paul J. Bautista. A Dry Low NOx Combustor for the MS3002 Regenerative Gas Turbine. *ASME 1994 International Gas Turbine and Aeroengine Congress and Exposition*, 3(78859):V003T06A010, 1994.

[37] A H. Lefebvre. Fuel effects on gas turbine combustion - Liner temperature, pattern factor and pollutant emissions. In *JA Aircraft*, volume 21, 1984.

[38] J. Odgers and D. Kretschmer. The Prediction of Thermal NOx in Gas Turbines. *ASME 1985 Beijing International Gas Turbine Symposium and Exposition*, 2(79436), 1985.

[39] G. D. Lewis. A new understanding of nox formation. *Tenth International Symposium on Air-Breathing Engines*, pages 625 –9, 1991.

[40] R.T. Watson, Groupe d'experts intergouvernemental sur l'évolution du climat, Intergovernmental Panel on Climate Change, D.L. Albritton, United Nations Environment Protection, Intergovernmental Panel on Climate Change Working Group III, I.P.O.N.C.C. WORKING, Intergovernmental Panel on Climate Change Working Group Science, and World Meteorological Organization. *Climate Change 2001: Synthesis Report: Third Assessment Report of the Intergovernmental Panel on Climate Change*. Climate change 2001. Cambridge University Press, 2001.

[41] Ibrahim Dincer and Marc A. Rosen. Exergy: Energy, environment and sustainable development. In Ibrahim Dincer and Marc A. Rosen, editors, *Exergy (Second Edition)*. Elsevier, 2013.

[42] Broomhead M.J Visser W.P.J. Gsp, a generic object-oriented gas turbine simulation environment. *ASME IGTI Turbo Expo conference*, 2000.

[43] Jorge Nocedal and Stephen J. Wright. *Numerical Optimization*. Springer, New York, NY, USA, second edition, 2006.

[44] Andrew M. Roltand Vishal Sethi Konstantinos G. Kyprianidis. *Progress in Gas Turbine Performance*, chapter On intercooled Turbofan Engines, pages 3–24. InTech, 2013.

[45] A. Žukauskas. *Heat Transfer from Tubes in Crossflow*, volume 8 of *Advances in Heat Transfer*. Elsevier, 1972.

[46] Feijia Yin, Floris S. Tiemstra, and Arvind G. Rao. Development of a Flexible Turbine Cooling Prediction Tool for Preliminary Design of Gas Turbines. *Journal of Engineering for Gas Turbines and Power*, 140(9), 2018. 091201.

[47] EASA. Edb emissions data, 2019. Issue: 26.

[48] EASA. *TYPE-CERTIFICATE DATA SHEET for GE90*, 2019. Issue: 04.

[49] Chi-Ming Lee, Kathleen M Tacina, and Changlie Wey. High pressure low nox emissions research: Recent progress at nasa glenn research center. *fuel*, 4, 2007.

[50] National Research Council. *Aeronautical Technologies for the Twenty-First Century*. The National Academies Press, Washington, DC, 1992.

[51] DA Sullivan. A simple gas turbine combustor no x correlation including the effect of vitiated air. *Journal of Engineering for Power*, 1977.

[52] J. M. Clarke and J. H. Horlock. Availability and propulsion. *Journal of Mechanical Engineering Science*, 17(4):223–232, 1975.

[53] H.D. Baehr. *THERMODYNAMIK: eine Einführung in die Grundlagen und ihre technischen Anwendungen*. "Springer, Berlin", 1978.

[54] Jansen S. and Woudstra N. Understanding the exergy of cold: theory and practical examples. *International Journal of Exergy*, 7(6):693, 2010.

[55] Glenn Brown. The history of the darcy-weisbach equation for pipe flow resistance. *Proc. Environ. Water Resour. Hist.*, 38, 2002.

A

Validation of intercooler modelling

The following code was used to validate the design choice for the intercooler, namely a constant pressure loss of 3% in cruise for an effectiveness of 50%. This is then scaled using Reynolds analogy for all other flight phases or varying effectiveness.

$$Nu_D = 0.023 Re_D^{4/5} Pr^n \tag{A.1}$$

The Prandtl number comes from the fluid used and the Reynolds number is found using equation A.2. The number n is a factor dependent on heat going out of the flow or heat going in to the flow where n is 0.3 or 0.4, respectively.

$$Re_D = \frac{\rho V D_{in}}{\mu} \tag{A.2}$$

The heat transfer coefficient can be calculated using the Nusselt number and the thermal conductivity.

$$h = \frac{N_u \cdot k}{D_{in}} \tag{A.3}$$

The thermal resistance to heat transfer is given as equation A.4.

$$R = \frac{1}{hA_{in}} \tag{A.4}$$

Where A_{in} is the total inside area of the tubes. The resistance of the tubes itself is given by equation A.5.

$$R_{wall} = \frac{ln(\frac{D_{out}}{D_{in}})}{2\pi k_{wall} L} \tag{A.5}$$

The resistance of the cooling flow is calculated using the layout of the intercooler. It is dependent on how the tubes are stacked together and the distance between them. The speed of the flow is dependent on the frontal size of the heat exchanger, and 2 parameters, the longitudinal pitch SL and the transversal pitch ST. The diagonal pitch SD is also used to define the smallest area in the intercooler for the cold side. The maximum speed in this configuration happens along the ST line or the SD line as can be seen in figure A.1. This all follows the procedures by Zukauskas et al. [45].

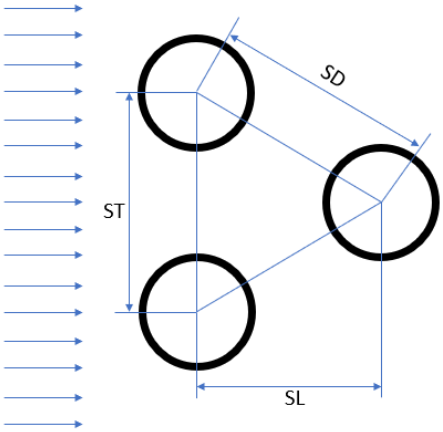

Figure A.1: Representation of staggered flow bank. The hot flow goes through the pipes and the cold flow goes around the pipes.

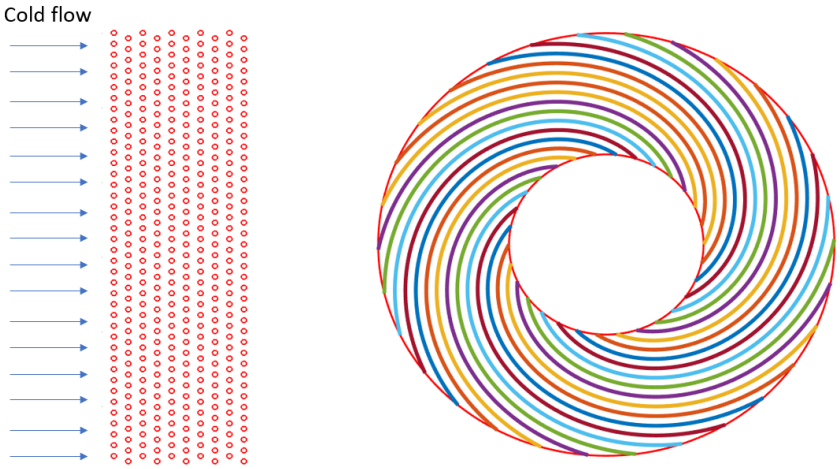

Figure A.2: Full view of HE, first top view of circumference. Second, frontal view where the core lies inside of the HE.

If the maximum speed happens along the SD line, it is given by equation A.6. On the ST line it is given by equation A.7.

$$V_{max} = V_i \frac{ST}{ST - D_{out}} \tag{A.6}$$

$$V_{max} = V_i \frac{ST}{2 \cdot (SD - D_{out})} \tag{A.7}$$

Now the Reynolds number is calculated using equation A.8

$$Re = \frac{\rho V_{max} D_{out}}{\mu} \tag{A.8}$$

The Nusselt factor calculated using equation A.9

$$Nu = C_3 C_2 Re^m Pr^n \frac{Pr}{Pr_s}^{0.25} \tag{A.9}$$

Where $C_2 = 1$, $n = 0.36$ and C_3 and m depend on the Reynolds number, and are summarized in Table

A.1.

Table A.1: C_3 and m based on Reynolds number [45]

Re	C_3	m
1<Re<40	0.75	0.4
40<Re<1000	0.51	0.5
1000<Re< 10^5	0.26	0.6
10^5 <Re< 10^6	0.076	0.7

Now the heat transfer coefficient is also calculated using equation A.3. The resistance is then calculated using equation A.4 where the surface area is replaced with the surface area on the outside of the tubes. Because the heat transfer happens in series from the inside of the tube to the outside, the equivalent R is the sum of the partial resistances. and the heat transfer is calculated using equation A.10

$$\dot{q} = (T_1 - T_2)/R_{eq} \tag{A.10}$$

Using the enthalpy and the mass flow, the temperature changes in both flows can be found. For the pressure loss along the heat exchanger, also Zukauskas et al. [45] is used. This is expressed as equation A.11

$$\Delta p = \chi N_L \left(\frac{\rho V_{max}^2}{2} \right) f \tag{A.11}$$

Where friction factor f and correction factor

$$\chi$$

are given in a graphical form dependent on Reynolds number and the geometry.

$$N_L$$

is the number of rows in the heat exchanger. The friction factor is shown in figure A.3 and the correction factor is shown in figure A.4.

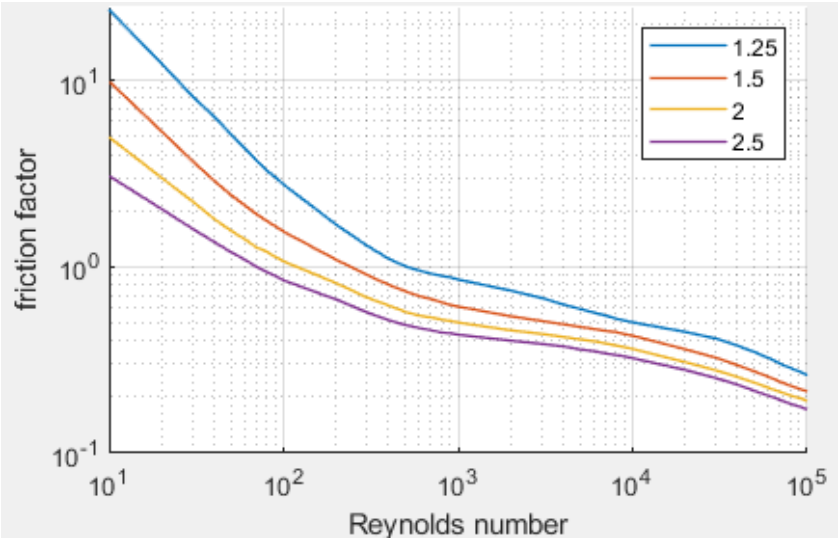

Figure A.3: Friction factor for pressure drop model from Zukauskas[45]. In the legend, the number represents the distance between the columns over the distance between the rows. P_T/P_L

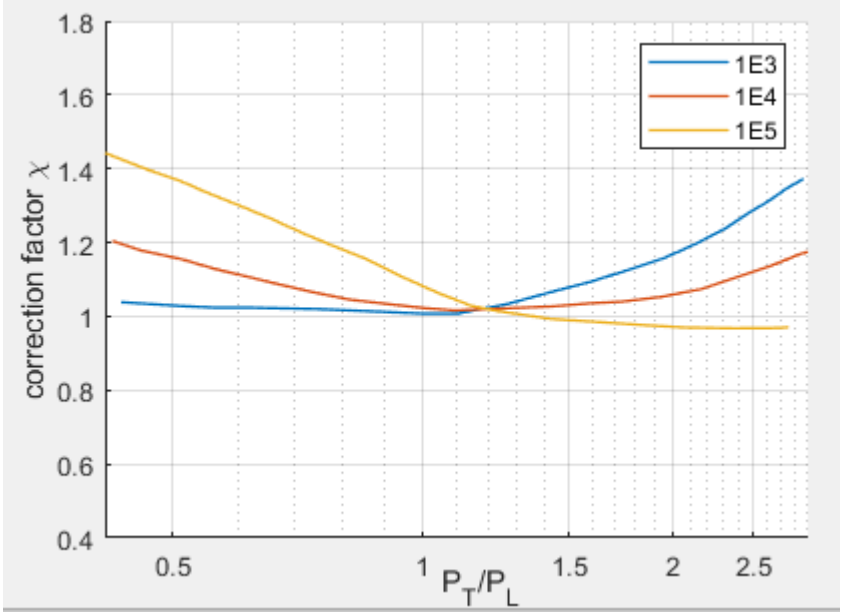

Figure A.4: Correction factor for pressure drop model from Zukauskas[45]. The legend represents the Reynolds number.

If the input in the heat exchanger is between 2 lines, an interpolation is used to find the corresponding factors. The pressure loss inside the tubes of the intercooler is found by equation A.12 and equation A.13. Which calculate the Darcy friction factor and the pressure loss by the Darcy-Weisbach equation [55].

$$\lambda = (0.79ln(Re) - 1.64)^{-2} \tag{A.12}$$

$$\Delta p = \lambda \left(\frac{L \rho V^2}{2 D_{in}} \right) \tag{A.13}$$

B

Efficiency loss factor of turbine cooling

The effect of the loss factor on the engine performance is looked upon here. This loss factor is well described by Horlock et al.[32] and by Wilcock et al. [24]. The effect on the engines is investigated changing the loss factor from 0 to 0.625.

In the following figures, the effects are shown when all the parameters are changed for different loss factors. In figure B.1, the effect on the TSFC for varying loss factor is presented. It is noted that since the BPR has no direct influence on the core cycle, it has only a small difference. This comes from the fact that the core cycle will produce less thrust for the same fuel.

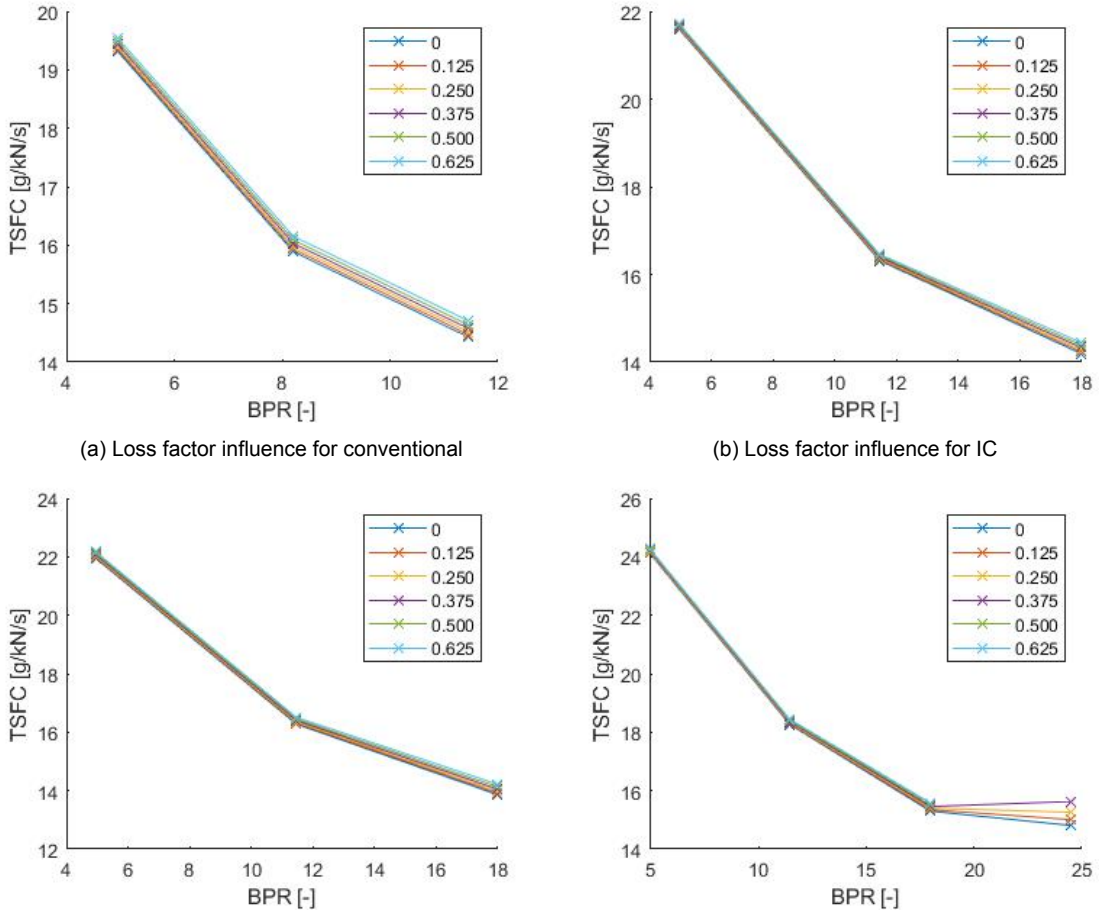

(a) Loss factor influence for conventional

(b) Loss factor influence for IC

(c) Loss factor influence for ITB

(d) Loss factor influence for IC-ITB

Figure B.1: Effect of loss factor and BPR.

Following this in figure B.2, the effect on the TSFC for varying FPR is shown. The same is seen, almost no influence since the FPR has no impact on the core except that the exhaust flow will have less energy. It is also seen that in the IC-ITB engine, the FPR can be higher.

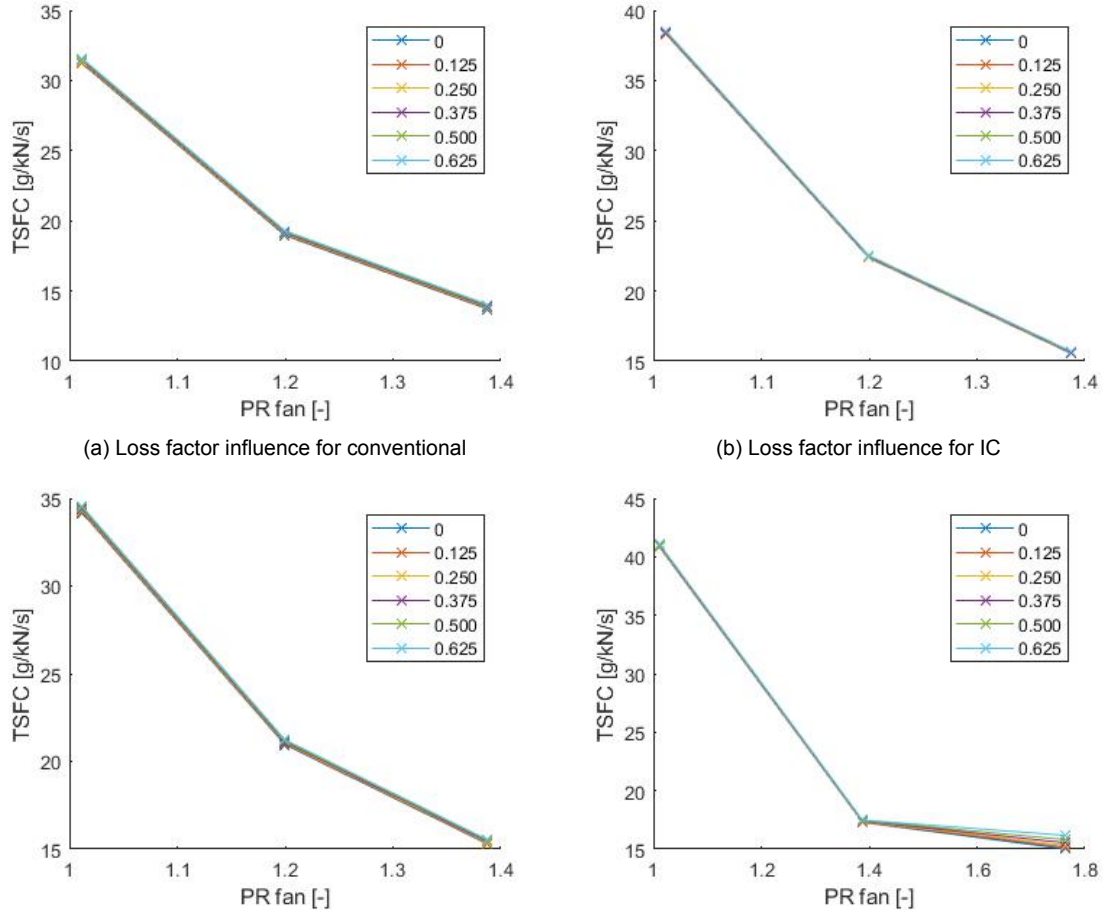

(a) Loss factor influence for conventional

(b) Loss factor influence for IC

(c) Loss factor influence for ITB

(d) Loss factor influence for IC-ITB

Figure B.2: Effect of loss factor and FPR.

In figure B.3 the effect of the loss factor on the TSFC for varying LPC PR is shown. The effect is more pronounced since now it affects the cooling temperature. They are all increased since the HPC starts at a higher pressure and thus also at a higher temperature. This effect is minimized for the IC-engine since in this engine, the flow between the LPC and HPC is cooled.

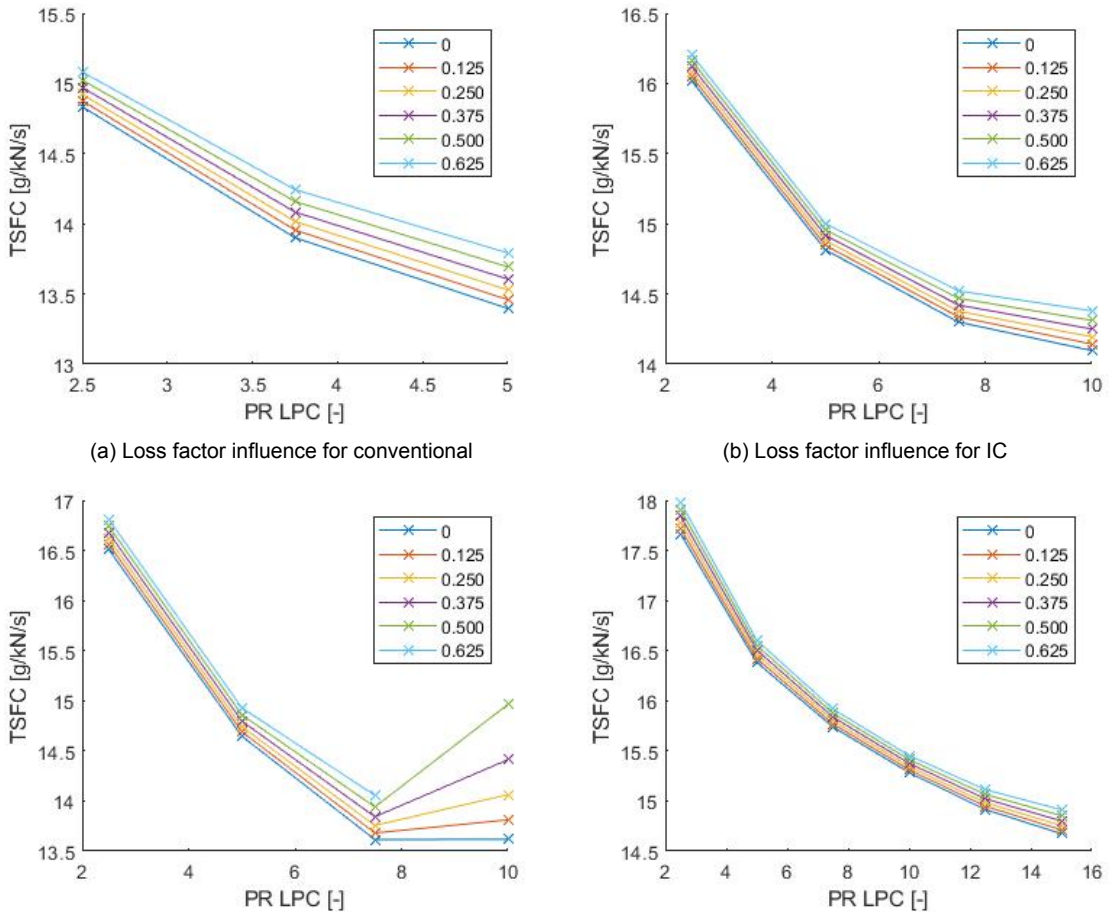

(a) Loss factor influence for conventional

(b) Loss factor influence for IC

(c) Loss factor influence for ITB

(d) Loss factor influence for IC-ITB

Figure B.3: Effect of loss factor and low pressure compressor pressure ratio.

In figure B.4, the effect of the loss factor for varying HPC PR is visible. This follows the same trend as the LPC pressure ratio. The IC case and the IC-ITB case have the smallest impact by this factor since the cooling flow enters colder and less cooling is required.

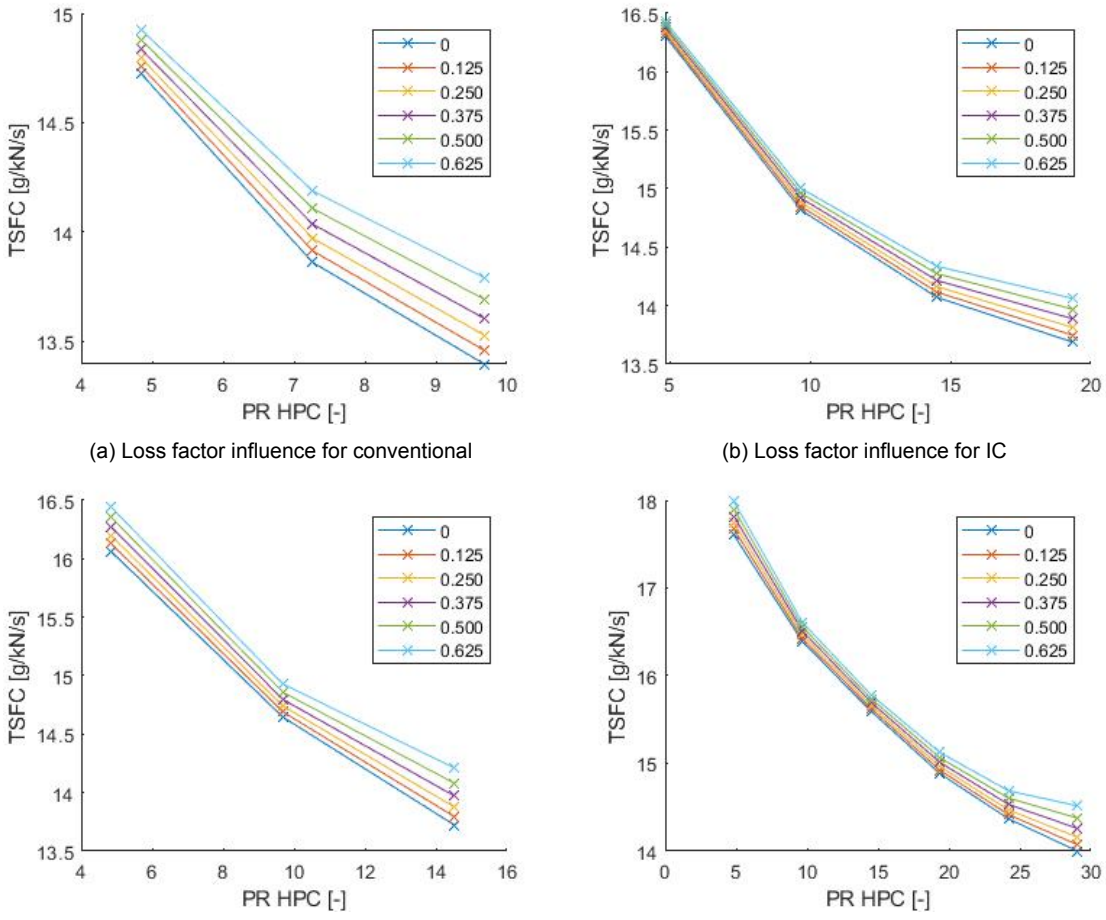

(a) Loss factor influence for conventional

(b) Loss factor influence for IC

(c) Loss factor influence for ITB

(d) Loss factor influence for IC-ITB

Figure B.4: Effect of loss factor and HPC pressure ratio.

In figure B.5, the effect of the TIT is visible. While the conventional engine shows the best TSFC, the influence of the loss factor is also the largest for the conventional engine. The IC-engine shows the best performance when changing the loss factor. The ITB engine is not much difference though, +3% for the IC and +4% for the temperature set at 1900K.

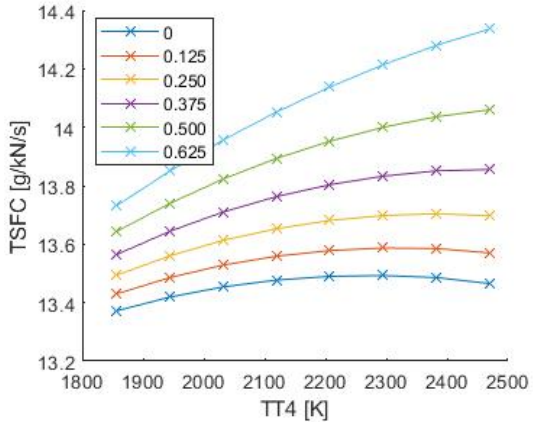

(a) Loss factor influence for conventional

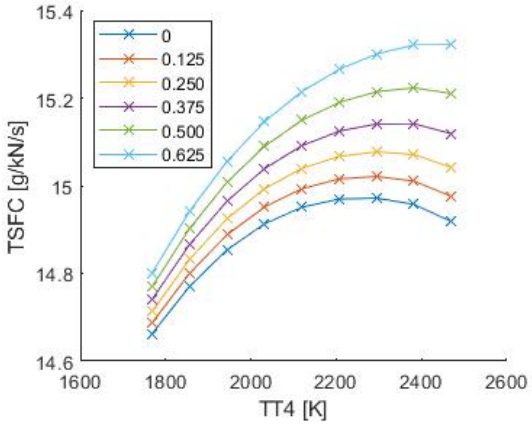

(b) Loss factor influence for IC

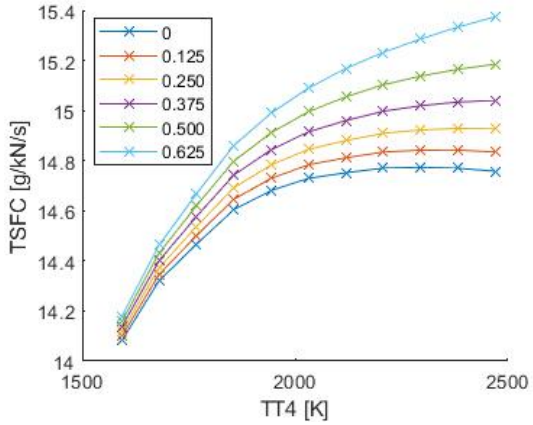

(c) Loss factor influence for ITB

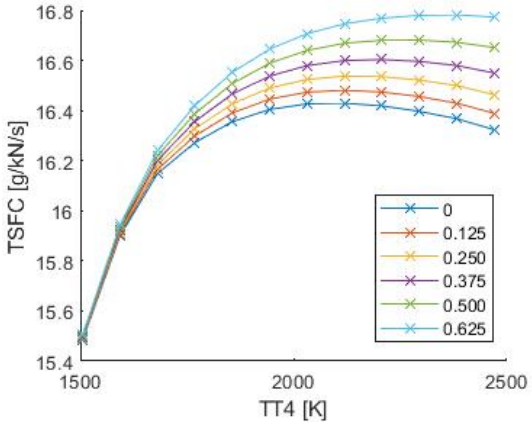

(d) Loss factor influence for IC-ITB

Figure B.5: Effect of loss factor and TIT.